博士論文

Studies on chemotaxis mechanism involved in the early stage of plant infection by bacterial wilt pathogen *Ralstonia pseudosolanacearum*

青枯病菌 *Ralstonia pseudosolanacearum* の植物感染初期段階に関与する走化性機構の解明

緋田　安希子

広島大学大学院先端物質科学研究科

2018 年 3 月

目次

1. 主論文

Studies on chemotaxis mechanism involved in the early stage of plant infection by bacterial wilt pathogen *Ralstonia pseudosolanacearum*

（青枯病菌 *Ralstonia pseudosolanacearum* の植物感染初期段階に関与する走化性機構の解明）

緋田　安希子

2. 公表論文

(1) Identification of the *mcpA* and *mcpM* genes, encoding methyl-accepting proteins involved in amino acid and L-malate chemotaxis, and involvement of McpM-mediated chemotaxis in plant infection by *Ralstonia pseudosolanacearum* (formerly *Ralstonia solanacearum* phylotype I and III).

Hida A, Oku S, Kawasaki T, Nakashimada Y, Tajima T, Kato J.

Applied and Environmental Microbiology **81**:7420-7430 (2015).

(2) Identification of boric acid as a novel chemoattractant and elucidation of its chemoreceptor in *Ralstonia pseudosolanacearum* Ps29.

Hida A, Oku S, Nakashimada Y, Tajima T, Kato J.

Scientific Reports **7**:8609 (10 pages) (2017).

2. 参考論文

(1) Identification and characterization of chemosensors for D-malate, unnatural enantiomer of malate, in *Ralstonia pseudosolanacearum*

Tunchai M, **Hida A**, Oku S, Nakashimada Y, Tajima T, Kato J.

Microbiology **163**:233-242 (2017).

(2) Negative chemotaxis of *Ralstonia pseudosolanacearum* to maleate and identification of the maleate chemosensory protein.

Tunchai M, **Hida A**, Oku S, Nakashimada Y, Nikata T, Tajima T, Kato J.

Journal of Bioscience and Bioengineering **124**:647-652 (2017).

(3) Involvement of many chemotaxis sensors in negative chemotaxis to ethanol in *Ralstonia pseudosolanacearum* Ps29.

Oku S, **Hida A**, Tunchai M, Tajima T, Nakashimada Y, Kato J.

Microbiology **163**: 1880-1889 (2017).

主論文

CONTENTS

CHAPTER 1
General introduction

The *Ralstonia solanacearum* species complex, composed of *R. solanacearum* (formerly *R. solanacearum* phylotype II), *Ralstonia pseudosolanacearum* (formerly *R. solanacearum* phylotypes I and III) and *Ralstonia syzyg*ii subsp. *indonesiensis* (formerly *R. solanacearum* phylotype IV)[1,2], is a bacterial group of gram-negative plant pathogen that causes bacterial wilt disease in more than 200 plant species in over 50 families, including economically important crops such as tomato, tobacco, potato and eggplant[3,4]. The *R. solanacearum* species complex is extremely damaging to agriculture because of its wide geographical distribution, wide host range, and high survivability. This soil-borne bacterium usually enters plant roots through wounds, the root tips, and secondary root emergence points, eventually invading the xylem vessels and spreading to the aerial parts of the plant[5]. Many factors contribute to bacterial wilt disease. For example, type III secretion system and exopolysaccharide, which are known as major factors, and plant cell wall-degrading enzymes and also motility including chemotaxis[6].

Chemotaxis, a universal phenomenon in motile bacteria, allows these organisms to move toward more favorable condition in response to chemical gradient in environment[7]. The molecular mechanisms that underlie bacterial chemotaxis have been studied intensively in *Escherichia coli* and *Salmonella enterica* serovar Typhimurium[8,9]. Chemotactic ligands are detected by transmembrane chemoreceptors called methyl-accepting chemotaxis proteins (MCPs). Upon ligands binding, MCPs generate chemotaxis signals that are communicated to the flagellar motor via a series of chemotaxis (Che) proteins (Fig. 1.1). In *E. coli*, five MCPs (Tsr, Tar, Trg, Tap, and Aer) and six Che

proteins (CheA, CheB, CheR, CheW, CheY, and CheZ) have been identified to date [9]. While this two-component signaling mechanism is mostly common to that of other chemotactic bacteria, the number of MCPs vary among different bacteria. Compared with enteric bacteria, free-living environmental bacteria such as soil-borne bacteria possess a large number of MCPs. For example, 26 putative MCPs in *Pseudomonas aeruginosa* PAO1[10], 27 putative MCPs in *Pseudomonas putida* F1[11], and 37 putative MCPs in *Pseudomonas fluorescens* Pf0-1[12]. The environmental bacteria therefore show chemotactic response to various compounds including not only amino acids, sugars and organic acids but also inorganic phosphate, aromatic compounds, and pollutants[10,11,13-16]. Because most of attractants are growth substrates, chemotaxis is believed to assist bacteria in efficiently moving to environments suitable for growth. Bacterial chemotaxis can be also viewed as an important prelude to ecological interactions such as nodulation by *Rhizobium leguminosarum*[17], root colonization by plant growth-promoting *P. fluorescens*[12,18,19], and infection by *R. solanacearum*[20].

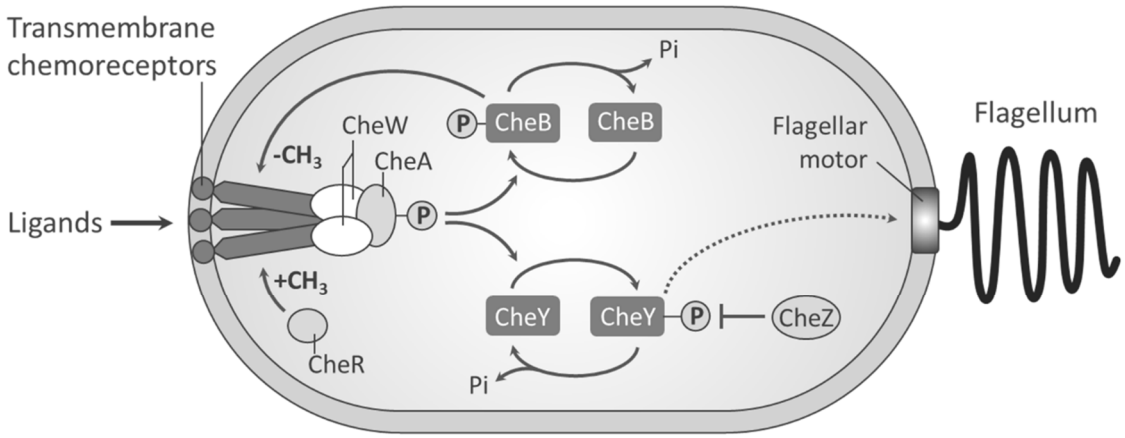

Fig. 1.1. Chemotaxis signal transduction pathway in *E. coli*. Ligands are recognized by transmembrane chemoreceptors. In response to decreased attractants, the chemoreceptors induce autophosphorylation of CheA. Phosphorylated CheA transfers the phosphoryl group to CheY and CheB. Phosphorylated CheY then binds to flagellar motor and causes cell to tumble by promoting a switch in the direction of flagellar rotation from counter clockwise to clockwise. Phosphorylated CheB and CheR, methyltransferase, mediate adaptation[9].

The *R. solanacearum* species complex is motile and shows chemotaxis to various compounds [20]. Tans-Kersten *et al*. (2001) reported that swimming motility was essential for invasive virulence on tomato in *R. solanacearum* strain K60[21]. Yao and Allen (2006) observed that *cheA* and *cheW* single mutants of strain K60, which are nonchemotactic but motile, were less infectious than the wild-type strain in sand-soak virulence assays. When tomato plants were coinoculated with a 1:1 mixture of each nonchemotactic mutant and its wild-type parent, the wild-type strain outcompeted these nonchemotactic mutants. From these results, authors concluded that *R. solanacearum* K60 requires chemotaxis for full virulence and depends on taxis to locate and colonize plant roots[20]. They also demonstrated that aerotaxis (energy taxis) contributed to efficient interaction of *R. solanacearum* K60 with host plants[22]. However, nonchemotactic mutants were more impaired in virulence than the mutant defective in aerotaxis. These data suggested that taxis other than aerotaxis is involved in migration of this pathogen to plant roots.

In this study, I tried to identify other taxis involved in plant infection by the *R. solanacearum* species complex. Complete genomic sequences have been generated for several strains of the *R. solanacearum* species complex[23]. Although genomic analysis revealed that these strains each encode more than 20 MCPs, all these MCPs except two aerotaxis sensors[22] have not yet been functionally characterized, which hampers the identification of chemoattractant(s) involved in plant infection by the *R. solanacearum* species complex. Therefore, I first attempted to characterize unknown MCPs function and then investigate involvements of the MCPs in plant infection using the *mcp* deletion mutants. In chapter 2 and 3, chemotaxis to L-amino acids, L-malate and citrate, main components of plant root exudate, were analyzed. In chapter 4, chemotaxis to boric acid, a novel chemoattractant, was analyzed.

CHAPTER 2

Identification of chemoreceptors for L-amino acids and L-malate, and its relationships with plant infection

2.1. Introduction

Chemotaxis plays an important role for plant-microbe interactions in beneficial bacteria such as *R. leguminosarum*[24], *P. fluorescens*[18] and *Bacillus subtilis*[25] as well as pathogenic bacteria such as *Dickeya dadantii* 3937[26] and the *R. solanacearum* species complex[20]. These soil-borne bacteria are believed to locate plant roots by sensing root exudate. Plant roots release a wide variety of compounds[27], many of which act as a chemoattractant for bacteria[28,29]. In several bacteria, specific molecules involved in chemotaxis to root exudate have been identified. *P. putida* KT2440 shows chemotaxis to aromatic metabolites in maize exudate[30]. *Sinorhizobium meliloti* is attracted to alfalfa exudate by sensing proline[31]. *P. fluorescens* Pf0-1 effectively locates and colonizes tomato roots by sensing amino acids in its exudate [12]. *R. solanacearum* is also reportedly attracted to plant root exudate and needs chemotaxis for full virulence and competitive fitness[20]. However, specific compound(s) detected by this pathogen is/are hitherto unknown.

Amino acids, sugars, and organic acids are quantitatively major components of plant root exudate. Yao and Allen reported that *R. solanacearum* strain K60 shows chemotactic response to certain amino acids, organic acids including citrate and malate, and sugars[20]. These compounds that are major components of root exudate and chemoattractants for the pathogen could be important molecules for the *R. solanacearum* species complex to migrate to plant roots in the early stage of infection. In this chapter, I investigated involvements of chemotaxis to these compounds in plant infection.

2.2 Experimental procedures

2.2.1. Bacterial strains, plasmids, and growth conditions

Bacterial strains and plasmids used in this chapter are listed in Table 2.1 and Table 2.2, respectively. *R. pseudosolanacearum* Ps29 (formerly *R. solanacearum* Ps29 [phylotype I, race I, biovar 3]; isolated from tobacco) and *R. pseudosolanacearum* MAFF106611 (formerly *R. solanacearum* MAFF106611 [phylotype I, race I, biovar 4]; isolated from eggplant) were obtained from the Leaf Tobacco Center (Japan Tobacco Inc.) and the National Institute of Agrobiological Sciences, Japan, respectively. A highly motile Ps29 strain and its derivatives were used for chemotaxis research, and a highly virulent MAFF106611 strain and its derivatives were used for tomato plant assay. *E. coli* strains JM109 and S17-1 were used for plasmid construction and transconjugation, respectively.

R. pseudosolanacearum strains were cultivated at 28°C in CPG medium or in *R. solanacearum* minimal (RSM) medium with shaking at 280 rpm. CPG medium[32] contained 10 g/l polypeptone, 1 g/l casamino acid, and 5 g/l glucose. RSM medium[33] contained 1.75 g/l K_2HPO_4, 0.75 g/l KH_2PO_4, 0.15 g/l trisodium citrate dihydrate, 1.25 g/l $(NH_4)_2SO_4$, 0.25 g/l $MgSO_4 \cdot 7H_2O$, and 5 g/l glucose (glucose was sterilized by 0.2 μm filter and supplemented into autoclaved media). *E.coli* strains were grown at 37°C in Luria-Bertani (LB) medium[34] containing 0.5% yeast extract, 1% NaCl, and 1% tryptone. For plasmid selection and maintenance, kanamycin was provided at 40 μg/ml.

2.2.2. DNA manipulation

Standard procedures were used for plasmid DNA preparations, transformations of *E. coli*, and agarose gel electrophoresis[34]. PCR, restriction enzyme digestions, and ligation reactions were conducted using KOD FX Neo polymerase (Toyobo, Osaka, Japan),

FastDigest (Thermo Fisher Scientific, Massachusetts, USA), and Ligation High Ver.2 (Toyobo, Osaka, Japan), respectively, according to the manufacturer's instructions. Primers used for PCR are listed in Table 2.3.

2.2.3 Chemotaxis assay

Computer-assisted capillary assay were carried out as described previously[35]. *R. pseudosolanacearum* Ps29 strains were grown in CPG medium (supplemented with 40 μg/ml kanamycin when necessary) for 20 h. Then, 100 μl of preculture cells were transferred into 5-ml RSM medium and grown for 4 h. *R. pseudosolanacearum* MAFF106611 strains were grown in RSM medium for 20 h without preculture. One ml of grown cells in 1.5 mL tube were harvested by centrifugation at 3,300×*g* for 1 min, and then gently suspended by 1 mL of 10 mM HEPES buffer (pH 7.0). The cells were again harvested and gently resuspended by same buffer. The washed cells were maintained at 28°C for 1 h before measurements.

Glass capillaries were prepared from micro-injection glass tubing type G-1 (Narishige, Tokyo, Japan) by using puller PB-7 (Narishige, Tokyo, Japan). A test compound plus 1% (v/v) agarose suspended by 10 mM HEPES buffer was put into glass capillaries by capillary action. Cell movement was observed under an inverted phase-

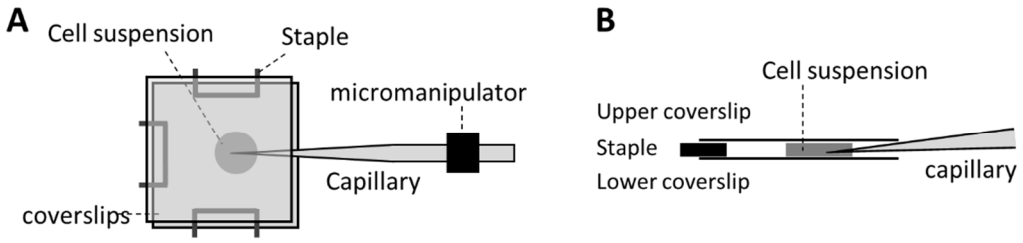

Fig. 2.1. A set on the stage of microscope for chemotaxis assay . **A**, top view; **B**, side view. Glass capillary contained test compounds plus 1%(v/v) agarose.

contrast microscope IMT-2 (Olympus, Tokyo, Japan) equipped with a micromanipulator MN-151 (Narishige, Tokyo, Japan). The microscope stage was set as depicted in Fig. 2.1. Cells in a 10-μl suspension were placed on a coverslip, and the assay was started by placing the coverslip upside down on another coverslip placed on three staples as spacer to fill around the mouth of the capillary with the cell suspension. Cells were videotaped, and the number of bacteria migrating toward the mouth of the capillary at the initial time (N_0) and at each given time interval (N_t) was counted using digital image processing and icy Spot Detector. The strength of the chemotactic response was determined and reported in terms of normalized cell number per frame (N_t/N_0). Unless stated otherwise, normalized cell numbers were calculated by dividing the number of cells at 1 min by that at the initiation of observation. As negative control, 10 mM HEPES buffer was used.

2.2.4. Construction of unmarked deletion mutants

The putative *mcp* and *cheA* genes in *R. pseudosolanacearum* Ps29 and MAFF106611 were deleted by an unmarked-gene-deletion technique using suicide plasmid pK18*mobsacB*[36] that harbors a kanamycin resistance gene (*kan*) as a selection marker and the *sacB* gene as a counter-selection marker. The general procedure was as follows. All PCR primers were designed based on the genome sequence of *R. pseudosolanacearum* GMI1000 (formerly *R. solanacearum* GMI1000), and additional nucleotides with appropriate restriction sites were added at the 5’ ends of primers for convenience of plasmid construction. Four primers were used to amplify 0.6- to 1.2-kb upstream and downstream regions, respectively, of the target gene from *R. pseudosolanacearum* Ps29 and MAFF106611. The amplified DNA fragments were digested with appropriate restriction enzymes and ligated with the backbone of

pK18*mobsacB* digested with appropriate restriction enzymes. Table 2.4 shows primer pairs and restriction enzymes used in construction of each plasmids for unmarked deletion of 22 *mcp* and *cheA* genes.

The resulting plasmid was introduced into *R. pseudosolanacearum* Ps29 or MAFF106611 by transconjugation using *E. coli* S17-1. Strain S17-1 harboring the plasmid for unmarked gene modification and *R. pseudosolanacearum* wild-type strain were grown overnight in liquid medium, and washed three times by sterile water. For transconjugation, 100 µL of 4:1 (OD_{600} ration) mixture of Ps29 cells and S17-1 cells (or 1:2 mixture of MAFF106611 cells and S17-1 cells) was dropped on CPG agar plate without kanamycin. Single-crossover recombination between homologous regions of genomic DNA and the plasmid resulted in the integration of the plasmid into the genome. After incubation overnight, cells on CPG plate were harvested, washed three times by sterile water, and spread Simmons Citrate Agar (SCA) plate containing 40 µg/ml kanamycin to select cells containing the integrated plasmid by kanamycin resistance. Colonies obtained on SCA plate after incubation for 2 or 3 days were inoculated into RSM liquid medium and cultivated overnight. Then, grown cells were spread and incubated for 2 or 3 days on CPG agar plate containing 6% sucrose to confirm sucrose sensitivity. Cells undergoing the second single-crossover recombination (plasmid excision) were selected on this plate, yielding sucrose-resistant and kanamycin-sensitive cells. Depending on the excision crossover, the resulting strain harbored either the wild type gene or an unmarked deletion of the target gene. The latter genotype was confirmed by visualizing the size of the fragment amplified by colony PCR using primers flanking the target gene.

2.2.5. Construction of complementing plasmids

pRCII was constructed to provide a plasmid vector for complementation analysis of *R. pseudosolanacearum* mutants. The construction scheme and physical map of pRCII are shown in Fig. 2.2. To construct pRCII, regions corresponding to the origin of replication from pKZ27[37], the *kan* gene from pUC4K[38], and the *lac* promoter and multiple-cloning sites from pUCP18[39] were amplified by PCR using primer pairs RCIIoriVf/RCIIoriVr, CLkanRf/CLkanRr2, and RCIIMCSf/RCIIMCSr, respectively. The amplified *kan* gene and the origin of replication were digested with *Nde*I and *Sac*II and ligated together to obtain pRC. The amplified region including the *lac* promoter and multiple-cloning sites was digested with *Nde*I and ligated with *Nde*I-digested pRC to obtain pRCII.

To construct pPS01, a 2.1-kb region containing the RS_RS03035 homolog gene of *R. pseudosolanacearum* Ps29 was amplified by PCR using primer pair CLRS01f/CLRS01r. The amplified fragments were digested with *Eco*RI and *Bam*HI and ligated with *Eco*RI- and *Bam*HI-digested pRCII. To construct pPS14, a 2.0-kb region containing the RS_RS19595 homolog gene of *R. pseudosolanacearum* Ps29 was amplified by PCR using primer pair CLRS14f/CLRS14r. The amplified fragments were

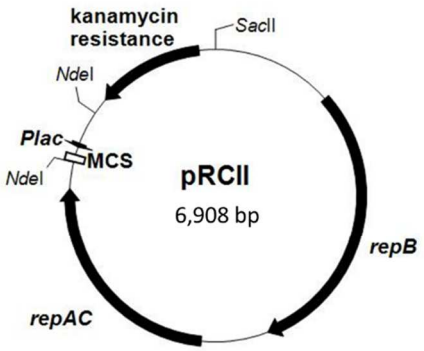

Fig. 2.2. Physical map of pRCII. The region between *Sac*II and *Nde*I including *repABC* was amplified from pKZ27. The region of kanamycin resistant gene was amplified from pUC4K. The region between *Nde*I sites including *lac* promoter and multiple cloning site (MCS) was amplified from pUCP18.

digested with *Eco*RI and *Bam*HI and ligated with the backbone of *Eco*RI-and *Bam*HI-digested pRCII.

2.2.6. Introduction of complementing plasmids into *R. pseudosolanacearum*

R. pseudosolanacearum Ps29 strains were cultured in CPG medium for 6 h after preculture in same medium for 20 h. Five ml of cells were centrifuged (3,300×*g* for 5 min), washed twice with ice-cold 10% (v/v) glycerol, and resuspended by 1 ml of same solution. The competent cells 400 μl were mixed with 2-μl plasmid in electroporation cuvette EP-202 (Cell projects, Kent, UK) and transformed by electroporation with 2.5 kV, 250 Ω, and 25 μF. The transformant cells were immediately curing by transfer 200 μl of it into 5 ml CPG liquid medium, placed at 28°C overnight without shaking, and then spread on CPG agar plate containing 40 μg/ml kanamycin. After incubation at 28°C for 2 days, transformant colonies were obtained.

2.2.7. Construction of kanamycin-resistant strain

Monterio *et al*. previously showed that one of the longest intergenic regions in *R. pseudosolanacearum* GMI1000 was permissive site, that is, that integration of insertion elements into this interval did not affect viability or pathogenicity[40]. The *kan* gene cassette was inserted into the corresponding intergenic region of *R. pseudosolanacearum* MAFF106611 to generate a kanamycin-resistant strain for use in competitive tomato colonization assays. For this purpose, suicide plasmid pINkanR was constructed. PCR using primer pairs TBSUf/TBSUr and TBSDf/TBSDr was conducted to amplify 0.8-kb and 1.2-kb regions from the intergenic region, respectively. The amplified regions were digested with *Bam*HI+*Eco*RV and *Eco*RV+*Pst*I, respectively, and ligated with the

backbone of *Bam*HI-, *Pst*I-digested pK18*mobsacB* to obtain pTBS. The *kan* gene was amplified from pUC4K by PCR using the CLkanRf/CLkanRr primer pair, and the PCR product was ligated with the *Eco*RV-digested pTBS to generate pINkanR.

The chromosomal insertion of the *kan* gene in *R. pseudosolanacearum* MAFF106611 was conducted by transforming the strain with pINkanR and selecting for kanamycin resistance, and thereby selecting for a homologous double cross-over recombination event as described in section 2.2.4 (except that second selection was performed on CPG containing 6% sucrose and 40μg/ml kanamycin). One such transformant showing a growth rate compatible to that of the wild-type strain was selected and designated MFK.

2.2.8. Virulence assay

Fifty grams of quartz sand (grain size 0.1 to 0.3 mm) (Paint-works, Japan) was placed in each glass tube (35-mm inner diameter, 40-mm outer diameter, 120-mm length). The open end of the tube was plugged with a silicone resin stopper. The tube then was autoclaved for 15 min at 121˚C. PNS (plant nutrient solution)[41] was formulated as, 0.295 g/l $Ca(NO_3)_2 \cdot 4H_2O$, 0.126 g/l KNO_3, 0.123 g/l $MgSO_4 \cdot 7H_2O$, 0.136 g/l KH_2PO_4, and trace elements (in mg/l): FeEDTA, 46; $B_4Na_2O_7$ $10H_2O$, 3.78; $ZnSO_4$ $7H_2O$, 0.21; $CuSO_4$ $5H_2O$, 0.07; Na_2MoO_4 $2H_2O$, 0.023. Sterile PNS (12.5 ml) was added to each autoclaved sand column. Tomato (*Solanum lycopersicum* cv. Oogata-fukuju) seeds were sterilized by gentle shaking for 10 min in a solution of 8.75% (v/v) sodium hypochlorite supplemented with 0.1% (v/v) Tween 20 and then were washed six times for 15 min/cycle in sterile deionized water. To synchronize germination, sterile seeds were kept overnight at 4˚C in the dark. Seeds then were placed on petri dishes containing PNS solidified with

1.5% (w/v) agar and incubated in a climate-controlled growth chamber (Sanyo, Osaka, Japan) for 7 days at 28˚C with a 16 h:8 h light:dark cycle. Seven-day-old tomato roots were wounded by cutting 1 cm away from the base of the stem. Bacterial cells were grown for 20 h in RSM medium, centrifuged (3,300×*g*, 2 min), washed twice with sterile deionized water, and adjusted to 10^6 CFU/ml (OD_{600} = 0.001) in sterile deionized water.

For the sand-soak inoculation method, the wounded seedling was planted near one wall of the tube and 50 µl of cell suspension was inoculated near the opposite wall of the tube (distance between the seedling and the inoculation spot was 30 mm). For the root-dip inoculation method, the wounded seedling was dipped in cell suspension for 10 seconds and planted in the center of the tube. For both methods, the plant were maintained in a climate-controlled growth chamber (28˚C, 16 h:8 h light:dark cycle) for 7-10 days and observed daily.

2.2.9. Collection of tomato root exudate

Root exudate was prepared from tomato plant (*S. lycopersicum* cv. Oogata-fukuju). Tomato seeds were sterilized as described in section 2.2.8 and germinated on PNS agar plate by incubation in a climate-controlled growth chamber (28˚C, 16 h:8 h light:dark cycle) for 3 days. Root exudate was collected in a Magenta™ vessel GA-7 (Sigma-Aldrich, Saint Louis, USA), equipped with a perforated tray and filled with a volume of 80 ml of sterile Milli-Q water up to the tray. Forty 3-day-old germinated seeds were placed on the tray with their roots in the solution. After 10 days of growth in a climate-controlled growth chamber (28˚C, 16 h:8 h light:dark cycle), an aliquot of exudate was taken directly from the Magenta™ vessel and tested for sterility on CPG and LB agar plates. The rest of the exudate was filtered to remove solid plant material, snap-frozen in

liquid nitrogen, and lyophilized; the resting solid material was redissolved in 2.0 ml of Milli-Q water. This 40-fold concentrated exudate was stored at -20˚C until use. Only root exudate in which no microbial growth was detected was used.

2.2.10. Competitive plant colonization assay

Twenty grams of quartz sand (grain size 0.1 to 0.3 mm) (Paint-works, Japan) was put in each glass tubes (22-mm inner diameter, 25-mm outer diameter, 120-mm length). The open end of the tube was plugged with a silicone resin stopper. The tube then was autoclaved for 15 min at 121˚C. Sterile PNS (5 ml) was added to each autoclaved sand column. A germinated tomato seed obtained as described in section 2.2.9 was aseptically placed at the center of each growth tube at 5 mm below the surface of the quartz sand and then grown in a climate-controlled growth chamber (28˚C, 16 h:8 h light:dark cycle) for another 3 days. Bacterial cells were grown for 20 h in RSM medium, centrifuged (3,300×*g*, 2 min), washed twice with sterile deionized water, and adjusted to 10^7 CFU/ml (OD_{600} = 0.02) in sterile deionized water.

For the competitive colonization assay, 50 µL of 1:1 (v/v) mixture of the tested strain and the competitor (the kanamycin-resistant strain of *R. pseudosolanacearum* MAFF106611) was inoculated to the edge of each plant growth tube. The plant growth tubes were incubated in a climate-controlled growth chamber (28˚C, 16 h:8 h light:dark cycle). After 2, 4, and 6 days of incubation, each tomato seedling was homogenized and shaken vigorously for 10 min in 0.5 ml of sterile deionized water to suspend the bacteria. The bacterial suspension was diluted and plated on CPG agar plates with and without kanamycin.

Table 2.1. Bacterial strains used in chapter 2.

Strain	Relevant characteristic(s)[a]	Reference.
Ralstonia pseudosolanacearum		
Ps29	Wild-type strain; race 1, biovar 3, phylotype, isolated from tobacco	[42]
DPS01	Ps29 derivative; Δ*mcpA* (LC005226)	This study
DPS02	Ps29 derivative; Δ*mcp02* (LC005227)	This study
DPS03	Ps29 derivative; Δ*mcpT* (LC005228)	This study
DPS04	Ps29 derivative; Δ*mcp04* (LC005229)	This study
DPS05	Ps29 derivative; Δ*mcpC* (LC005230)	This study
DPS06	Ps29 derivative; Δ*mcp06* (LC005231)	This study
DPS07	Ps29 derivative; Δ*mcp07* (LC005232)	This study
DPS08	Ps29 derivative; Δ*mcp08* (LC005233)	This study
DPS09	Ps29 derivative; Δ*mcp09* (LC005234)	This study
DPS10	Ps29 derivative; Δ*mcp10* (LC005235)	This study
DPS11	Ps29 derivative; Δ*mcpB* (LC005236)	This study
DPS12	Ps29 derivative; Δ*mcp12* (LC005237)	This study
DPS13	Ps29 derivative; Δ*aer2* (LC005238)	This study
DPS14	Ps29 derivative; Δ*mcpM* (LC005239)	This study
DPS15	Ps29 derivative; Δ*mcp15* (LC005240)	This study
DPS16	Ps29 derivative; Δ*mcpP* (LC005241)	This study
DPS17	Ps29 derivative; Δ*mcp17* (LC005242)	This study
DPS18	Ps29 derivative; Δ*mcp18* (LC005243)	This study
DPS19	Ps29 derivative; Δ*mcp19* (LC005244)	This study
DPS20	Ps29 derivative; Δ*aer1* (LC005245)	This study
DPS21	Ps29 derivative; Δ*mcp21* (LC005246)	This study
DPS22	Ps29 derivative; Δ*mcp22* (LC005247)	This study
MAFF106611	Wild-type strain; race 1, biovar 4, phylotype I, isolated from eggplant	[42]
DMA01	MAFF106611 derivative; Δ*mcpA* (LC005224)	This study
DMF14	MAFF106611 derivative; Δ*mcpM* (LC005225)	This study
DMFcheA	MAFF106611 derivative; Δ*cheA* (LC005222)	This study
MFK	MAFF106611 derivative; Km^r	This study
Escherichia coli		
JM109	*recA1*, *endA1*, *gyrA96*, *thi-1*, *hsdR17* (r_k^- m_k^+), *e14*$^-$ (*mcrA*$^-$), *supE44*, *relA1*, Δ(*lac-proAB*)/F' [*traD36*, *proAB*$^+$, *lacI*^{q}, *lacZ* ΔM15]	[34]
S17-1	MM294 derivative, RP4-2 Tc::Mu-Km::Tn7; chromosomally integrated	[43]

[a] LC005222 and LC005224 to LC005247 in parenthesis indicate the accession no.

Table 2.2. Plasmids used in chapter 2.

Plasmid	Relevant characteristic(s)	Reference
Unmarked gene modification		
pK18*mobsacB*	Km^r pUC18 derivative, *lacZα*, mobs site, *sacB*	[36]
pNMPS01	pK18*mobsacB* with a 1.2-kb PCR fragment upstream of *mcpA* and a 1.1-kb PCR fragment downstream of *mcpA* from Ps29 genome; Km^r	This study
pNMPS02	pK18*mobsacB* with a 0.7-kb PCR fragment upstream of *mcp02* and a 1.1-kb PCR fragment downstream of *mcp02* from Ps29 genome; Km^r	This study
pNMPS03	pK18*mobsacB* with a 0.9-kb PCR fragment upstream of *mcpT* and a 1.2-kb PCR fragment downstream of *mcpT* from Ps29 genome; Km^r	This study
pNMPS04	pK18*mobsacB* with a 0.8-kb PCR fragment upstream of *mcp04* and a 0.6-kb PCR fragment downstream of *mcp04* from Ps29 genome; Km^r	This study
pNMPS05	pK18*mobsacB* with a 1.0-kb PCR fragment upstream of *mcpC* and a 0.8-kb PCR fragment downstream of *mcpC* from Ps29 genome; Km^r	This study
pNMPS06	pK18*mobsacB* with a 1.5-kb PCR fragment upstream of *mcp06* and a 1.8-kb PCR fragment downstream of *mcp06* from Ps29 genome; Km^r	This study
pNMPS07	pK18*mobsacB* with a 0.6-kb PCR fragment upstream of *mcp07* and a 0.7-kb PCR fragment downstream of *mcp07*from Ps29 genome; Km^r	This study
pNMPS08	pK18*mobsacB* with a 1.3-kb PCR fragment upstream of *mcp08* and a 1.0-kb PCR fragment downstream of *mcp08* from Ps29 genome; Km^r	This study
pNMPS09	pK18*mobsacB* with a 1.0-kb PCR fragment upstream of *mcp09* and a 1.3-kb PCR fragment downstream of *mcp09* from Ps29 genome; Km^r	This study
pNMPS10	pK18*mobsacB* with a 1.0-kb PCR fragment upstream of *mcp10* and a 1.2-kb PCR fragment downstream of *mcp10* from Ps29 genome; Km^r	This study
pNMPS11	pK18*mobsacB* with a 1.3-kb PCR fragment upstream of *mcpB* and a 1.1-kb PCR fragment downstream of *mcpB* from Ps29 genome; Km^r	This study
pNMPS12	pK18*mobsacB* with a 0.8-kb PCR fragment upstream of *mcp12* and a 1.3-kb PCR fragment downstream of *mcp12* from Ps29 genome; Km^r	This study
pNMPS13	pK18*mobsacB* with a 1.3-kb PCR fragment upstream of *aer2* and a 1.0-kb PCR fragment downstream of *aer2* from Ps29 genome; Km^r	This study
pNMPS14	pK18*mobsacB* with a 0.9-kb PCR fragment upstream of *mcpM* and a 0.6-kb PCR fragment downstream of *mcpM* from Ps29 genome; Km^r	This study
pNMPS15	pK18*mobsacB* with a 1.2-kb PCR fragment upstream of *mcp15* and a 1.1-kb PCR fragment downstream of *mcp15* from Ps29 genome; Km^r	This study
pNMPS16	pK18*mobsacB* with a 0.3-kb PCR fragment upstream of *mcpP* and a 0.8-kb PCR fragment downstream of *mcpP* from Ps29 genome; Km^r	This study
pNMPS17	pK18*mobsacB* with a 0.8-kb PCR fragment upstream of *mcp17* and a 0.7-kb PCR fragment downstream of *mcp17* from Ps29 genome; Km^r	This study

Table 2.2. (Continued)

Plasmid	Relevant characteristic(s)	Reference
pNMPS18	pK18*mobsacB* with a 1.6-kb PCR fragment upstream of *mcp18* and a 0.7-kb PCR fragment downstream of *mcp18* from Ps29 genome; Km^r	This study
pNMPS19	pK18*mobsacB* with a 0.9-kb PCR fragment upstream of *mcp19* and a 1.2-kb PCR fragment downstream of *mcp19* from Ps29 genome; Km^r	This study
pNMPS20	pK18*mobsacB* with a 0.9-kb PCR fragment upstream of *aer1* and a 0.6-kb PCR fragment downstream of *aer1* from Ps29 genome; Km^r	This study
pNMPS21	pK18*mobsacB* with a 1.1-kb PCR fragment upstream of *mcp21* and a 0.8-kb PCR fragment downstream of *mcp21* from Ps29 genome; Km^r	This study
pNMPS22	pK18*mobsacB* with a 1.0-kb PCR fragment upstream of *mcp22* and a 0.8-kb PCR fragment downstream of *mcp22* from Ps29 genome; Km^r	This study
pNMMF01	pK18*mobsacB* with a 1.2-kb PCR fragment upstream of *mcpA* and a 1.1-kb PCR fragment downstream of *mcpA* from MAFF106611 genome; Km^r	This study
pNMMF14	pK18*mobsacB* with a 0.9-kb PCR fragment upstream of *mcpM* and a 0.6-kb PCR fragment downstream of *mcpM* from MAFF106611 genome; Km^r	This study
pNMMFcheA	pK18*mobsacB* with a 0.8-kb PCR fragment upstream of *cheA* and a 0.9-kb PCR fragment downstream of *cheA* from MAFF106611 genome; Km^r	This study
mcp complementation		
pUCP18	*E. coli-Pseudomonas* shuttle vector derived from pUC18; *lac* promoter, *lacZ*; Cb^r	[39]
pKZ27	Broad-host-range transcriptional fusion vector; IncQ, *lacZ*; Km^r	[37]
pUC4K	Origin of *kan*; Km^r	[38]
pRCII	*E. coli-Ralstonia* shuttle vector derived from pKZ27; IncQ, *lac* promoter; Km^r	This study
pPS01	pRCII with a 2.1-kb PCR fragment including *mcpA* of Ps29	This study
pPS14	pRCII with a 2.0-kb PCR fragment including *mcpM* of Ps29	This study
MFK construction		
pTBS	pK18*mobsacB* with a 0.8-kb and 1.2 kb PCR fragment of longest intergenic region from MAFF106611 genome; Km^r	This study
pINkanR	pTBS with 1.0-kb PCR fragment including kanamycin-resistant gene from pUC4K; Km^r	This study

Table 2.3. Oligonucleotides used in chapter 2.

Oligonucleotide	Sequence (5’ to 3’)[a]
Unmarked gene modification	
NMRS01Uf	ATTGGATCCCTCCTCAGTACAGGACCAC
NMRS01Ur	ATAGAATTCACGTTTGCTGTGCCTACCC
NMRS01Df	ATGAATTCATCAACGAGAGCAGCAAGAAG
NMRS01Dr	ATTAGTCGACCGCTCAACCTCAAGACGAATG
NMRS02Uf	AGAATTCCGCGATCTGTTTCTTACCAC
NMRS02Ur	ACTCGAGCTACGGACTGTCTATCGGCAAC
NMRS02Df	ACTCGAGCTGGGAAACCTTCTGAACCGTC
NMRS02Dr	AGGATCCAGCGTTCTCGGAGTTGTTGGTG
NMRS03Uf	AGAATTCGCTCGATCAATGCGTCCTC
NMRS03Ur	ACTCGAGAAGCGTTCCACAGTTGTCTCC
NMRS03Df	ACTCGAGATCTGTCTGTGCAGGTGAGG
NMRS03Dr	AGGATCCAGGTGGAAAGCTGGGACAAG
NMRS04Uf	AAGAATTCGCCTGTGGCCGAAGGGCATC
NMRS04Ur	GACATATGGGGATTCCGTAGAGACGACTGTC
NMRS04Df	AACATATGCGGGCATCGCGCATCGTGTG
NMRS04Dr	AAAGCTTTTCGCACCGACGCAGGGTC
NMRS05Uf	AGAATTCGAAGATGCCCACAACCTG
NMRS05Ur	ACTCGAGATCGGTAGCCCGTTCTCAAAC
NMRS05Df	ACTCGAGCCGCCAAAGAGATCAAGGAG
NMRS05Dr	AGGATCCGATCATGAAGGAAGGGCTGAAC
NMRS06Uf	ATTGGTCGACGTTGGCGTTGCACAAAGG
NMRS06Ur	AACAGATCTTGTGCAAAGAAACGAGGAAAG
NMRS06Df	AACAGATCTCATGCTACGATGCCTCAACTC
NMRS06Dr	TTCCGAATTCTTGTCTCCTCCCACCCTTTC
NMRS07Uf	ATGGATCCTCTCTCCGCCAGGAATACAAG
NMRS07Ur	ATCTCGAGGTGATTGGTTTGGGTGGTC
NMRS07Df	ATCTCGAGGATTGCCTTCCAGACCAAC
NMRS07Dr	ATTCTGCAGCTGTCGCACGATGTGTATTTCC
NMRS08Uf	AGAATTCGCAGCACCGTATCAGCACTC
NMRS08Ur	ATCTAGATTAATGGAGCGGCGCAAAG
NMRS08Df	ATCTAGATGAACCAGATGGACGAGGTGAC
NMRS08Dr	ATAAGCTTCACTGTGCGTAGGCTTGCAG
NMRS09Uf	GATCTAGACCGGCGTGCTCAACATGAACG
NMRS09Ur	AGGCCTGCAGGGGGGCGTTTTCGGATGATCG
NMRS09Df	GGCCCTGCAGCTCGATGGATGAGGTGACGCAG

Table 2.3. (Continued)

Oligonucleotide	Sequence (5’ to 3’)[a]
NMRS09Dr	GTCTAAGCTTTGGTCGCCCTGGCAGCCTTC
NMRS10Uf	AGAATTCGCCAACGAAATAGGCATGAAAG
NMRS10Ur	ATCTAGAGGGCTCATCAAGTCAGCAAAG
NMRS10Df	ATCTAGACCGCATCGTTCAACACCTTC
NMRS10Dr	ATAAGCTTGTCTTCCGTACGCCCTTCTTC
NMRS11Uf	TACTGGAATTCGTTCACGCTGGCTGTGCTTC
NMRS11Ur	CGTTCTCTAGACTTTCTTGAGTGACGCGCTAAGG
NMRS11Df	GCTAATCTAGACCGCAGGCAACAAGAAGAGC
NMRS11Dr	TACATAAGCTTGCAATGGGCATGCCAATAATC
NMRS12Uf	GAGAATTCCCGCGCGCAGATGTTTAACCC
NMRS12Ur	CGATCTAGAAGGACCCTCTTGTCTTGTCGATGC
NMRS12Df	GACTCTAGAGCAGGACATCGCAGACGGTGAC
NMRS12Dr	CTGAAAGCTTCAGGCCGACGATCAGCAGTGC
NMRS13Uf	ATGAATTCATCTTCAACCGCACACAAG
NMRS13Ur	ACTCTAGACAAAGCGGGTGTTCCTC
NMRS13Df	ACTCTAGAGCCTTCCAGACCAACATCCTC
NMRS13Dr	ATTAAGCTTACCATCGCGGTCAACGTATC
NMRS14Uf	TAGGGATCCGATGAGCGGGTTTGGTTG
NMRS14Ur	TTGGAATTCGGCGGCTTGAAGTGCTTAG
NMRS14Df	TTAGAATTCCTGACGGTGCGATAAACC
NMRS14Dr	GGTTGTCGACGGCGATCACTGACGATGCAC
NMRS15Uf	AGAATTCTTGTCCGAATAAAGTTACGAAGCAC
NMRS15Ur	ATCTAGAGCACTTCTTGAGCGGGTTTG
NMRS15Df	ACTCTAGATAGGCCGCGATCATGTCTG
NMRS15Dr	ATTAAGCTTGTGCGTTTGGAGGTGAGG
NMRS16Uf	ATGAATTCATGCCGAATGCCTTGATGAC
NMRS16Ur	ATCTCGAGGAAGACAGCCAGAACGAAGAG
NMRS16Df	ACTCGAGATGAAGCCGTCACGCAGATG
NMRS16Dr	AGGATCCGGTGTCCCAGGTGAAGTCAAG
NMRS17Uf	AGAATTCCAGAAGAATCGCAGGATGG
NMRS17Ur	ACTCGAGCGACGCTGGAAACCTGAAGAG
NMRS17Df	ACTCGAGCACGCAGATGGACGAGGTTAC
NMRS17Dr	AGGATCCTTCCCTGATGCCTTTCGTC
NMRS18Uf	GAAAGCTTGTGGATGACGCGCTTGTCCAG
NMRS18Ur	GACATATGGCTTTCCTCCAAGGTGTCTTTCGTG
NMRS18Df	GACATATGGGCTGTGGGTGACGGAAAAAGAAC

Table 2.3. (Continued)

Oligonucleotide	Sequence (5' to 3')[a]
NMRS18Dr	CCGAATTCCGCAATTCCGCAGATGTCGGG
NMRS19Uf	ATGAATTCATGAAGAACTGCACGAACAGGAC
NMRS19Ur	ATCTCGAGAATGACCGATACGCCACCAC
NMRS19Df	ATCTCGAGTGAACCAGATGGACGAGGTGAC
NMRS19Dr	ATGGATCCGGCTACGAACTGGTGTGCTC
NMRS20Uf	ATGAATTCTGCCGGTCCGTCTATACCTG
NMRS20Ur	ATCTCGAGCGGCGAAACATCAAGCAAC
NMRS20Df	ATCTCGAGAAATCCGCCGATCCTTCTG
NMRS20Dr	ATGGATTCATCACCGAGGTGTGGTACTG
NMRS21Uf	ATTAGTCGACATCTGGAATGTCCGCAACC
NMRS21Ur	ATTAGATCTGCCTTGTAGCCGTTGTTCTTG
NMRS21Df	TTCAGATCTCGCAGTGCTGTTGCTGTAAAC
NMRS21Dr	AGCCTGCAGAGAAAGACCTGTCGCACACC
NMRS22Uf	ATGAATTCGAACGGAACATCACCTACTCAATC
NMRS22Ur	ATCTCGAGGACTTGGCGAGAAACATCC
NMRS22Df	ATCTCGAGATTGCATTCCAGACCAACATCC
NMRS22Dr	ATGGATCCGCACACCACAAACACACACGAG
NMRScheAUf	AACCTTCTAGAGGTCGGTTAATGCGTGGAC
NMRScheAUr	TACTGGAATTCGGCTACAGCAACTGGGAAC
NMRScheADf	TACATAAGCTTCATAGGTCGCCTGCACAC
NMRScheADr	GGTAGTCTAGATCGCCTGAACGGAACATCAC
pRCII construction	
RCIIoriVf	ATTACCGCGGCACTCCCGTACTAACTGTCACGAA
RCIIoriVr	GGCCATATGGAGCAGAAGAGCATACATCTGGAAGC
RCIIMCSf	TAACATATGAAGCTTGCATGCCTGCAGGTCG
RCIIMCSr	AGACATATGTGCGTTATCCCCTGATTCTGTGGA
CLkanRf	GTAAGACATATGCGGGAAGATGCGTGATCTG
CLkanRr	ATTACCGCGGGGAAAGCCACGTTGTGTCTC
Gene cloning for sequencing or complementation analysis	
CLRS01f	CTATGAATTCATTTCCAGGCGATGGCGGCTTTG
CLRS01r	CATAGGATCCCGGTCGCCACCTGAACTGAAACC
CLRS02f	CATAGGATCCCGCGCAAGTTGCCGATAGACAGTC
CLRS02r	CAGATCTAGACAGGAAGCGTTCCACAGTTGTCTCC
CLRS03f	CAGATCTAGAGATGCCGACTGGGAAACCTTCTG

Table 2.3. (Continued)

Oligonucleotide	Sequence (5' to 3')[a]
CLRS03r	GTCTAAGCTTCTGGACGTGCTCTACCGGAACATG
CLRS04f	CTATGAATTCGTGAGGCGTTAAGTAGCCGATAAGG
CLRS04r	CATAGGATCCCGATATGCACCCTATGCACACGATG
CLRS05f	CTATGAATTCGGCTCAAGTTTGAGAACGGGCTACC
CLRS05r	CATAGGATCCCATATCGCGCAGGCGTACTGGAAC
CLRS06f	ATGTGAATTCCGCCTTCATCCTGTCAACTAATACG
CLRS06r	TTCTGGTACCCGAAACAAGAGTTGAGGCATCGTAG
CLRS07f	CTATGAATTCCGCAACCTGGTCCTCGTGATCAAG
CLRS07r	CATAGGATCCGCGGTCAGCGTGTACTACATCTTCG
CLRS08f	CTATGAATTCGTGGGCAAGACAAGTGGAGAAAGC
CLRS08r	CATAGGATCCGGTTGCGCTCGGGCATGATAATTTC
CLRS09f	TTCTGAATTCGCGCAGCATGTGGAGTTGGCATG
CLRS09r	TAATCTGCAGCCAAGATGCTGCTCAAGCCGCTG
CLRS10f	TTATGAATTCCGTCGTGCCCTGTTCTTTGCTGAC
CLRS10r	AATCGGATCCTGTTCCACCGCGTGGATGTCGAC
CLRS11f	ATGAATTCTAGCGCGTCACTCAAGAAAGG
CLRS11r	ATGGATCCAAGACATGGAAGCCAAGCTG
CLRS12f	CTATGAATTCGATGGGAAATCCATGCCGTCACTC
CLRS12r	CATAGGATCCGGCGGAAGATGGATGATGCATGAG
CLRS13f	TAATGAATTCGATCTCCATCAAATCCCGCCACG
CLRS13r	TTTCGGATCCGCAGGGCTATTACTTCTCCGAGC
CLRS14f	CTATGAATTCCGGTGCCGTACTAAGCACTTCAAGC
CLRS14r	CATAGGATCCGTCAGGCAATACAGCACTGGAGACC
CLRS15f	TTTAGAATTCGGCGGCGAATCTTCAACTATCTTC
CLRS15r	TTCTGGTACCCTATGCATGGACAATGGCTGCATC
CLRS16f	ATGAATTCAGCGGCACTAAAGGTGTGG
CLRS16r	ATGGATCCAGCGCATTGCCTACGAGTC
CLRS17f	TTTAGAATTCCACCTATTGGAGGTGTTCCGCATCG
CLRS17r	TTTACTGCAGGAGATGAACGGCGGAGCGTGATG
CLRS18f	TTTAGAATTCGTTTCATTGCCTCCAGCCCGATAG
CLRS18r	TTCTAGATCTCATGAACAAGGCCGGCGATATTTG
CLRS19f	TTTAGAATTCCGATATGTCCTTCTGGAGCAGCACG
CLRS19r	TTTCGGATCCGATGTCATCCAGGGCTACCTGCTG
CLRS20f	TTTAGAATTCGACCCGCGGGACTTAATCAAGCATG
CLRS20r	TTTCGGATCCGGTTATGGTGCGATACAGCATCG
CLRS21f	CTATGAATTCCGTGATGTCTCTCTCTTTGAAGCTG

Table 2.3. (Continued)

Oligonucleotide	Sequence (5’ to 3’)[a]
CLRS21r	CATAGGATCCGGAGAAAGAGACACCGTTAGTTGC
CLRS22f	TTTCGAATTCACCGAGCGACACAACGAAC
CLRS22r	TAACGGATCCCACCACAAACACACACGAGAG
CLRScheA	CACAACGATGGCAAGGACAC
CLRScheA	ATCGCGTGTTTCTTGACTT
MFK construction	
TBSUf	ATTGGATCCTAAGTCTGTGACGGTGGAGTGAGG
TBSUr	ATTGATATCTCGTTGCCATGATGCGATTTG
TBSDf	ATTGATATCGACATTGGTGGTTGCTATGGAG
TBSDr	ATTCTGCAGCTCAGTACGTGGTCTGCGATG
CLkanRf	GTAAGACATATGCGGGAAGATGCGTGATCTG
CLkanRr2	ATGATGCATATGGGAAAGCCACGTTGTGTCTC

[a] Underlined sequences indicate restriction enzyme sites.

Table 2.4. PCR primer pairs and restriction enzymes used in construction of plasmids for unmarked gene modification.

Target gene	DNA fragment or vector	PCR primer		Restriction enzymes	Resulting Plasmid
		forward	reverse		
mcpA	Upstream	NMRS01Uf	NMRS01Ur	*Bam*HI, *Eco*RI	pNMPS01,
	downstream	NMRS01Df	NMRS01Dr	*Eco*RI, *Sal*I	pNMMF01
	pK18*mobsacB*	-	-	*Bam*HI, *Sal*I	
mcp02	Upstream	NMRS02Uf	NMRS02Ur	*Eco*RI, *Xho*I	pNMPS02
	downstream	NMRS02Df	NMRS02Dr	*Xho*I, *Bam*HI	
	pK18*mobsacB*	-	-	*Eco*RI, *Bam*HI	
mcpT	Upstream	NMRS03Uf	NMRS03Ur	*Eco*RI, *Xho*I	pNMPS03
	downstream	NMRS03Df	NMRS03Dr	*Xho*I, *Bam*HI	
	pK18*mobsacB*	-	-	*Eco*RI, *Bam*HI	
mcp04	Upstream	NMRS04Uf	NMRS04Ur	*Eco*RI, *Nde*I	pNMPS04
	downstream	NMRS04Df	NMRS04Dr	*Nde*I, *Hin*dIII	
	pK18*mobsacB*	-	-	*Eco*RI, *Hin*dIII	
mcpC	Upstream	NMRS05Uf	NMRS05Ur	*Xho*I	pNMPS05
	downstream	NMRS05Df	NMRS05Dr	*Xho*I, *Bgl*II	
	pK18*mobsacB*	-	-	*Sma*I, *Bgl*II	
mcp06	Upstream	NMRS06Uf	NMRS06Ur	*Eco*RI, *Bgl*II	pNMPS06
	downstream	NMRS06Df	NMRS06Dr	*Bgl*II, *Sal*I	
	pK18*mobsacB*	-	-	*Eco*RI, *Sal*I	
mcp07	Upstream	NMRS07Uf	NMRS07Ur	*Bam*HI, *Xho*I	pNMPS07
	downstream	NMRS07Df	NMRS07Dr	*Xho*I, *Pst*I	
	pK18*mobsacB*	-	-	*Eco*RI, *Sal*I	
mcp08	Upstream	NMRS08Uf	NMRS08Ur	*Eco*RI, *Xba*I	pNMPS08
	downstream	NMRS08Df	NMRS08Dr	*Xba*I, *Hin*dIII	
	pK18*mobsacB*	-	-	*Eco*RI, *Hin*dIII	
mcp09	Upstream	NMRS09Uf	NMRS09Ur	*Hin*dIII, *Pst*I	pNMPS09
	downstream	NMRS09Df	NMRS09Dr	*Pst*I, *Xba*I	
	pK18*mobsacB*	-	-	*Hin*dIII, *Xba*I	
mcp10	Upstream	NMRS10Uf	NMRS10Ur	*Eco*RI, *Xba*I	pNMPS10
	downstream	NMRS10Df	NMRS10Dr	*Xba*I, *Hin*dIII	
	pK18*mobsacB*	-	-	*Eco*RI, *Hin*dIII	
mcpB	Upstream	NMRS11Uf	NMRS11Ur	*Eco*RI, *Xba*I	pNMPS11
	downstream	NMRS11Df	NMRS11Dr	*Xba*I, *Hin*dIII	
	pK18*mobsacB*	-	-	*Eco*RI, *Hin*dIII	
mcp12	Upstream	NMRS12Uf	NMRS12Ur	*Eco*RI, *Xba*I	pNMPS12
	downstream	NMRS12Df	NMRS12Dr	*Xba*I, *Hin*dIII	
	pK18*mobsacB*	-	-	*Eco*RI, *Hin*dIII	

Table 2.4. (Continued)

Target gene	DNA fragment or vector	PCR primer		Restriction enzymes	Resulting Plasmid
		forward	reverse		
aer2	Upstream	NMRS13Uf	NMRS13Ur	*Bam*HI, *Eco*RI	pNMPS13
	downstream	NMRS13Df	NMRS13Dr	*Eco*RI, *Sal*I	
	pK18*mobsacB*	-	-	*Bam*HI, *Sal*I	
mcpM	Upstream	NMRS14Uf	NMRS14Ur	*Eco*RI, *Xho*I	pNMPS14,
	downstream	NMRS14Df	NMRS14Dr	*Xho*I, *Bam*HI	pNMMF14
	pK18*mobsacB*	-	-	*Eco*RI, *Bam*HI	
mcp15	Upstream	NMRS15Uf	NMRS15Ur	*Eco*RI, *Xho*I	pNMPS15
	downstream	NMRS15Df	NMRS15Dr	*Xho*I, *Bam*HI	
	pK18*mobsacB*	-	-	*Eco*RI, *Bam*HI	
mcpP	Upstream	NMRS16Uf	NMRS16Ur	*Eco*RI, *Nde*I	pNMPS16
	downstream	NMRS16Df	NMRS16Dr	*Nde*I, *Hin*dIII	
	pK18*mobsacB*	-	-	*Eco*RI, *Hin*dIII	
mcp17	Upstream	NMRS17Uf	NMRS17Ur	*Xho*I	pNMPS17
	downstream	NMRS17Df	NMRS17Dr	*Xho*I, *Bgl*II	
	pK18*mobsacB*	-	-	*Sma*I, *Bgl*II	
mcp18	Upstream	NMRS18Uf	NMRS18Ur	*Eco*RI, *Bgl*II	pNMPS18
	downstream	NMRS18Df	NMRS18Dr	*Bgl*II, *Sal*I	
	pK18*mobsacB*	-	-	*Eco*RI, *Sal*I	
mcp19	Upstream	NMRS19Uf	NMRS19Ur	*Bam*HI, *Xho*I	pNMPS19
	downstream	NMRS19Df	NMRS19Dr	*Xho*I, *Pst*I	
	pK18*mobsacB*	-	-	*Eco*RI, *Sal*I	
aer1	Upstream	NMRS20Uf	NMRS20Ur	*Eco*RI, *Xba*I	pNMPS20
	downstream	NMRS20Df	NMRS20Dr	*Xba*I, *Hin*dIII	
	pK18*mobsacB*	-	-	*Eco*RI, *Hin*dIII	
mcp21	Upstream	NMRS21Uf	NMRS21Ur	*Hin*dIII, *Pst*I	pNMPS21
	downstream	NMRS21Df	NMRS21Dr	*Pst*I, *Xba*I	
	pK18*mobsacB*	-	-	*Hin*dIII, *Xba*I	
mcp22	Upstream	NMRS22Uf	NMRS22Ur	*Eco*RI, *Xba*I	pNMPS22
	downstream	NMRS22Df	NMRS22Dr	*Xba*I, *Hin*dIII	
	pK18*mobsacB*	-	-	*Eco*RI, *Hin*dIII	
cheA	Upstream	NMRScheAUf	NMRScheAUr	*Eco*RI, *Xba*I	pNMMFcheA
	downstream	NMRScheADf	NMRScheADr	*Xba*I, *Hin*dIII	
	pK18*mobsacB*	-	-	*Eco*RI, *Hin*dIII	

Table 2.5. The *mcp* genes of *R. pseudosolanacearum* strains.

mcp No.	Gene of GMI1000[a]		Number of amino acids		Identity[b] (%)	Accession No.[c]
			GMI1000	Ps29		
01	RS_RS03035	(RSc0606)	600	600	100	LC005226
02	RS_RS05755	(RSc1155)	623	623	99	LC005227
03	RS_RS05760	(RSc1156)	600	600	99	LC005228
04	RS_RS06185	(RSc1234)	514	514	100	LC005229
05	RS_RS07350	(RSc1460)	513	513	99	LC005230
06	RS_RS09565	(RSc1894)	521	521	99	LC005231
07	RS_RS09805	(RSc1950)	329	329	99	LC005232
08	RS_RS13995	(RSc2799)	515	515	99	LC005233
09	RS_RS15755	(RSc3136)	661	661	99	LC005234
10	RS_RS16570	(RSc3307)	600	600	99	LC005235
11	RS_RS17100	(RSc3412)	515	515	99	LC005236
12	RS_RS03375	(RSc0671)	743	743	99	LC005237
13	RS_RS18385	(RSp0255)	529	529	99	LC005238
14	RS_RS19595	(RSp0507)	600	600	99	LC005239
15	RS_RS21140	(RSp0840)	518	518	99	LC005240
16	RS_RS18600	(RSp0303)	515	515	99	LC005241
17	RS_RS22085	(RSp1027)	524	524	99	LC005242
18	RS_RS22425	(RSp1099)	513	513	100	LC005243
19	RS_RS22970	(RSp1209)	522	522	99	LC005244
20	RS_RS23045	(RSp1224)	514	514	99	LC005245
21	RS_RS23695	(RSp1363)	543	543	99	LC005246
22	RS_RS23910	(RSp1406)	608	608	99	LC005247

[a] Locus tags in parenthesis indicate old locus tags.
[b] Identity between amino acid sequences of GMI1000 and Ps29 orthologs.
[c] Accession No. of the *mcp* genes of Ps29.

2.3 Results

2.3.1. Chemotactic reposes of wild-type strain to various compounds

It is important to select a strain that shows superior motility under chemotaxis assay conditions to effectively carry out chemotaxis research. Microscopic observations and swimming plate assays found that motility of *R. pseudosolanacearum* Ps29 was superior to that of *R. pseudosolanacearum* MAFF106611 (Fig. 2.3A, B). In addition, strain Ps29 shows stronger chemotactic response to aspartate than that of strain MAFF106611 (Fig. 2.3C). Although the genome sequence of *R. pseudosolanacearum* Ps29 has not been determined, I presumed that the *R. pseudosolanacearum* GMI1000 database could be used as a reference for identification of methyl-accepting chemotaxis protein genes (*mcp* genes) and chemotaxis-related genes, given that both strains GMI1000 and Ps29 belong to former *R. solanacearum* phylotype I, race 1,and biovar 3. To confirm my prediction, I performed PCR analysis of the Ps29 genome based on the GMI1000 sequence. *R.*

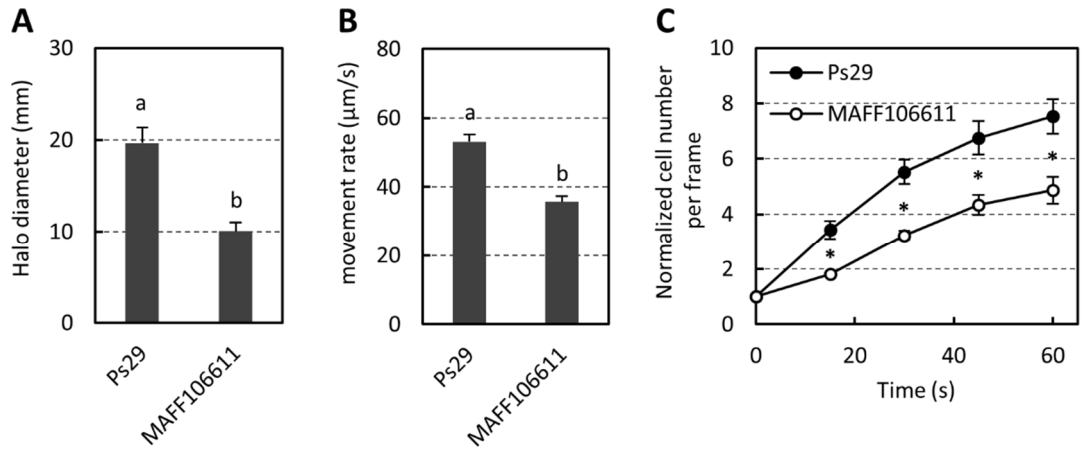

Fig. 2.3. Motility and chemotaxis of *R. pseudosolanacearum* Ps29 and MAFF106611. **A**, swimming assay in semi-solid agar plates. Bacterial cells were inoculated into semi-solid agar plates containing 1 g/l tryptone, 5 g/l KCl, and 3 g/l agar and incubated at 28˚C. After 3 days, halo diameter was measured. Vertical bars represent the standard errors of measurements done in six independent experiments. **B**, microscope observation. Bacterial cells were observed by microscope and movement rate of cells were measured. Vertical bars represent the standard errors of measurements done about 30 cells in three independent experiments. **C**, chemotaxis to 5 mM aspartate. Vertical bars represent the standard errors of measurements done at least in triplicate. Different letters or asterisks indicate statistically significant differences between Ps29 and MAFF106611 ($P < 0.05$ by Student's *t*-test).

pseudosolanacearum GMI1000 possesses 22 putative *mcp* genes. PCR using primers specific to each of 22 putative *mcp* genes in GMI1000 (Table 2.3, 2.4) and genomic DNA of Ps29 as a template yielded PCR products of sizes matching those predicted from the GMI1000 genome (data not shown). Furthermore, DNA sequencing confirmed that the amplified DNA fragments from the Ps29 genome contained open reading frames encoding proteins with more than 99% identity to the counterparts of GMI1000 MCPs (Table 2.5). These results demonstrated that Ps29 possesses homologs of 22 GMI1000 *mcp* genes. Thus, I selected *R. pseudosolanacearum* Ps29 as a model strain for further chemotaxis research.

To identify chemoattractants, I measured chemotactic responses of wild-type *R. pseudosolanacearum* Ps29 toward amino acids, organic acids, and sugars known to be major components of root exudate[44] by the computer-assisted capillary assay[35] (Fig. 2.4). In comparison with responses to a negative control (HEPES buffer), Ps29 showed significant responses to L-malate, citrate, fumarate, succinate, and all 20 standard amino acids except arginine, glycine, lysine, and proline ($P < 0.05$ by Student's *t* test). Ps29 also

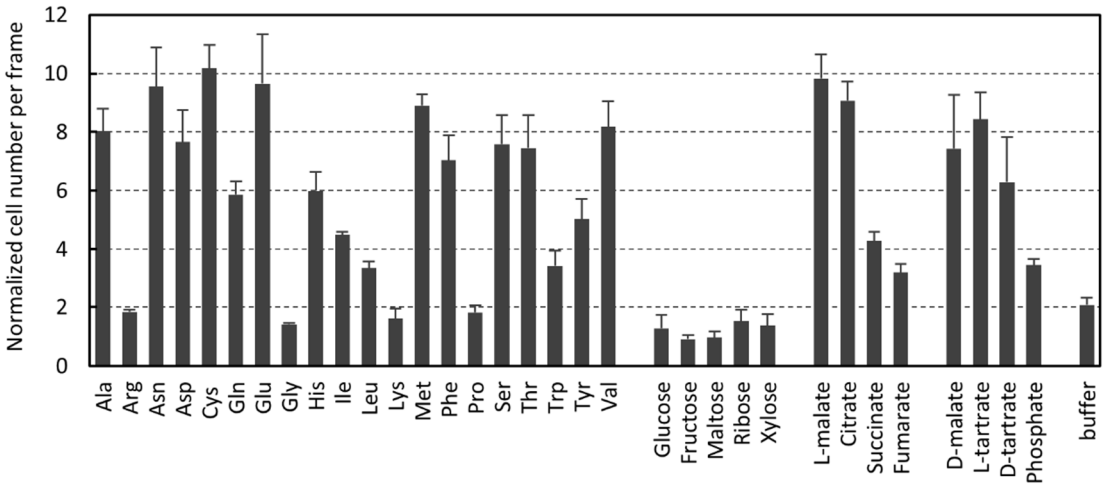

Fig. 2.4. Chemotactic responses to various compounds by *R. pseudosolanacearum* wild-type strain Ps29. Compounds were used at a concentration of 5 mM. Vertical bars represent the standard errors for measurements done at least in triplicate.

was attracted by growth substrates including inorganic phosphate and L-tartrate. However, this strain did not respond to any of the tested utilizable (glucose and fructose) or unutilizable sugars (maltose, ribose and xylose). Interestingly, Ps29 showed chemotactic responses to not only naturally-occurring L-malate and L-tartrate but also to D-malate and D-tartrate, which are a non-physiological isomer of malate and tartrate, respectively, and does not support growth of *R. pseudosolanacearum* Ps29 as a carbon and energy source (data not shown).

2.3.2. Identification of chemoreceptor for L-malate

To identify genes encoding MCPs for specific chemoattractants, I constructed a library of *R. pseudosolanacearum* Ps29 single mutants harboring unmarked deletions in each of the 22 *mcp* genes. I then attempted to identify a MCP for organic acids such as L-malate, citrate, succinate, and fumarate, which are major organic compounds contained in plant root exudate, by screening the library for mutants deficient in chemotactic response to these compounds (Fig. 2.5). However, all mutant showed responses to citrate, succinate, and fumarate comparable to that of the wild-type strain (Fig. 2.5B to D). In contrast to screening for MCPs involved in chemotaxis to these compounds, screening for L-malate MCP found that strain DPS14, a mutant deleted for a homolog of *R .pseudosolanacearum* GMI1000 RS_RS19595 (old locus tag RSp0507), showed significantly lower responses to L-malate than did wild-type Ps29 among 22 *mcp* single-deletion mutants ($P < 0.01$ by Student's *t* test) (Fig. 2.5A). The other 21 *mcp* single deletion mutants showed responses to L-malate comparable to that of wild-type Ps29. Introduction of plasmid pPS14, which harbors the Ps29 RS_RS19595 homolog, restored the ability of strain DPS14 to respond to L-malate (Fig. 2.6), demonstrating that the RS_RS19595 homolog encodes a MCP for

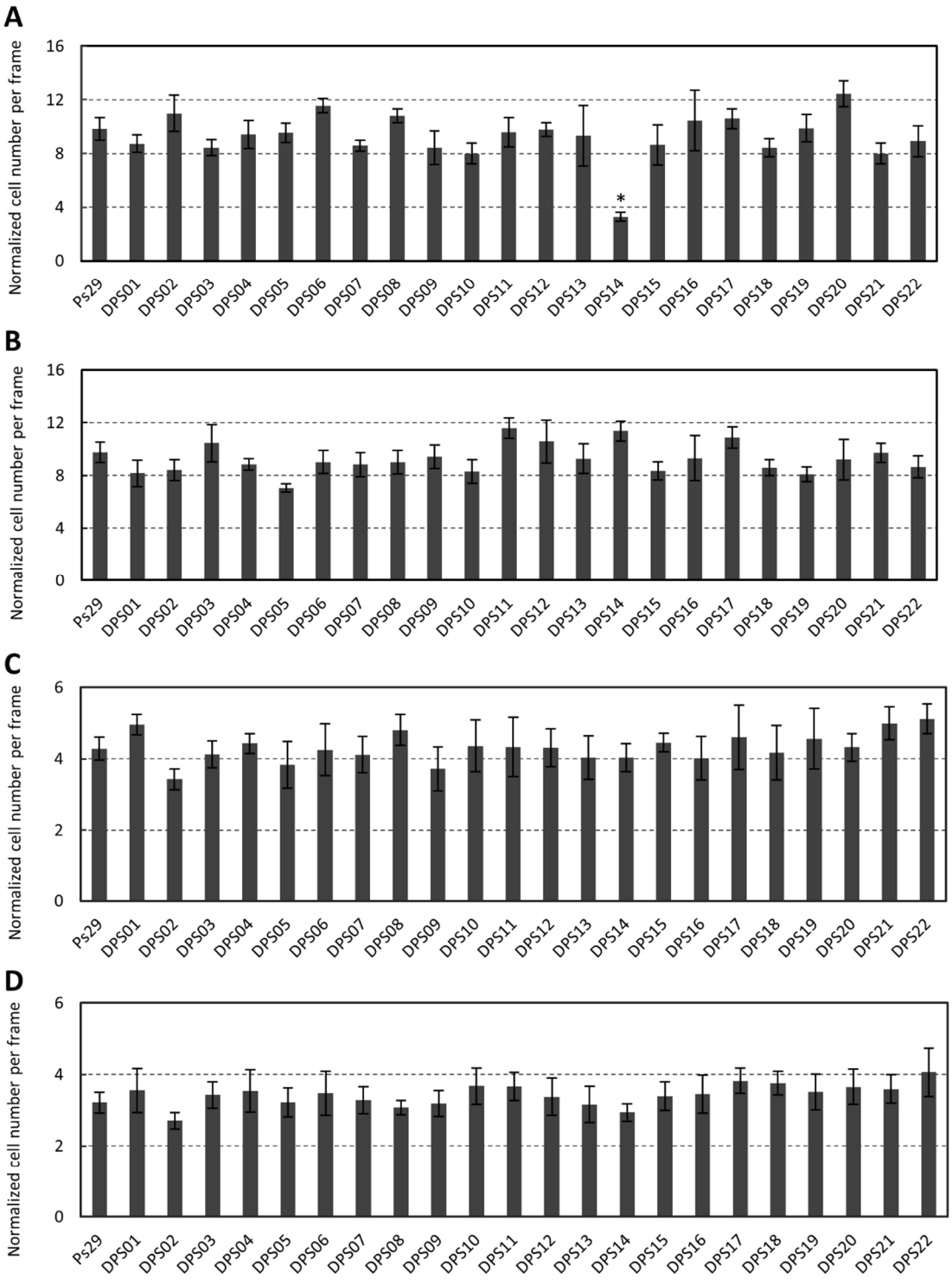

Fig. 2.5. Screening for organic acids MCPs using the library of 22 *mcp* single-deletion mutants of *R. pseudosolanacearum* Ps29. Chemotaxis to L-malate (**A**), citrate (**B**), succinate (**C**), and fumarate (**D**). Compounds were used at a concentration of 5 mM. Ps29, wild-type strain; DPS01 to DPS22, *mcp* single-deletion mutants. Vertical bars represent the standard errors for measurements done at least in triplicate. Asterisk indicates significant difference in chemotaxis between wild-type and *mcp* mutant ($P < 0.01$ by Student's *t* test).

L-malate. DNA sequencing revealed that the predicted RS_RS19595-homologous protein of Ps29 is 99% identical (596 in 600 amino acids overlap) to the GMI1000 RS_RS19595 protein (Table 2.5). I designated the RS_RS19595 homolog as *mcpM* (MCP for L-malate). The chemotactic responses of strain DPS14 toward citrate, succinate, and fumarate did not differ significantly in comparison to those of wild-type Ps29 (Fig. 2.5), suggesting that McpM is not involved in chemotaxis towards organic acids other than L-malate. This result does not necessarily rule out the ability of McpM to sense these organic acids, but I infer that McpM is the major MCP for L-malate in *R. pseudosolanacearum* Ps29.

McpM shows structural characteristics typical of MCPs: a positively charged N-terminus followed by a hydrophobic membrane-spanning region; a hydrophilic periplasmic domain; a second hydrophobic membrane-spanning region and a hydrophilic cytoplasmic domain[45]. Chemotactic ligands are known to bind to the periplasmic domains (ligand binding domains, LBDs) of MCPs, thereby initiating chemotactic signaling. The diverse ligand specificities among MCPs reflect amino acid sequence diversity of the LBDs. BLASTP analysis against the National Center for Biotechnology Information database using the putative LBD of McpM (155 amino acids; residues 33 to

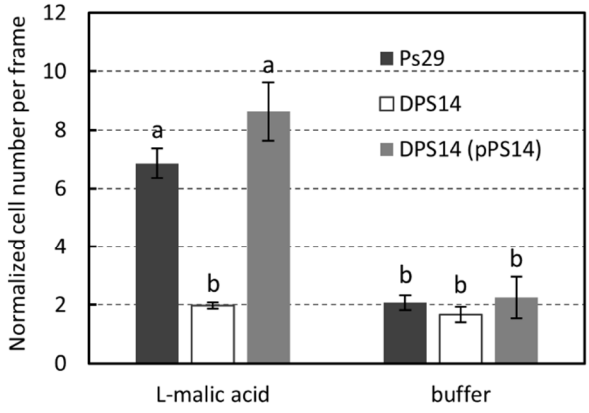

Fig. 2.6. Chemotactic responses to 0.5 mM L-malate by R. pseudosolanacearum Ps29 strains. Ps29, wild-type strain; DPS14, *mcpM* deletion mutant; DPS14 (pPS14), DPS14 harboring the complementing plasmid. Different letters indicate significant differences ($P < 0.05$ by Student's *t* test).

187) as a query sequence revealed that other strains of the *R. solanacearum* species complex and *Ralstonia pickettii* strains possess MCPs with LBDs highly similar to that of McpM (78-100% identity), while the MCPs of *Burkholderia* species such as *Burkholderia ambifaria* and *Burkholderia cenocepacia* shared up to 43% identity with the LBD of McpM. *P. putida* F1 McfS (Pput_4520)[46], *P. putida* KT2440 McpS (PP4658)[47], *P. aeruginosa* PAO1 McpS (PA2652)[48], and *P. fluorescens* Pf0-1 McpS (Pfl01_0728) and McpT (Pfl01_3768)[19] have been identified as MCPs for malate. However, I did not detect apparent similarity between the LBDs of these known MCPs for malate and that of *R. pseudosolanacearum* Ps29 McpM (data not shown).

2.3.3. Identification of chemoreceptor for amino acids

To identify a Ps29 MCP for amino acid(s), I also screened the mutant library for the ability to respond to leucine. Strain DPS01, a deletion mutant of a homolog of *R. pseudosolanacearum* GMI1000 RS_RS03035 (old locus tag RSc0606), was defective in chemotaxis to leucine (Fig. 2.7A). Other mutants strains showed responses to leucine comparable to that of wild-type Ps29. Out of the 16 amino acid attractants, strain DPS01 failed to respond to 12 amino acids and showed significantly lower responses to 4 amino acids (asparagine, aspartate, cysteine, and glutamine) than wild-type Ps29 ($P < 0.05$ by Student's *t* test) (Fig. 2.7B). The introduction of plasmid pPS01, which harbors the Ps29 RS_RS03035 homolog, restored the ability of strain DPS01 to respond to 16 amino acids (Fig. 2B), demonstrating that the RS_RS03035 homolog is a MCP for amino acids in *R. pseudosolanacearum* Ps29. I additionally noted that strain DPS01 harboring pPS01 showed significant chemotactic responses to arginine, lysine, glycine, and proline, amino

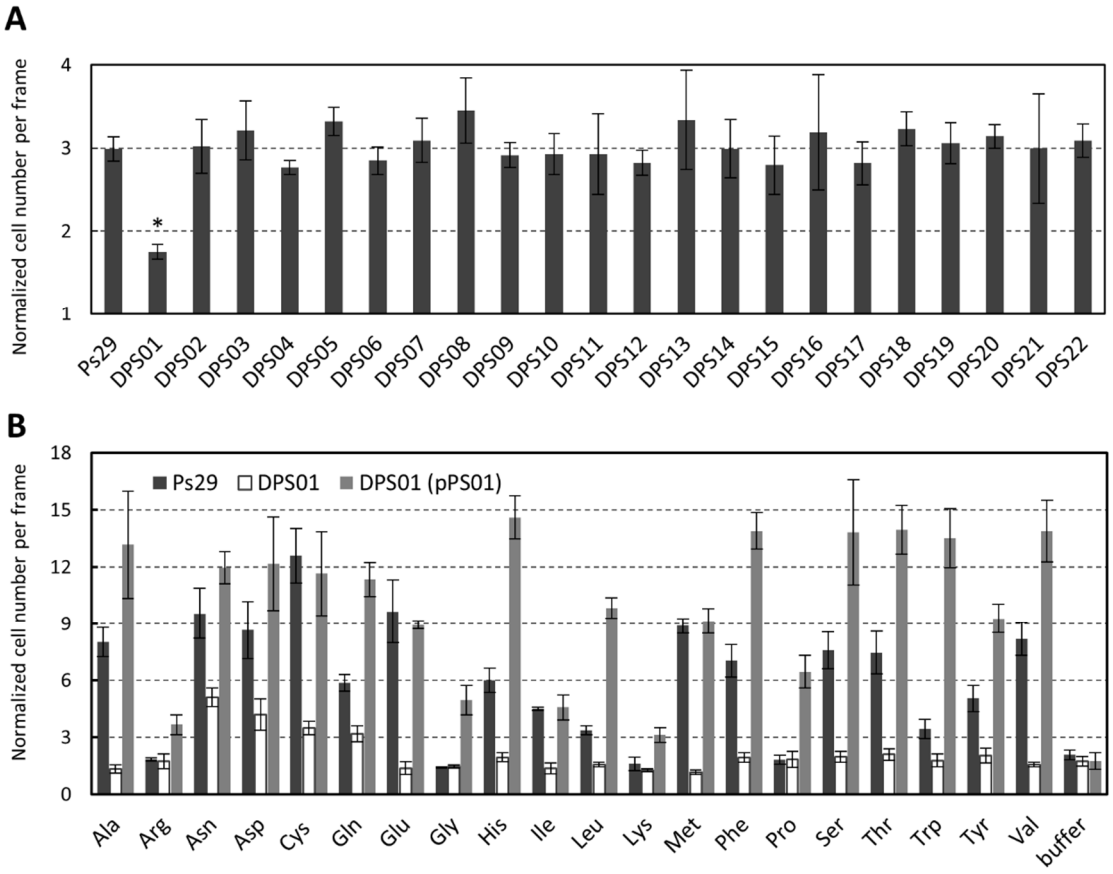

Fig. 2.7. Identification of amino acids MCP in *R. pseudosolanacearum* Ps29. **A**, chemotactic responses to 0.5 mM L-leucine by wild-type strain (Ps29) and 22 *mcp* single-deletion mutants (DPS01 to DPS22). Asterisk indicates significant difference in chemotaxis between wild-type and *mcp* mutant ($P < 0.05$ by Student's *t* test). **B**, chemotactic responses to 5 mM naturally occurring amino acids by wild-type strain (Ps29), *mcpA* deletion mutant (DPS01), and DPS01 harboring the complementing plasmid [DPS01(pPS01)]. Chemotactic responses to Asp and Cys were analyzed 1.5 min after initiation. There are significant differences in chemotaxis toward naturally occurring amino acids other than Arg, Gly, Lys, and Pro between the wild-type and DPS01 ($P < 0.05$ by Student's *t* test) and between DPS01 and DPS01 (pPS01) ($P < 0.05$ by Student's *t* test). Chemotactic responses to Arg, Gly, Lys, and Pro by DPS01 and DSP01 (pPS01) were significantly different ($P < 0.05$ by Student's *t* test). Vertical bars represent the standard errors for measurements done at least in triplicate.

acids to which wild-type *R. pseudosolanacearum* Ps29 did not respond, when compared to a response to HEPES buffer as a negative control ($P < 0.05$ by Student's *t* test) (Fig. 2.7B). I postulate that this effect is due to overexpression of the RS_RS03035 homolog in strain DPS01. The result suggests that the RS_RS03035 MCP has the potential to sense all 20 naturally-occurring amino acids. DNA sequence data revealed that the RS_RS03035 homologous protein from Ps29 is completely identical to GMI1000

RS_RS03035 protein (Table 2.5). I designated the RS_RS03035 gene as *mcpA* (MCP for amino acids).

Protein BLAST analysis revealed that, like McpM, MCPs with LBDs similar to that of McpA (239 amino acids, residues 49 to 287) are distributed in the *R. solanacearum* species complex and *R. pickettii* strains (80-100% identity) and *Burkholderia* species (up to 66% identity). The LBD of McpA showed 27% identity to that of *P. aeruginosa* PAO1 PctA (PA4309), a protein that is the major MCP for amino acids in that pseudomonad[49].

2.3.4. Identification of chemoreceptor/chemotaxis involved in plant infection

Although *R. pseudosolanacearum* Ps29 was used for chemotaxis assays, I noted that Ps29 yielded weaker virulence on tomato plants (Fig. 2.8). I therefore returned to *R. pseudosolanacearum* MAFF106611 for assessing the role of *mcpA* and *mcpM* in bacterial wilt disease on tomato. PCR analysis and DNA sequencing revealed that *R. pseudosolanacearum* MAFF106611 also possesses *mcpA* and *mcpM* homologs, the respective products of which are more than 99% identical to the *R. pseudosolanacearum*

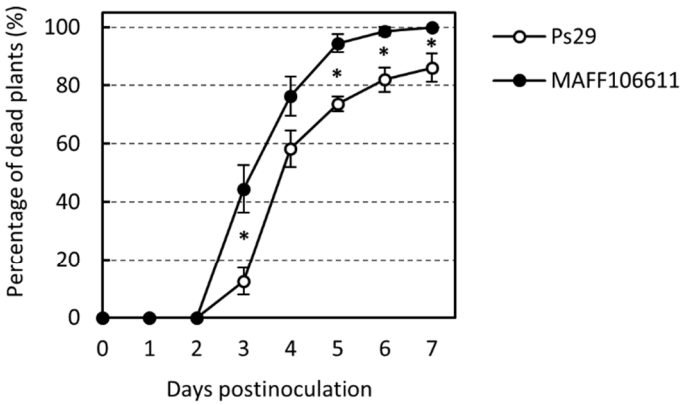

Fig. 2.8. Virulence of *R. pseudosolanacearum* Ps29 and MAFF106611. Bacterial cells were inoculated 7-day-old wounded tomato seedling by dipping root-tip into cell suspension. In each experiment, 8 tomato seedlings were examined and observed to calculate the percentage of dead plants. Means and standard errors were calculated from nine independent experiments. Asterisks indicate significant differences ($P < 0.05$ by Student's *t* test)

Ps29 counterparts. Unmarked *R. pseudosolanacearum* MAFF106611 *mcpA* deletion mutant (DMF01) and *mcpM* deletion mutant (DMF14) showed chemotactic phenotypes similar to those of *R. pseudosolanacearum* Ps29 *mcpA* and *mcpM* deletion mutants, respectively (Fig. 2.9). I also constructed an unmarked *R. pseudosolanacearum* MAFF106611 *cheA* deletion mutant (DMFcheA); as expected, this *cheA* mutant was nonchemotactic but motile (data not shown). I confirmed that there were no significant differences in growth in PNS medium supplemented with glucose between these mutants and wild-type MAFF106611 (data not shown), suggesting that these mutations did not affect the growth of *R. pseudosolanacearum* MAFF106611.

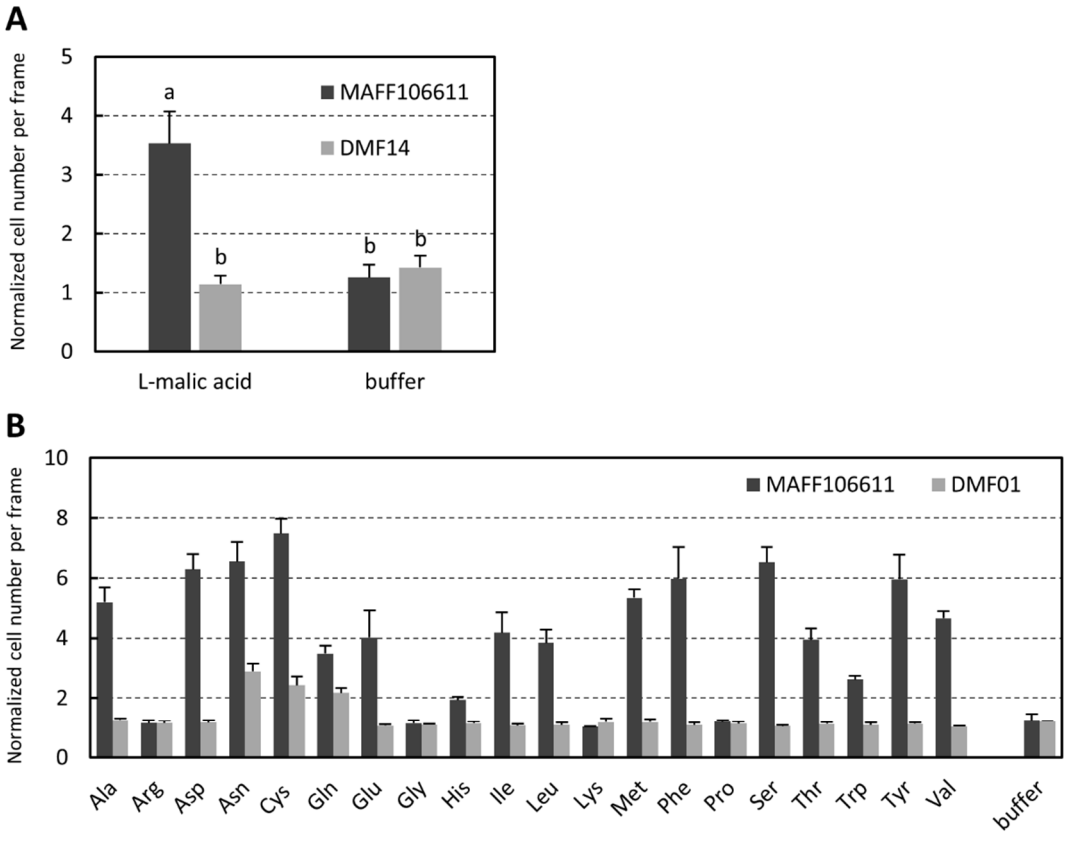

Fig. 2.9. Chemotactic responses to L-malate (A) and amino acids (B) by *R. pseudosolanacearum* MAFF1106611 strains. MAFF106611, wild-type strain; DMF14, *mcpM* deletion mutant; DMF01, *mcpA* deletion mutant. Videotape frames were analyzed at the initiation of observation and 2 min after initiation. Compounds were used at a concentration of 5 mM. Different letters indicate significant differences ($P < 0.05$ by Student's *t* test). There are significant differences in chemotaxis to amino acids other than Arg, Gly, Lys, and Pro between wild-type strain and DMF01 ($P < 0.05$ by Student's *t* test). Vertical bars represent the standard errors of measurements done at least in triplicate.

Virulence of the mutant strains was tested by the root-dip inoculation method. In this method, the root tips of 7-day-old tomato plants were cut and then challenged by root-dip inoculation with a cell suspension of *R. pseudosolanacearum* MAFF106611. Tomato plants inoculated with wild-type MAFF106611 started wilting 3 days postinoculation (dpi) and died by 7 dpi. The time line of wilting in response to mutant strains DMF01, DMF14, and DMFcheA was similar to that seen with the wild-type parent, indicating that neither *mcpA*, *mcpM*, or *cheA* were required for virulence when bacterial cells were directly introduced into tomato plants (Fig. 2.10A).

I then tested plant infection by the mutants using the sand-soak inoculation method. In this method, a bacterial cell suspension was inoculated into the sand at a spot about 30 mm away from a tomato plant. Plant infection by this assay requires bacterial cells to locate and invade host plants from a distance. Wild-type MAFF106611 yielded

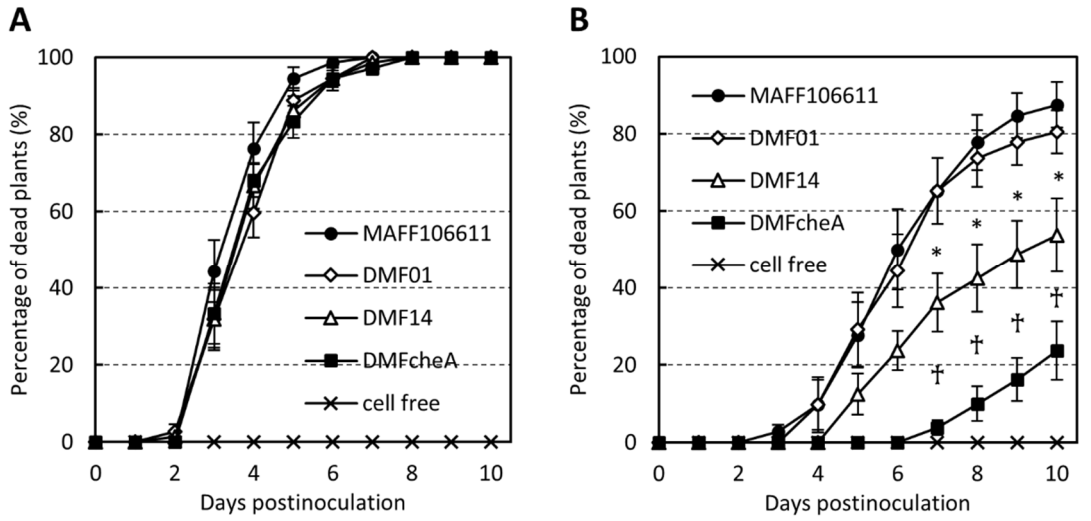

Fig. 2.10. Virulence of *R. pseudosolanacearum* MAFF106611 strains on tomato seedlings. MAFF106611, wild-type strain; DMF01, *mcpA* deletion mutant; DMF14, *mcpM* deletion mutant; DMFcheA, *cheA* deletion mutant. In each experiment, 8 tomato seedlings were examined and observed to calculate the percentage of dead plants. Means and standard errors were calculated from at least nine independent experiments. **A**, root-dip inoculation virulence assay. Bacterial cells were inoculated onto 7-day-old wounded tomato seedlings by dipping the root tip in a cell suspension. **B**, sand-soak inoculation virulence assay. Bacterial cells were inoculated -30mm away from 7-day-old wounded tomato seedlings. Asterisks and crosses indicate significant differences in the percentages of dead plants between the wild-type strain and DMF14 and between DMF14 and DMFcheA, respectively ($P < 0.05$ by Student's *t* test).

wilting at 4 dpi, killing 90% of tomato plants at 10 dpi, while strain DMFcheA was significantly less infectious (Fig. 2.10B). This result suggested that the virulence assay using sand-soak inoculation method permits evaluation of chemotactic effects on plant infection. Testing of the *mcp* mutant strains revealed that strain DMF14 was significantly less infectious than wild-type MAFF106611 ($P < 0.05$ by Student's *t* test), killing only 54% of tomato plants at 10 dpi in sand-soak inoculation virulence assays (Fig. 2.10B). The infectivity of strain DMF01 did not differ significantly from that the wild-type MAFF106611 (Fig. 2.10B). These results suggest that McpM-mediated chemotaxis is required for full virulence by *R. pseudosolanacearum* MAFF106611; in contrast, McpA-mediated chemotaxis to amino acids does not play a crucial role in initial location of plant roots by the bacterium in this sand-soak inoculation virulence assay. Notably, the infectivity of strain DMF14, though attenuated compared to the wild-type strain, remained significantly higher than that of strain DMFcheA ($P < 0.05$ by Student's *t* test).

2.3.5. Chemotactic responses to root exudate and competitive plant colonization.

The attenuated infectivity of *R. pseudosolanacearum* MAFF106611 DMF14 in the sand-soak inoculation virulence assay presumably reflected decreased ability of the mutant strain to locate tomato roots. To test this hypothesis, I evaluated the chemotactic responses of *R. pseudosolanacearum* MAFF106611 *mcp* mutants to tomato root exudate. Strain DMF14 showed significantly lower chemotactic response to root exudate than wild-type MAFF106611 ($P < 0.05$ by Student's *t* test); response did not differ significantly between DMF01 and wild-type parent (Fig. 2.11A). Similar effects were observed in comparisons between wild-type and mutant strains of the highly motile *R. pseudosolanacearum* Ps29 (Fig. 2.11B).

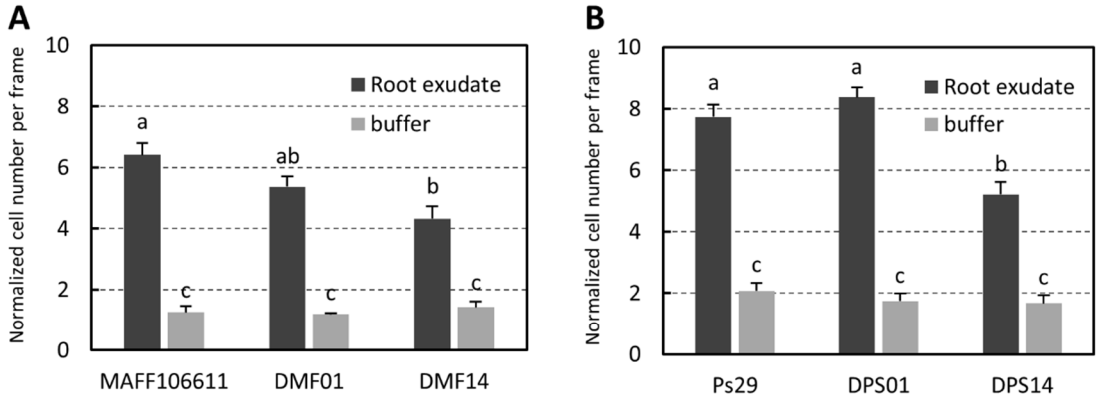

Fig. 2.11. Chemotactic responses to tomato root exudate by *R. pseudosolanacearum* MAFF106611 and Ps29 strains. The total organic carbon content of tomato root exudate used in this assay was 3.59 g-C/L. **A**, chemotaxis of MAFF106611 wild-type strain, *mcpA* deletion mutant (DMF01), and *mcpM* deletion mutant (DMF14). Videotape frames were analyzed at the initiation of observation and 2 min after initiation. **B**, chemotaxis of Ps29 wild-type strain, *mcpA* deletion mutant (DPS01), and *mcpM* deletion mutant (DPS14). Vertical bars represent the standard errors for measurements done at least in triplicate. Different letters indicate significant differences ($P < 0.05$ by Student's *t* test).

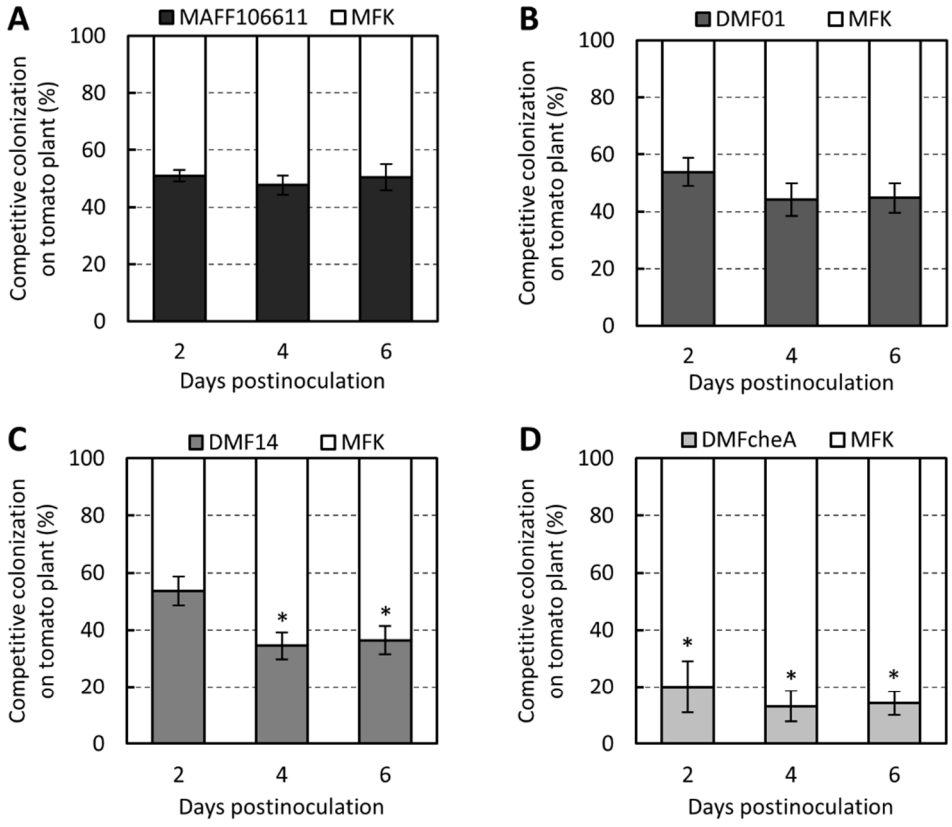

Fig. 2.12. Plant colonization assay for competition between the *R. pseudosolanacearum* MAFF106611 kanamycin-resistant strain (MFK) and wild-type strain MAFF106611 (**A**), *mcpA* deletion mutant (DMF01) (**B**), *mcpM* deletion mutant (DMF14) (**C**), or *cheA* deletion mutant (DMFcheA) (**D**). Tomato plants were sampled in at least six independent experiments conducted in triplicate per time point. Vertical bars represent the standard errors for measurements. Asterisks indicate statistically significant differences between MFK and mutants ($P < 0.05$ by Student's *t* test).

I further tested this hypothesis using competitive tomato colonization assays, specifically by inoculating tomato seedlings with a 1:1 mixture of a test and competitor strains. Because the *R. pseudosolanacearum* MAFF106611 kanamycin-resistant mutant (MFK) competed fully with wild-type strain MAFF106611 (Fig. 2.12A), I used MFK as the competitor strain in competitive plant colonization assays to distinguish the competitor strain from test strains. The results of the competitive plant colonization assays were consistent with those of virulence assays. Strain DMF14 as well as DMFcheA showed inferior plant colonization ability compared to MFK, while strain DMF01 fully competed with MFK (Fig. 2.12B to D).

2.4 Discussion

Genomic analysis revealed that *R. pseudosolanacearum* GMI1000 possesses 22 putative *mcp* genes (Table 2.5 for accession numbers of genome sequences). In the present study, I demonstrated that *R. pseudosolanacearum* Ps29 possesses homologs of all 22 *R. pseudosolanacearum* GMI1000 *mcp* genes. Complete genome sequences of *R. pseudosolanacearum* FQY 4 (formerly named *R. solanacearum* FQY4 [phylotype I]), *R. pseudosolanacearum* CMR15 (formerly named *R. solanacearum* CMR15 [phylotype III]), *R. solanacearum* CFBP2957 (phylotype IIA), *R. solanacearum* Po82 (phylotype IIB), and *R. syzygii* subsp. *indonesiensis* PSI07 (formerly named *R. solanacearum* [phylotype IV]) have been determined. Although these strains belong to different phylotypes, all the sequenced strains possess 21-23 putative *mcp* genes, of which 19-21 genes are homologs of the *R. pseudosolanacearum* GMI1000 *mcp* genes. Notably, the LBDs of nominally homologous MCPs exhibit more than 71% respective identity. Thus, *mcp* genes are conserved among the *R. solanacearum* species complex.

R. pseudosolanacearum Ps29 showed chemotactic responses to amino acids, dicarboxylic acids (malate, succinate, fumarate, and tartrates), tricarboxylic acid (citrate), and inorganic phosphate but any of the tested sugars. Yao and Allen previously reported the chemotactic responses of *R. solanacearum* K60 (phylotype IIB, isolated from tomato) to various plant-related organic compounds[20]. The response pattern of Ps29 is similar to that of K60, although there are minor differences. Specifically, Ps29 did not respond to arginine, glycine, lysine, and proline, while K60 was attracted by proline, glycine, and lysine but failed to respond to arginine, cysteine, histidine, threonine, and tryptophan. Additionally, Ps29 was attracted by succinate but K60 did not respond to succinate. Partial genome sequence of *R. solanacearum* K60 is available on the GenBank database. A BLAST search of this partial genome sequence detected the presence of a gene encoding McpA homolog (GenBank accession number CCF97014). The LBD of the putative *R. solanacearum* K60 McpA exhibits 93% identity to the *R. pseudosolanacearum* Ps29 and MAFF106611 McpA proteins (data not shown). Differences in patterns of chemotactic responses to 20 naturally occurring amino acids between Ps29/MAFF106611 and K60 may be attributed to differences in the amino acid sequence in LBDs of their respective McpAs. Yao and Allen measured chemotactic responses to 8 compounds, including sugars and organic acids, by eight different strains of the *R. solanacearum* species complex and found that the strains varied significantly in their attraction to these compounds[20]. Based on these results, those authors noted the possibility that chemotactic responses may be differentially selected traits that confer adaptation to various hosts or ecological conditions. Given that *mcp* genes are conserved among the *R. solanacearum* species complex, differences in expression patterns of a set of *mcp* genes may make a bigger contribution to diverse chemotactic responses among

the *R. solanacearum* species complex than diversity of MCPs. Therefore, comprehensive analysis of expression of a set of *mcp* genes is important to understand the chemotactic response pattern in each strain of the *R. solanacearum* species complex.

LBDs of bacterial MCPs can be classified according to their sizes into cluster-I (120 to 210 amino acids) and cluster-II (220 to 299 amino acids) domains[50]. The MCPs for amino acids in *E. coli* (Tar and Tsr) contain cluster-II LBDs with 4-helix-bundle (4HB) domains[51]. Ligand specificity of Tar and Tsr is relatively narrow, and these MCPs sense limited numbers of amino acids (Tar, aspartate and glutamate; Tsr, serine, alanine, and glycine)[52]. The PctA protein of *P. aeruginosa* PAO1, which senses as many as 18 naturally occurring amino acids[14], contains cluster-II LBD with a double-PDC (PhoQ/DcuS/CitA) domain [53,54]. *R. pseudosolanacearum* McpA, which is a MCP able to potentially sense 20 naturally occurring amino acids as shown here, also contains a cluster-II LBD with a predicted LBD size of 243 amino acids. Structure prediction by Phyre^2 program [55] indicated that the *R. pseudosolanacearum* McpA contains a double PDC domain in its LBD (Fig. 2.13). In contrast, the LBD of *R. pseudosolanacearum* McpM is classified as a member of cluster I, with a predicted LBD size of 153 amino acids. Phyre^2 structure analysis predicted the presence of 4-helix-bundle domain in the LBD of McpM (Fig. 2.13). Several MCPs have been reported as chemoreceptors for malate. These MCPs include *P. aeruginosa* PAO1 McpS (PA2652)[48], *P. putida* KT2440 McpS (PP4658)[47], *P. putida* F1 McfS (Pput_4520)[46], and *P. fluorescens* Pf0-1 McpS (Pfl01_0728) and McpT (Pfl01_3768)[19]. *P. aeruginosa* PAO1 McpS and *P. fluorescens* Pf0-1 McpT contain cluster-I LBDs with CACHE (Ca^{2+}channels and chemotaxis receptors) domains[56] while the LBDs of *P. putida* KT2440 McpT, *P. putida* F1 McfS, and *P. fluorescens* Pf0-1 McpS belong to cluster II and contain helical-bimodular (HBM)

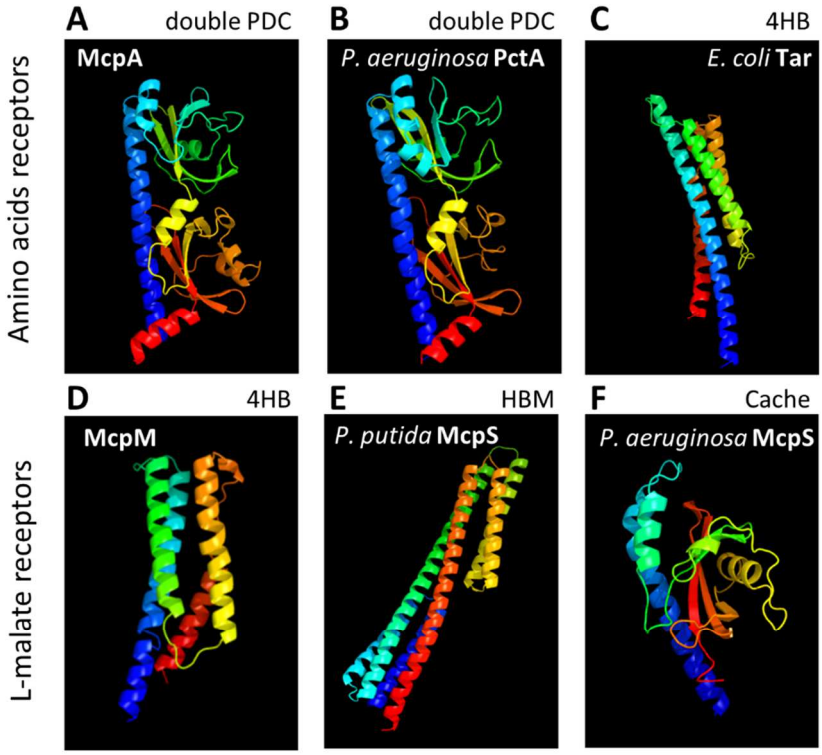

Fig. 2.13. The predicted three-dimensional (3D) structures of bacterial MCP LBDs. **A**, McpA LBD of *R. pseudosolanacearum* Ps29 and MAFF106611; **B**, PctA LBD of *P. aeruginosa* PAO1; **C**, Tar LBD of *E. coli*; **D**, McpM LBD of *R. pseudosolanacearum* Ps29; **E**, McpS LBD of *P. putida* KT2440; **F**, McpS LBD of *P. aeruginosa* PAO1. 3D structures of MCP LBDs were predicted by using Phyre^2 algorithm. Blue color, N-terminus; red color, C-terminus.

domains[57]. Thus, the LBD of *R. pseudosolanacearum* McpM contains a different type of domain compared to the LBDs of *Pseudomonas* MCPs for malate, consistent with the lack of observed sequence similarity between the LBDs of *R. pseudosolanacearum* McpM and *Pseudomonas* MCPs for malate.

Our results showed that nonchemotactic but motile mutant DMFcheA (*cheA* deletion mutant) displayed decreased infectivity to tomato plants in sand-soak inoculation virulence assays, and exhibited decreased tomato plant colonization in competitive plant colonization assays when compared to the wild-type parent. These data are consistent with those reported by Yao and Allen[20]. These results confirmed that taxis is involved in migration to plants in soils and in plant infection by the *R. solanacearum* species complex. Our assays also demonstrated decreased plant infection, attenuated colonization,

and weakened response to tomato root exudate by a *mcpM* deletion mutant (strain DMF14) when compared to the wild-type strain. These results indicate that in addition to Aer-mediated aerotaxis, McpM-mediated chemotaxis to certain components of root exudate is required for effective plant infection by the *R. solanacearum* species complex. Compared to the parent strain, the *mcpM* mutant showed decreased responses to malate, but was not altered in responses to other organic acids (succinate, fumarate, and citrate). Notably, malate has been reported to constitute a major component of tomato root exudate[44]. Therefore, it is highly likely that McpM-mediated chemotaxis to malate is involved in tomato plant infection by *R. pseudosolanacearum*. Although amino acids also were reported as major components of tomato root exudate[58], the *mcpA* deletion mutant (strain DMF01) was as infectious as the wild-type strain in sand-soak inoculation plant virulence assays and competed fully with the wild-type strain in competitive plant colonization assays. Since the response of the *mcpA* mutant to root exudate was as strong as that of the wild-type strain, it seems that the concentrations of amino acids in root exudate were too low to elicit strong chemotactic responses in *R. pseudosolanacearum*.

The DMFcheA had decreased infectivity compared to the *mcpM* mutant. This distinction may reflect the fact that the *cheA* mutant is also deficient in Aer-mediated energy taxis as well as chemotaxis[22]. Alternatively, root exudate component(s) other than L-malate may be involved in plant colonization and plant infection by *R. pseudosolanacearum*. Citrate, which is abundant in tomato root exudate [44] and is a strong attractant of *R. pseudosolanacearum*, is a likely candidate for such a component. However, analysis of 22 *mcp* single-deletion mutants cannot identified MCP for citrate, suggesting that citrate taxis is mediated by multiple receptors. Alternative approach to *mcp* single mutant library might be needed to identify MCP(s) for citrate.

CHAPTER3

Identification of chemoreceptors for citrate and its relationships with plant infection

3.1 Introduction

In chapter 2, I identified McpA and McpM as a chemoreceptor for amino acids and L-malate, respectively, and revealed that McpM-mediated L-malate taxis is required for the early stage of plant infection in *R. pseudosolanacearum*. Furthermore, comparison infectivity of *mcpM* mutant and that of *cheA* mutant, which is nonchemotactic but motile, suggested that chemotaxis other than L-malate taxis may be important for locating plant roots when the *R. solanacearum* species complex infect plants. Although our research group also successfully identified McpT as a chemoreceptor for L-tartrate, one of component of root exudate[24], by using the library of Ps29 *mcp* single-deletion mutants, virulence assay and competitive colonization assay using the *mcpT* deletion mutant showed that McpT-mediated chemotaxis, possibly reflecting chemotaxis to L-tartrate, dose not facilitate this pathogen motility to tomato roots [59].

Citrate is known as a major component of plant root exudate. There are several studies reported that citrate is the most abundant organic acid in root exudate[44,60]. It is therefore possible that citrate taxis plays an important role for plant-associated bacteria that locate roots by sensing root exudate, including the *R. solanacearum* species complex.

In several bacteria, chemotaxis to citrate and its receptors has been reported, which are Tcp of *S. enterica* serovar Typhimurium[61], McpS and McpQ of *P. putida* KT2440[46,47], McfS and McfQ of *P. putida* F1[46], and MCP2201 and MCP2901 of *Comamonas testosteroni* CNB-1[62,63]. The *R. solanacearum* species complex also shows strong response to citrate. I therefore tried to identify citrate MCP(s) by using the library

of *mcp* single-deletion mutants in previous chapter, but it resulted in failure, suggesting that multiple MCPs are involved in citrate taxis. In this chapter, I constructed another *mcp* mutant library of *R. pseudosolanacearum* Ps29 to identify citrate MCP(s) and analyzed on citrate taxis and its involvement in plant infection.

3.2 Experimental procedures

3.2.1. Bacterial strains, plasmids, and growth conditions

Bacterial strains and plasmids used in this chapter are listed in Table 3.1 and Table 3.2, respectively. *R. pseudosolanacearum* Ps29 and MAFF106611 were used for chemotaxis research and tomato plant assay, respectively. *E. coli* strains JM109 and S17-1 were used for plasmid construction and transconjugation, respectively. Each strains were grown as described in section 2.2.1.

3.2.2. DNA manipulation

Standard procedures were used for plasmid DNA preparations, transformations of *E. coli*, and agarose gel electrophoresis[34]. PCR, restriction enzyme digestions, and ligation reactions were conducted using KOD FX Neo polymerase (Toyobo, Osaka, Japan), FastDigest (Thermo Fisher Scientific, Massachusetts, USA), and Ligation High Ver.2 (Toyobo, Osaka, Japan), respectively, according to the manufacturer's instructions. Primers used for PCR are listed in Table 3.3.

3.2.3. Chemotaxis assay

Chemotaxis responses were measured by computer-assisted capillary assays as described in section 2.2.3. In this chapter, all measurements of *R. pseudosolanacearum* Ps29 strains

were started at 40 to 80 cells per frame.

In measurements of chemotaxis to citrate/metal^{2+} complexes, all tested compounds (citrate, magnesium chloride, calcium chloride, and L-alanine as control) were adjusted pH to 7.0 by 5 N NaOH, and cell suspension was supplemented with 1 mM magnesium chloride or calcium chloride just before the beginning of each measurements to prevent dissociation of citrate/metal^{2+} complex diffused out of the capillary mouth.

3.2.4. Construction of multiple *mcp* deletion mutants

Twenty two *mcp* genes of *R. pseudosolanacearum* Ps29 were deleted one by one by repeating unmarked-gene-deletion process described in section 2.2.4 to obtain a total-chemoreceptor-deletion mutant, strain POC22. The order of *mcp* deletion and plasmids used for construction of POC22 were listed in Table 3.4. Derivatives of suicide plasmid pK18*mobsacB*, which have been constructed in chapter 2, were used for deletion of *mcp* genes other than *mcpT*. Because *mcpT* and homolog of RS_RS05755 (old locus tag RSc1155) lie next to each other, pNMPS0203 was constructed to disrupt *mcpT* in a mutant containing a deletion of the RS_RS05755 homolog

The construction procedure was as follow. A 0.7-kb upstream region of *mcp02* and a 1.2-kb downstream region of *mcpT* were amplified by PCR using the NMRS02Uf/NMRS02Ur and NMRS03Df/NMRS03Dr primer pairs, respectively, and genomic DNA of *R. pseudosolanacearum* Ps29. The amplified fragments were digested with *Eco*RI+*Xho*I and *Xho*I+*Bam*HI, and ligated with the backbone of *Eco*RI- and *Bam*HI- digested pK18*mobsacB* to obtain pNMPS0203.

3.2.5. Construction of *mcp* single- and double-deletion mutants

The *mcp* genes of *R. pseudosolanacearum* Ps29 and MAFF106611 were deleted by an unmarked-gene-deletion technique described in section 2.2.4. The RS_RS07350 (old locus tag RSc1460) homolog gene (*mcpC*) and RS_RS18600 (old locus tag RSc0303) homolog gene (*mcpP*) double-deletion mutant of Ps29 was constructed using plasmid for deletion of the *mcpP* (pNMPS16) and the *mcpC* deletion mutant (DPS05) as based strain. The *mcpC* and *mcpP* single- and double-deletion mutants of MAFF106611 were constructed using plasmids for deletion of the *mcpC* (pNMMF05) and *mcpP* (pNMMF16). These plasmids were constructed in the similar way to that for Ps29 (pNMPS05 and pNMPS16) using primer sets NMRS05Uf/Ur/Df/Dr and NMRS16Uf/Ur/Df/Dr, respectively, and MAFF106611 genome.

3.2.6. Complementation of *mcp* genes

To construct the pPS05 and pPS16 plasmids for use in the complementation analysis, CLRS05f/CLRS05r and CLRS16f/CLRS16r primer pairs were used to amplify 1.7-kb regions containing the *mcpC* and *mcpP* of *R. pseudosolanacearum* Ps29, respectively. The amplified fragments were digested with *Eco*RI and *Bam*HI, and ligated with *Eco*RI- and *Bam*HI-digested pRCII. The resulting plasmids, pPS05 and pPS16, were then introduced into Ps29 *mcp* mutants by electroporation, as described in section 2.2.6.

3.2.7. Sand-soak inoculation virulence assay

Virulence of *R. pseudosolanacearum* MAFF106611 strains were investigated by sand-soak inoculation method as described in section 2.2.8. In this chapter, Mikawa quartz sand standard no.6 (grain size 0.1 to 0.3 mm) (Mikawa-keiseki Co., Ltd., Aichi, Japan)

was used instead of quartz sand of Paint works.

3.2.8. Competitive plant colonization assay

Competitive plant colonization of *R. pseudosolanacearum* MAFF106611 strains were tested as described in section 2.2.9 with some modifications. In this chapter, large tubes (35-mm inner diameter, 40-mm outer diameter, 120-mm length) were used instead of small tubes. Gnotobiotic system containing Mikawa quartz sand standard no.6 (grain size 0.1 to 0.3 mm) (Mikawa-keiseki Co., Ltd., Aichi, Japan), PNS medium and wounded tomato seedling was prepared as described in section 2.2.8. Bacterial cells were grown for 20 h in RSM medium, centrifuged (3,300×*g*, 2 min), washed twice with sterile deionized water, and adjusted to 10^6 CFU/ml (OD_{600} = 0.001) in sterile deionized water.

For the competitive colonization assay, 50 µL of 1:1 (v/v) mixture of the tested strain and the competitor (the kanamycin-resistant strain of *R. pseudosolanacearum* MAFF106611) was inoculated near the opposite wall of the tube (distance between the seedling and the inoculation spot was 30 mm). The plant growth tubes were incubated in a climate-controlled growth chamber (28˚C, 16 h:8 h light:dark cycle). After 2, 4, and 6 days of incubation, each tomato seedling was homogenized and shaken vigorously for 10 min in 0.5 ml of sterile deionized water to suspend the bacteria. The bacterial suspension was diluted and plated on CPG agar plates with and without kanamycin.

Table 3.1. Bacterial strains used in chapter 3.

Strain	Relevant characteristic(s)[a]	Reference.
Ralstonia pseudosolanacearum		
Ps29	Wild-type strain; race 1, biovar 3, phylotype, isolated from tobacco	[42]
POC10	Ps29 derivative; Δ*mcpA* (LC005226) Δ*mcp02* (LC005227) Δ*mcp09* (LC005234) Δ*mcp10* (LC005235) Δ*mcp12* (LC005237) Δ*mcpM* (LC005239) Δ*mcp15* (LC005240) Δ*mcp17* (LC005242) Δ*mcp18* (LC005243) Δ*mcp19* (LC005244)	This study
POC11	Ps29 derivative; POC10 Δ*mcpC* (LC005230)	This study
POC12	Ps29 derivative; POC11 Δ*mcpP* (LC005241)	This study
POC22	Ps29 derivative; Δ*mcpA* (LC005226) Δ*mcp02* (LC005227) Δ*mcpT* (LC005228) Δ*mcp04* (LC005229) Δ*mcpC* (LC005230) Δ*mcp06* (LC005231) Δ*mcp07* (LC005232) Δ*mcp08* (LC005233) Δ*mcp09* (LC005234) Δ*mcp10* (LC005235) Δ*mcpB* (LC005236) Δ*mcp12* (LC005237) Δ*aer2* (LC005238) Δ*mcpM* (LC005239) Δ*mcp15* (LC005240) Δ*mcpP* (LC005241) Δ*mcp17* (LC005242) Δ*mcp18* (LC005243) Δ*mcp19* (LC005244) Δ*aer1* (LC005245) Δ*mcp21* (LC005246) Δ*mcp22* (LC005247)	This study
DPS05	Ps29 derivative; Δ*mcpC* (LC005230)	This study (chapter 2)
DPS16	Ps29 derivative; Δ*mcpP* (LC005241)	This study (chapter 2)
DPS0516	Ps29 derivative; Δ*mcpC* (LC005230) Δ*mcpP* (LC005241)	This study
MAFF106611	Wild-type strain; race 1, biovar 4, phylotype I, isolated from eggplant	[42]
DMF05	MAFF106611 derivative; Δ*mcpC* (LC381281)	This study
DMF16	MAFF106611 derivative; Δ*mcpP* (MF138068)	This study
DMF0516	MAFF106611 derivative; Δ*mcpC* Δ*mcpP*	This study
MFK	MAFF106611 derivative; Km^r	This study (chapter 2)
Escherichia coli		
JM109	*recA1*, *endA1*, *gyrA96*, *thi-1*, *hsdR17* (r_k^- m_k^+), *e14*$^-$ (*mcrA*$^-$), *supE44*, *relA1*, Δ(*lac-proAB*)/F' [*traD36*, *proAB*$^+$, *lacI*^{q}, *lacZ* ΔM15]	[34]
S17-1	MM294 derivative, RP4-2 Tc::Mu-Km::Tn7; chromosomally integrated	[43]

[a] LC005226 to LC005247, and MF138068 in parenthesis indicate the accession no. of the *mcp* genes.

Table 3.2. Plasmids used in chapter 3.

Plasmid	Relevant characteristic(s)	Reference.
Unmarked gene modification		
pK18*mobsacB*	Km^r pUC18 derivative, *lacZα*, mobs site, *sacB*	[36]
pNMPS01	pK18*mobsacB* with a 1.2-kb PCR fragment upstream of *mcpA* and a 1.1-kb PCR fragment downstream of *mcpA* from Ps29 genome; Km^r	This study (chapter 2)
pNMPS02	pK18*mobsacB* with a 0.7-kb PCR fragment upstream of *mcp02* and a 1.1-kb PCR fragment downstream of *mcp02* from Ps29 genome; Km^r	This study (chapter 2)
pNMPS0203	pK18*mobsacB* with a 0.7-kb PCR fragment upstream of *mcp02* and a 1.2-kb PCR fragment downstream of *mcpT* from Ps29 genome; Km^r	This study
pNMPS04	pK18*mobsacB* with a 0.8-kb PCR fragment upstream of *mcp04* and a 1.2-kb PCR fragment downstream of *mcp04* from Ps29 genome; Km^r	This study (chapter 2)
pNMPS05	pK18*mobsacB* with a 1.0-kb PCR fragment upstream of *mcpC* and a 0.8-kb PCR fragment downstream of *mcpC* from Ps29 genome; Km^r	This study (chapter 2)
pNMPS06	pK18*mobsacB* with a 1.5-kb PCR fragment upstream of *mcp06* and a 1.8-kb PCR fragment downstream of *mcp06* from Ps29 genome; Km^r	This study (chapter 2)
pNMPS07	pK18*mobsacB* with a 0.6-kb PCR fragment upstream of *mcp07* and a 0.7-kb PCR fragment downstream of *mcp07*from Ps29 genome; Km^r	This study (chapter 2)
pNMPS08	pK18*mobsacB* with a 1.3-kb PCR fragment upstream of *mcp08* and a 1.0-kb PCR fragment downstream of *mcp08* from Ps29 genome; Km^r	This study (chapter 2)
pNMPS10	pK18*mobsacB* with a 1.0-kb PCR fragment upstream of *mcp10* and a 1.2-kb PCR fragment downstream of *mcp10* from Ps29 genome; Km^r	This study (chapter 2)
pNMPS11	pK18*mobsacB* with a 1.3-kb PCR fragment upstream of *mcpB* and a 1.1-kb PCR fragment downstream of *mcpB* from Ps29 genome; Km^r	This study (chapter 2)
pNMPS12	pK18*mobsacB* with a 0.8-kb PCR fragment upstream of *mcp12* and a 1.3-kb PCR fragment downstream of *mcp12* from Ps29 genome; Km^r	This study (chapter 2)
pNMPS13	pK18*mobsacB* with a 1.3-kb PCR fragment upstream of *aer2* and a 1.0-kb PCR fragment downstream of *aer2* from Ps29 genome; Km^r	This study (chapter 2)
pNMPS14	pK18*mobsacB* with a 0.9-kb PCR fragment upstream of *mcpM* and a 0.6-kb PCR fragment downstream of *mcpM* from Ps29 genome; Km^r	This study (chapter 2)
pNMPS15	pK18*mobsacB* with a 1.2-kb PCR fragment upstream of *mcp15* and a 1.1-kb PCR fragment downstream of *mcp15* from Ps29 genome; Km^r	This study (chapter 2)
pNMPS16	pK18*mobsacB* with a 0.3-kb PCR fragment upstream of *mcpP* and a 0.8-kb PCR fragment downstream of *mcpP* from Ps29 genome; Km^r	This study (chapter 2)
pNMPS17	pK18*mobsacB* with a 0.8-kb PCR fragment upstream of *mcp17* and a 0.7-kb PCR fragment downstream of *mcp17* from Ps29 genome; Km^r	This study (chapter 2)
pNMPS18	pK18*mobsacB* with a 1.6-kb PCR fragment upstream of *mcp18* and a 0.7-kb PCR fragment downstream of *mcp18* from Ps29 genome; Km^r	This study (chapter 2)

Table 3.2. (Continued)

Plasmid	Relevant characteristic(s)	Reference.
pNMPS19	pK18*mobsacB* with a 0.9-kb PCR fragment upstream of *mcp19* and a 1.2-kb PCR fragment downstream of *mcp19* from Ps29 genome; Km^r	This study (chapter 2)
pNMPS20	pK18*mobsacB* with a 0.9–kb PCR fragment upstream of *aer1* and a 0.6–kb PCR fragment downstream of *aer1* from the Ps29 genome	This study (chapter 2)
pNMPS21	pK18*mobsacB* with a 1.1-kb PCR fragment upstream of *mcp21* and a 0.8-kb PCR fragment downstream of *mcp21* from Ps29 genome; Km^r	This study (chapter 2)
pNMPS22	pK18*mobsacB* with a 1.0-kb PCR fragment upstream of *mcp22* and a 0.8-kb PCR fragment downstream of *mcp22* from Ps29 genome; Km^r	This study (chapter 2)
pNMMF05	pK18*mobsacB* with a 1.0-kb PCR fragment upstream of *mcpC* and a 0.8-kb PCR fragment downstream of *mcpC* from MAFF106611 genome; Km^r	This study
pNMMF16	pK18*mobsacB* with a 0.3-kb PCR fragment upstream of *mcpP* and a 0.8-kb PCR fragment downstream of *mcpP* from MAFF106611 genome; Km^r	This study
Unmarked gene modification		
pRCII	*E. coli-Ralstonia* shuttle vector derived from pKZ27; IncQ, *lac* promoter; Km^r	This study (chapter 2)
pPS05	pRCII with a 1.7-kb PCR fragment including *mcpC* of Ps29	This study
pPS16	pRCII with a 1.7-kb PCR fragment including *mcpP* of Ps29	This study

Table 3.3. Oligonucleotides used in chapter 3.

Oligonucleotide	Sequence (5' to 3')[a]
Unmarked gene modification	
NMRS05Uf	AGAATTCGAAGATGCCCACAACCTG
NMRS05Ur	ACTCGAGATCGGTAGCCCGTTCTCAAAC
NMRS05Df	ACTCGAGCCGCCAAAGAGATCAAGGAG
NMRS05Dr	AGGATCCGATCATGAAGGAAGGGCTGAAC
NMRS16Uf	ATGAATTCATGCCGAATGCCTTGATGAC
NMRS16Ur	ATCTCGAGGAAGACAGCCAGAACGAAGAG
NMRS16Df	ACTCGAGATGAAGCCGTCACGCAGATG
NMRS16Dr	AGGATCCGGTGTCCCAGGTGAAGTCAAG
NMRS02Uf	AGAATTCCGCGATCTGTTTCTTACCAC
NMRS02Ur	ACTCGAGCTACGGACTGTCTATCGGCAAC
NMRS03Df	ACTCGAGATCTGTCTGTGCAGGTGAGG
NMRS03Dr	AGGATCCAGGTGGAAAGCTGGGACAAG
Complementation assay	
CLRS05f	CTATGAATTCGGCTCAAGTTTGAGAACGGGCTACC
CLRS05r	CATAGGATCCCATATCGCGCAGGCGTACTGGAAC
CLRS16f	ATGAATTCAGCGGCACTAAAGGTGTGG
CLRS16r	ATGGATCCAGCGCATTGCCTACGAGTC

[a] Underlined sequences indicate restriction enzyme sites.

Table 3.4. Construction of *R. pseudosolanacearum* Ps29 multiple *mcp* deletion mutants.

Disruption order	Deletion target gene[a]	Materials		Resulting strain
		Based strain	Plasmid[b]	
1	*mcp12* (LC005234)	DPS09	pNMPS12	DPS0912
2	*mcpM* (LC005239)	DPS0912	pNMPS14	POC3
3	*mcpA* (LC005226)	POC3	pNMPS01	POC4
4	*mcp10* (LC005235)	POC4	pNMPS10	POC5
5	*mcp19* (LC005244)	POC5	pNMPS19	POC6
6	*mcp18* (LC005243)	POC6	pNMPS18	POC7
7	*mcp02* (LC005227)	POC7	pNMPS02	POC8
8	*mcp15* (LC005240)	POC8	pNMPS15	POC9
9	*mcp17* (LC005242)	POC9	pNMPS17	POC10
10	*mcpC* (LC005230)	POC10	pNMPS05	POC11
11	*mcpP* (LC005241)	POC11	pNMPS16	POC12
12	*mcp22* (LC005247)	POC12	pNMPS22	POC13
13	*mcpB* (LC005236)	POC13	pNMPS11	POC14
14	*mcp06* (LC005231)	POC14	pNMPS06	POC15
15	*mcp04* (LC005229)	POC15	pNMPS04	POC16
16	*mcp08* (LC005233)	POC16	pNMPS08	POC17
17	*mcpT* (LC005228)	POC17	pNMPS0203	POC18
18	*mcp21* (LC005246)	POC18	pNMPS21	POC19
19	*mcp07* (LC005232)	POC19	pNMPS07	POC20
20	*aer2* (LC005238)	POC20	pNMPS13	POC21
21	*aer1* (LC005245)	POC21	pNMPS20	POC22

[a] LC005226 to LC005247 in parenthesis indicate the accession no. of the *mcp* genes.
[b] Plasmids for unmarked deletion of *mcp* genes

3.3 Results

3.3.1. Identification of chemoreceptors for citrate

Computer-assisted capillary assays showed that citrate taxis by *R. pseudosolanacearum* Ps29 was concentration-dependent (Fig. 3.1). In previous chapter, analysis of 22 *mcp* single-deletion mutants revealed that none of the mutants showed a significant decrease in response to citrate ($P < 0.01$ by Student's t-test) (Fig. 2.5B), suggesting that citrate taxis is mediated by multiple receptors or a receptor(s) other than the 22 putative MCPs. To examine the latter possibility, POC22, total-*mcp*-deletion mutant of *R. pseudosolanacearum* Ps29, was constructed by unmarked-gene-deletion technique. The POC22 mutant was completely unable to respond to citrate (Fig. 3.2A), excluding the possibility that citrate taxis is mediated by chemoreceptor other than 22 MCPs and indicating that these 22 MCPs include chemoreceptor(s) for citrate. I therefore attempted to identify MCPs for citrate by screening a library of multiple-mcp-deletion mutants (designated POC*n*, where *n* is the number of deleted *mcp* genes) obtained in the course of construction of the 22-*mcp*-deletion mutant POC22. Although the response to citrate by strain POC10 (a mutant with deletion of 10 *mcp*s) was comparable to that of wild-type

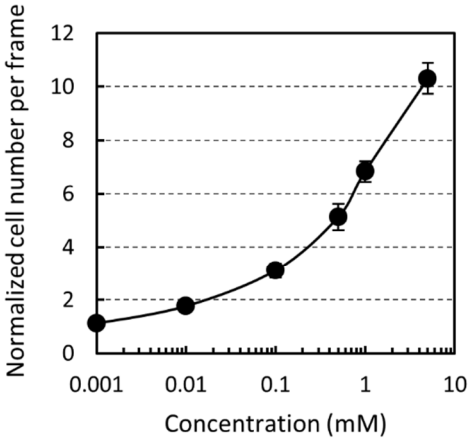

Fig. 3.1. Concentration-dependent chemotaxis toward citrate by *R. pseudosolanacearum* wild-type Ps29. Vertical bars represent the standard error of measurement for experiments performed at least nine.

strain, POC11 (the POC10 with additional deletion of the homolog of *R. pseudosolanacearum* GMI1000 RS_RS07350), showed a significantly lower-level response to citrate than did POC10 ($P < 0.05$ by Student's *t* test) (Fig. 3.2B). Deletion of the *mcpP* gene, which has been identified as gene encoding phosphate sensor by co-worker[64], in POC11 to create POC12 resulted in loss of the ability to respond to 0.5 mM citrate (Fig. 3.2B). These results suggested that the RS_RS07350 homolog and *mcpP* are involved in citrate taxis.

Careful review of the responses by the RS_RS07350 single-deletion mutant (DPS05) and the *mcpP* single-deletion mutant (DPS16) revealed that both single mutants

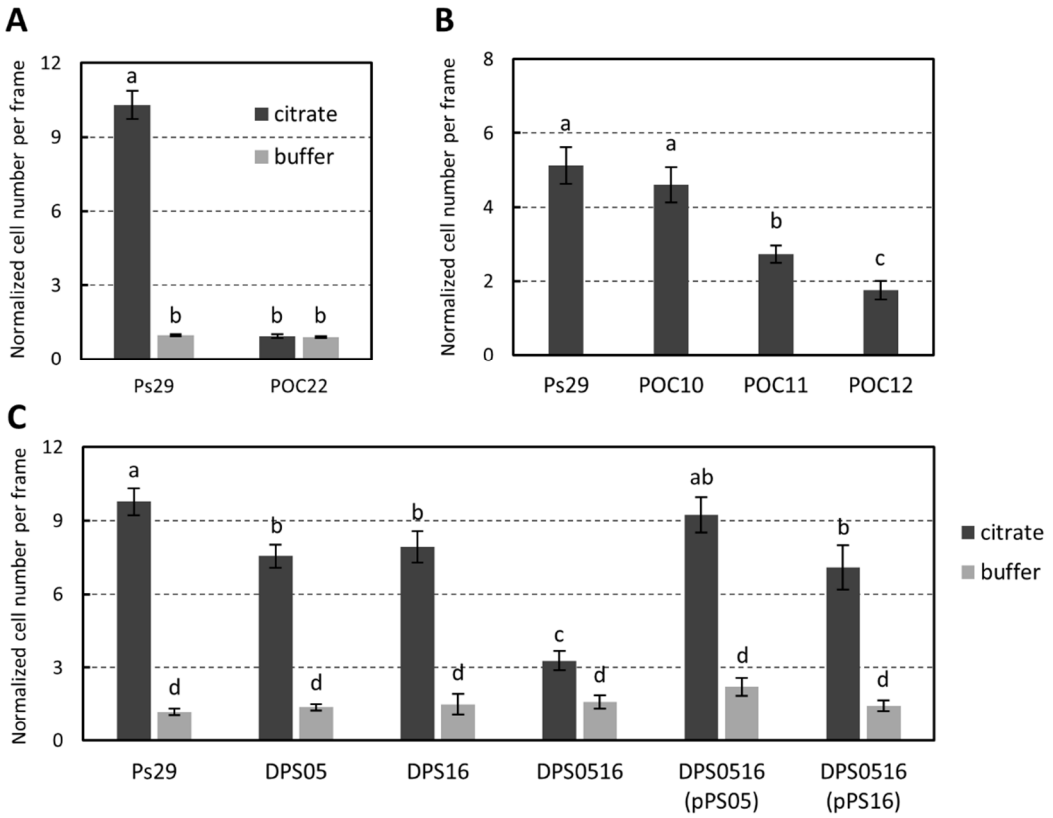

Fig. 3.2. Chemotactic responses to citrate by *R. pseudosolanacearum* Ps29. **A**, chemotaxis to 5 mM citrate by wild-type strain (Ps29) and total-*mcp*-deletion mutant (POC22). **B**, chemotaxis to 0.5 mM citrate by wild-type strain (Ps29) and multiple-*mcp* deletion mutant (POC*n*, where *n* is the number of deleted *mcp*s). **C**, chemotaxis to 5 mM citrate by wild-type strain (Ps29), *mcpC* deletion mutant (DPS05), *mcpP* deletion mutant (DPS16), *mcpC* and *mcpP* double-deletion mutant (DPS0516), DPS0516 harboring complementing plasmids. pPS05, pRCII containing *mcpC*; pPS16, plasmid containing *mcpP*. Different letters indicate significant differences ($P < 0.05$ by Student's *t* test). Vertical bars represent the standard errors of measurements done at least in triplicate.

showed a slight but statistically significant decrease in chemotaxis to 5 mM citrate compared with the wild-type strain ($P < 0.05$ by Student's *t* test) (Fig. 3.2C). Double deletion of these *mcp* genes resulted in a marked reduction in the response to citrate. Introduction of pPS05 (harboring the RS_RS07350 homolog) and pPS16 (harboring the *mcpP*) restored the ability of the double mutant DPS0516 to respond to citrate (Fig. 3.2C), demonstrating that the RS_RS07350 homolog and McpP are MCPs for citrate in *R. pseudosolanacearum* Ps29. I designated the RS_RS07350 homolog as *mcpC* (MCP for citrate). However, DPS0516 still able to show moderate but statistically significant response to 5 mM citrate compared to that to buffer ($P < 0.05$ by Student's *t* test). (Fig. 3.2C).

3.3.2. Ligand specificities of McpC and McpP

I next investigated the ligand specificities of McpC and McpP. Co-worker have already revealed that McpP can sense not only phosphate as a attractant but also maleate as a repellent[64]. To assess whether McpC and McpP are involved in chemotaxis to other organic acids, I examined an *mcpC* and *mcpP* double-deletion mutant (DPS0516) for

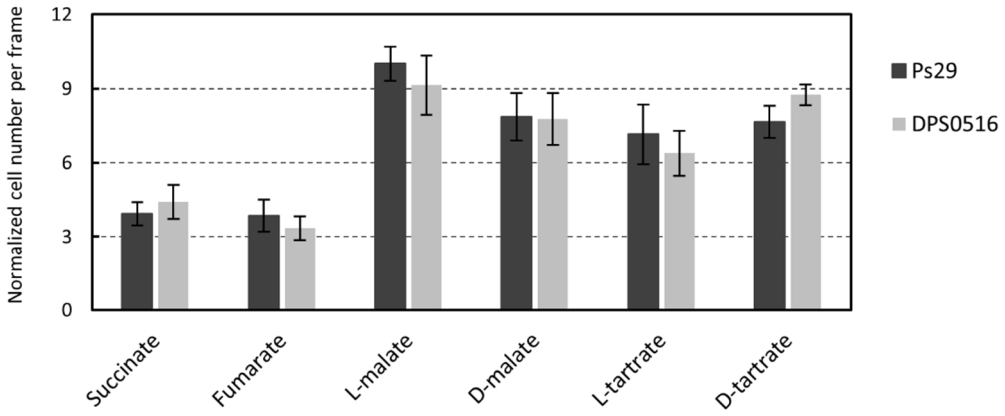

Fig. 3.3. Chemotactic responses to 5 mM organic acids other than citrate by *R. pseudosolanacearum* Ps29 wild-type strain and *mcpC* and *mcpP* double-deletion mutant (DPS0516). Vertical bars represent the standard errors of measurements done at least triplicate.

chemotactic response to organic acids identified as *R. pseudosolanacearum* Ps29chemoattractants in chapter 2, including L-malate, D-malate, succinate, fumarate, L-tartrate, and D-tartrate. The DPS0516 strain showed responses to each compounds comparable to those of wild-type strain Ps29 (Fig. 3.3), suggesting that McpC and McpP are not involved in chemotaxis to these organic acids. Although this result does not completely rule out the possibility that McpC and McpP are capable of sensing these compounds, it does clearly indicate that McpC and McpP are primarily chemoreceptors for citrate in *R. pseudosolanacearum* Ps29.

Citrate is known to form complexes with divalent metal cations like magnesium or calcium[65]. As several citrate chemoreceptors are known to also recognize metal cation-citrate complexes[66,67], the involvements of McpC and McpP in chemotaxis to metal cation-citrate complexes was investigated. Wild-type *R. pseudosolanacearum* Ps29 showed chemotactic response to Mg^{2+}- and Ca^{2+}-citrate complexes although these responses were not as strong as the response to free citrate (Fig. 3.4A) This reduction in the strength of the chemotactic response in the presence of metal ion was not observed in the analysis of chemotaxis to L-alanine, which dose not form complex with metal ions (Fig. 3.4A). These results suggested that metal cation-citrate complexes elicit weaker chemotactic responses than free citrate in *R. pseudosolanacearum* Ps29. In the *mcpC* and *mcpP* double-deletion mutant (DPS0516), there were no significant differences between the response to Mg^{2+}- and Ca^{2+}-citrate complexes versus the control buffer. Introduction of plasmid pPS05, which harbors the Ps29 *mcpC* gene, restored the ability of strain DPS0516 to respond to both Mg^{2+}- and Ca^{2+}-citrate complexes (Fig. 3.4B), demonstrating that McpC senses metal cation-citrate complexes as well as free citrate. Conversely, introduction of plasmid pPS16, which harbors the Ps29 *mcpP*, did not enable strain

DPS0516 to respond to metal cation-citrate complexes (Fig. 3.4B), suggesting that McpP is specific for free citrate.

3.3.3. Distribution of McpC and McpP homologous proteins

McpM and McpP have typical structure of MCP. Dense alignment surface (DAS) analysis[68] identified the LBD of McpC and McpP as a region spanning 159 amino acids (residues 31 to 189) and 168 amino acids (residues 29 to 187), respectively. Protein

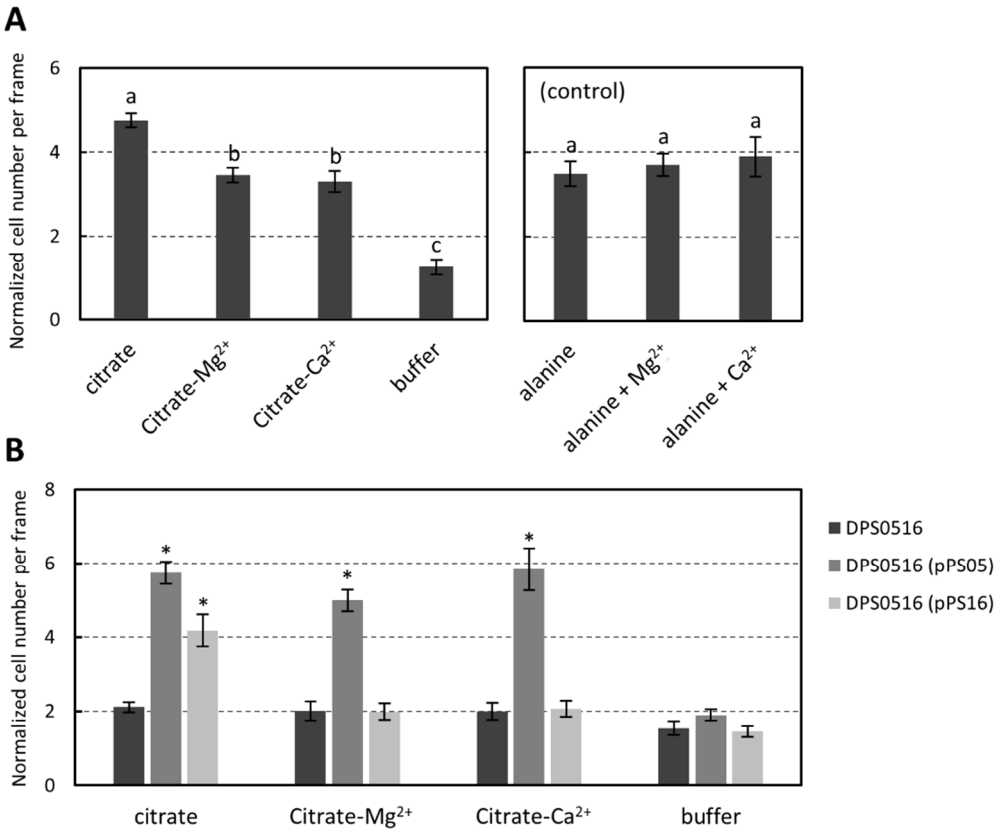

Fig. 3.4. Chemotactic responses to citrate and metal cation-citrate complexes by *R. pseudosolanacearum* Ps29 strains. Mg^{2+}- and Ca^{2+}-citrate were 0.5 mM citrate with 10 mM $MgCl_2$ and $CaCl_2$, respectively. In measurements of chemotaxis to compound with metal chloride, cell suspension was supplemented with 1 mM $MgCl_2$ or $CaCl_2$. **A**, chemotaxis of wild-type strain. As control, 0.5 mM L-alanine with and without 10 mM metal chloride were used. Different letters indicate significant differences ($P < 0.05$ by Student's *t* test). **B**, chemotaxis of *mcpC* and *mcpP* double-deletion mutant (DPS0516) and DPS0516 harboring complementing plasmid. pPS05, pRCII containing the *mcpC*; pPS16, plasmid containing the *mcpP*. Asterisks indicate significant differences in the chemotactic responses between DPS0516 and its complementation strains ($P < 0.05$ by Student's *t* test). Vertical bars represent the standard errors of measurements done at least six.

BLAST analyses using the putative LBD of McpC and McpP sequences, respectively, as a query revealed that MCPs with LBDs similar to those of McpC and McpP are distributed among members of the *R. solanacearum* species complex and that those LBDs exhibit high similarity (90 to 100% identity) to the *R. pseudosolanacearum* Ps29 McpP LBD or McpC LBD. Homologous proteins with LBDs similar to McpC LBD also distributed other *Ralstonia* species including *Ralstonia insidiosa, R. pickettii* and *Ralstonia mannitolilytica*, *Mumia flava*, *Capriavidus* sp., and *Burkholderiaceae* sp. while those LBDs are less similar to the Ps29 McpC LBD (53 to 80% identity). *R. pickettii*, *R. mannitolilytica*, and blood disease bacterium possess MCPs with LBDs similar to McpP LBD (31 to 75% identity). These results suggested that the homologous proteins of McpC and McpP are differentially distributed among *Ralstonia* species and its related genus.

3.3.4. Relationship between citrate taxis and plant infection

The role of citrate taxis in bacterial wilt disease on tomato was investigated. In these experiments, the highly virulent *R. pseudosolanacearum* MAFF106611 strain was used instead of strain Ps29. PCR analysis and DNA sequencing of strain MAFF106611 demonstrated the presence of *mcpC* and *mcpP*, the respective products of which are 99% identical to their Ps29 counterparts. The *mcpC* deletion mutant (DMF05), *mcpP* deletion mutant (DMF16), and these *mcp*s double-deletion mutant (DMF0516) showed chemotactic phenotypes similar to the strain Ps29 mutants (Fig. 3.5).

I tested plant infection by the mutants using the sand-soak inoculation method (Fig. 3.6), in which bacteria are inoculated into sand 3 cm away from a tomato seedling. Plant infection in this assay therefore requires cells to locate the host plants from a distance and move to them to invade. Wild-type strain MAFF106611 started wiling at 4

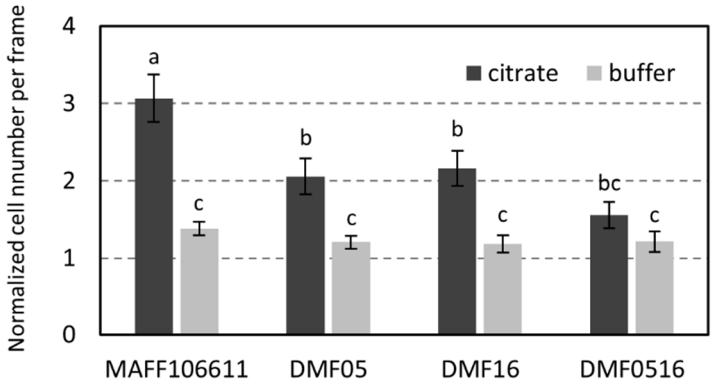

Fig. 3.5. Chemotactic responses to 5 mM citrate by *R. pseudosolanacearum* MAFF1106611 strains. MAFF106611, wild-type strain; DMF05, *mcpC* deletion mutant; DMF16, *mcpP* deletion mutant; DMF0516, *mcpC* and *mcpP* double-deletion mutant. Videotape frames were analyzed at the initiation of observation and 2 min after initiation. Different letters indicate significant differences ($P < 0.05$ by Student's *t* test). Vertical bars represent the standard errors of measurements done at least triplicate.

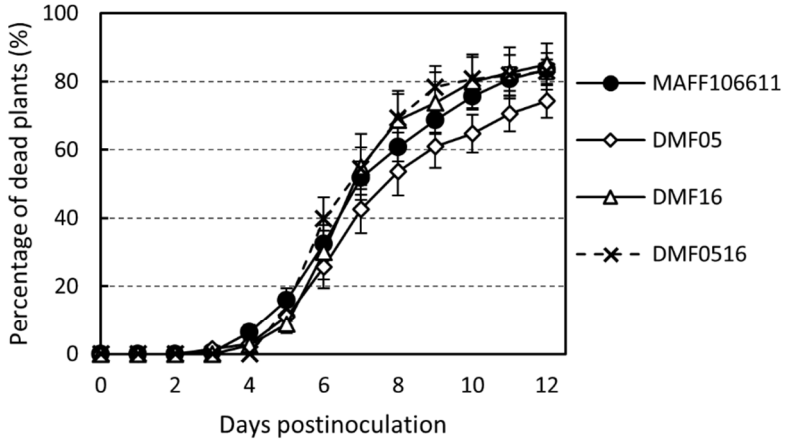

Fig. 3.6. Sand-soak inoculation virulence assay on *R. pseudosolanacearum* MAFF106611 strains on tomato seedlings. MAFF106611, wild-type strain; DMF05, *mcpC* deletion mutant; DMF16, *mcpP* deletion mutant; DMF0516, *mcpC* and *mcpP* double-deletion mutant. In each experiment, 8 tomato seedlings were examined and observed to calculate the percentage of dead plants. Means and standard errors were calculated from at least nine independent experiments.

dpi and killed 80% of the tomato plants by 12 dpi. The time line of wilting in response to challenge with strain DMF05, DMF16, or DMF0516 was similar to that seen with the wild-type parent. I also conducted a competitive tomato colonization assay by sand soak inoculating tomato seedlings with a 1:1 mixture of strain DMF0516 and a kanamycin-resistant strain (MFK) as competitor that competed fully with wild-type strain (Fig. 3.7A). Strain DMF0516 showed the same level of competitive plant colonization with MFK as

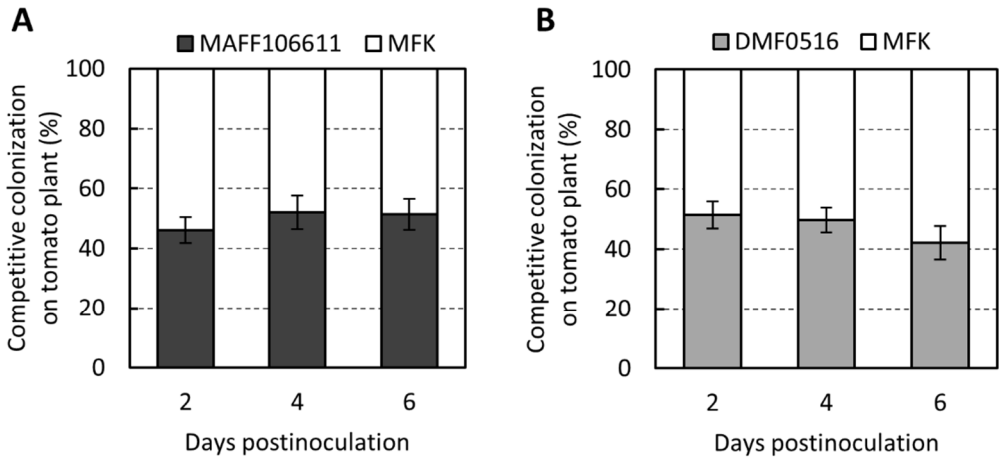

Fig. 3.7. Plant colonization assay for competition between the *R. pseudosolanacearum* MAFF106611 kanamycin-resistant strain (MFK) and wild-type strain MAFF106611 (**A**), *mcpC* and *mcpP* double-deletion mutant (DMF0516) (**B**). Means and standard errors were calculated from at least four independent experiments conducted in 5 plants per time point.

the wild-type strain (Fig. 3.7B), consistent with the results of virulence assay. These suggested that citrate taxis mediated by McpC and McpP does not play a crucial role in initial localization of plant roots by *R. pseudosolanacearum* MAFF106611.

3.4 Discussion

In this chapter, I identified McpC and McpP as chemoreceptors for citrate using a library of *R. pseudosolanacearum* Ps29 multiple-*mcp*-gene deletion mutants. In addition, I showed that McpC can sense citrate in complexes with Mg^{2+} and Ca^{2+} as well as free citrate, although McpP, which has been identified as being involved in both positive chemotaxis to phosphate and negative chemotaxis to maleate[64], cannot sense metal cation-citrate complexes. Analysis of chemotaxis using *mcpC* and *mcpP* double-deletion mutant (DPS0516) suggested that these two MCPs are not involved in chemotaxis to other organic acids (e.g., malate, tartrate, succinate, and fumarate). Thus, McpC and McpP, both of which act as a major MCP for citrate, have some differences in ligand specificity. However, the LBDs of McpC and McpP exhibit sequence similarity of 29%. Both of these

MCPs belong to the cluster-I group (MCPs with LBD containing 120 to 210 amino acid residues) based on size of the LBD and are annotated as a 4 helix bundle (4HB) in Pfam and InterPro. Protein structure predictions using the Phyre^2 fold recognition server [55] also suggested the presence of the 4HB domain in the *R. pseudosolanacearum* Ps29 McpC and McpP LBDs (Fig. 3.8).

To date, MCPs for citrate have been reported in several bacteria. McpS of *P. putida* KT2440[47] and McfS of *P. putida* F1[46] are citrate receptors with a broad ligand range, and they sense not only citrate but also other TCA cycle intermediates such as malate, succinate, and fumarate. MCP2201 and MCP2901 of *C. testosteroni* CNB-1 also recognize many compounds such as aromatic compounds and/or TCA cycle intermediates including citrate[62,63]. Conversely, citrate MCPs with a narrow ligand range also have been identified. Citrate chemotaxis of *Salmonella enterica* serovar Typhimurium is mediated by the Tcp receptor, which can sense both free citrate and Mg^{2+}-citrate complexes as attractants[67] (similar to McpC) and phenol as a repellent[61] (similar to McpP). The Tcp receptor belongs to cluster I based on the size of the LBD (160 amino acids), which forms a 4HB, similar to McpC and McpP of *R. pseudosolanacearum* Ps29. Martín-Mora *et al*. showed that the McpS paralogue McpQ of *P. putida* KT2440 is also chemoreceptor specific to citrate and that it mediates chemotaxis preferentially to citrate in complex with Mg^{2+} or Ca^{2+} [65], whereas McpS cannot recognize these

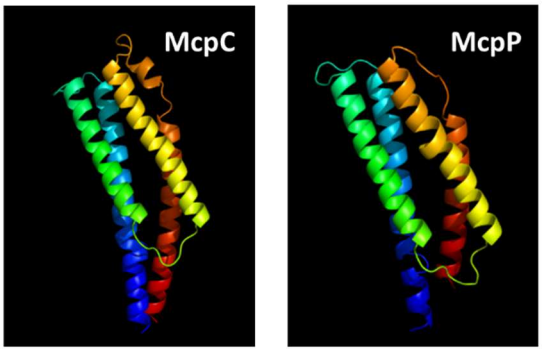

Fig. 3.8. The predicted three-dimensional (3D) structures of McpC LBD and McpP LBD of *R. pseudosolanacearum* Ps29. The 3D structures were predicted by using Phyre² algorithm. Blue color, N-terminus; red color, C-terminus.

metal cation-citrate complexes[65]. In contrast to the Tcp receptor of *S. enterica* and McpC and McpP of *R. pseudosolanacearum*, McpQ (with an LBD containing 253 amino acids) of *P. putida* KT2440 falls into cluster II, and its LBD assumes a helical-bimodular (HBM) fold. Thus, there are some similarities and differences between known citrate MCPs and McpC and McpP of *R. pseudosolanacearum*.

Chemotaxis plays an important role in facilitating ecological interactions, including plant infection by the *R. solanacearum* species complex[20]. In previous chapter, I demonstrated that chemotaxis to L-malate, which is a major component of plant root exudate[44], facilitates migration of *R. pseudosolanacearum* to tomato plants. As citrate is also a strong chemoattractant and major component of root exudate[44,60], it seems likely that citrate serves as a chemotactic signaling compound that enables bacteria to locate and interact with plant roots. However, the results of the present virulence assay and competitive plant colonization assay using the sand-soak inoculation method revealed that the infectivity and competitive colonization ability of the *mcpC* and *mcpP* double-deletion mutant of MAFF106611 (DMF0516) did not differ significantly in comparison with the wild-type strain. Several possibilities can be considered from these results. (i) The most likely possibility is that the concentration of citrate released from tomato roots was too low in this assay system, while tomato exudate reportedly contains 3-110 μg/plant citrate (46 to 70% of the total pool of organic acids), depending on the stage of plant growth and cultivation condition[44]. (ii) It is possible that citrate taxis of *R. pseudosolanacearum* does not play an important role in soil environment. Because citrate forms complexes with metal cations like Mg^{2+} or Ca^{2+}[65],which are abundant in soil [70,71] and plant root exudate[72,73], citrate could be primarily present as a metal complex in soil environment. The magnitude of responses to both Mg^{2+}- and Ca^{2+}-citrate complexes

mediated by McpC are lower than the response to free citrate mediated by both McpC and McpP in wild-type *R. pseudosolanacearum* Ps29. This phenomenon is completely opposite to that of *P. putida* KT2440, which shows a response of much greater magnitude to Mg^{2+}-citrate than free citrate[66]. (iii) Alternatively, differences in expression levels of *mcp* genes in plant assay versus chemotaxis assay could cause the unexpected results in plant experiments. López-Farfán and co-workers recently demonstrated that environmental conditions determine *mcp* expression levels in *P. putida* KT2440 as a model bacterium with a large number of chemoreceptors[74]. The DPS0516 mutant still exhibited moderate response to citrate (Fig. 3.2C), clearly indicating the presence of citrate receptor(s) other than McpC and McpP. In plant assay system, if the unidentified citrate MCP(s) was/were expressed much higher levels than in the chemotaxis assay, the DMF0516 mutant could have responded strongly to citrate released from tomato roots. To form a final conclusion regarding the involvement of citrate taxis in plant infection by member of the *R. solanacearum* species complex, identification of all citrate receptors, including minor MCP(s), will be needed.

CHAPTER4

Identification of boric acid as a novel chemoattractant and elucidation of its chemoreceptor

4.1 Introduction

As described in chapter 2 and 3, *R. pseudosolanacearum* Ps29 shows chemotaxis to amino acids, organic acids and phosphate. Yao and Allen reported that *R. solanacearum* K60 shows chemotaxis not only to amino acids and organic acids but also to sugars [20]. Does the *R. solanacearum* species complex responds to only typical chemoattractants like these compounds? The hitherto characterized MCPs other than McpM (McpA for amino acids; McpT for L-tartrate; McpP for phosphate and citrate; McpC for citrate) were not important for plant infection whereas ligands of these MCPs are known as major components of plant root exudate. Hence, chemotaxis involved in plant infection are not revealed completely. There is possibly an unknown chemotaxis and it could contribute to plant infection.

In the course of my chemotaxis research, a unique phenomenon was observed in *R. pseudosolanacearum* strain Ps29. I used computer-assisted capillary assays to analyze chemotaxis behavior in *Pseudomonas* strains as well as *R. pseudosolanacearum*. HEPES buffer was used for cell suspensions and as a negative control for the chemotaxis assays. *Pseudomonas* strains showed no response to HEPES buffer, whereas *R. pseudosolanacearum* showed weak response to HEPES buffer and occasionally, strongly responded to the “negative” control. I investigated this phenomenon in detail and found that *R. pseudosolanacearum* was attracted to boric acid. In this chapter, I describe chemotaxis toward boric acid by *R. pseudosolanacearum* and the identification and characterization of its chemotaxis sensor and discuss its biological meaning.

4.2 Experimental procedures

4.2.1. Bacterial strains, plasmids, and growth conditions

Bacterial strains and plasmids used in this chapter are listed in Table 4.1. *R. pseudosolanacearum* Ps29 and MAFF106611 were used for chemotaxis research and tomato plant assay, respectively. *E. coli* JM109, S17-1 and BL21(DE3) were used for plasmid construction, transconjugation, and protein expression, respectively.

R. pseudosolanacearum strains and *E. coli* strains were grown as described in section 2.2.1. *Pseudomonas* strains were grown for 20 h in LB medium with shaking at 280 rpm, then 100 µl of the preculture cells were transferred into 5 ml of T0 medium[37] containing 2.0 g/l glucose, 0.15 g/l NaCl, 1.0 g/l NH_4Cl, 0.1 g/l KCl, 0.01 g/l $CaCL_2$ $2H_2O$, 0.01 g/l $MgCl_2$ $6H_2O$, 0.1 g/l Na_2SO_4, 0.001 g/l $FeCl_3$, and 10 g/l Tris buffer (pH7.6), and grown for 6 h with shaking at 280 rpm. *P. aeruginosa* PAO1 was grown at 37°C. *P. fluorescens* Pf0-1 and *P. putida* F1 were grown at 28°C.

4.2.2. DNA manipulation

Standard procedures were used for plasmid DNA preparations, transformations of *E. coli*, and agarose gel electrophoresis[34]. PCR, restriction enzyme digestions, and ligation reactions were conducted using KOD plus Neo polymerase (Toyobo, Osaka, Japan), FastDigest (Thermo Fisher Scientific, Massachusetts, USA), and Ligation High Ver.2 (Toyobo, Osaka, Japan), respectively, according to the manufacturer's instructions. Primers used for PCR are listed in Table 4.2.

4.2.3. Chemotaxis assay

Chemotaxis responses were measured by computer-assisted capillary assays as described in section 2.2.3. In this chapter, 10 mM HEPES buffer (pH 7.0) stored in a plastic tube was used as chemotaxis buffer, unless stated otherwise.

4.2.4. Complementation of *mcpB*

To construct the pPS11 plasmid for use in the complementation analysis, a 1.9-kb region encoding the RS_RS17100 (old locus tag RSc3412) homolog gene (*mcpB*) of *R. pseudosolanacearum* Ps29 was amplified by PCR using the CLRS11f/CLRS11r primer pair. The amplified fragments were digested with *Eco*RI and *Bam*HI, and cloned between the *Eco*RI and *Bam*HI sites of pRCII. pPS11 was then introduced into strain DPS11 by electroporation, as described in section 2.2.6.

4.2.5. Expression and purification of McpB LBD

A DNA fragment encoding the McpB-LBD (30 to 186 amino acid residues) was amplified by PCR using genomic DNA of *R. pseudosolanacearum* Ps29 and primers McpB_LBDf and McpB_LBDr, which contained the restriction sites for *Nde*I and *Eco*RI, respectively. The amplified fragments were digested with *Nde*I and *Bam*HI and cloned between the *Nde*I and *Bam*HI sites of pET28b(+) (Novagen) to construct pET28_PsMcpB_LBD, which was then used to transform *E. coli* BL21(DE3).

The transformed strain was cultured in LB medium supplemented with 40 μg/ml of kanamycin at 37°C Then, 4 ml of the preculture cells were transferred into 1 L Erlenmeyer flasks containing 400 ml of LB medium supplemented with 40 μg/ml kanamycin and grown for 2 to 3 h at 28°C with rotary shaking at 160 rpm. After reaching

an OD_{600} value of 0.5, 0.1 mM IPTG was added to induce expression of the McpB LBD, and cultivation was continued overnight at 18°C with rotary shaking at 120 rpm. The bacterial cells were harvested by centrifugation for 10 min at 5,000×*g* and lysed by using B-PER™ Bacterial Protein Extraction Reagent (Thermo Fisher Scientific, Massachusetts, USA) according to the manufacturer's instruction. After centrifugation at 20,000×g for 1 h, the supernatant was loaded onto a His GraviTrap TALON column (GE Healthcare, Buckinghamshire, UK) equilibrated with buffer (20 mM sodium phosphate, 500 mM NaCl, pH 7.0) containing 30 mM imidazole. McpB LBD was eluted with the same buffer containing 300 mM imidazole and analyzed by SDS-PAGE. The protein concentration was determined by Bicinchoninic acid (BCA) assay using BCA Protein Assay Kit (Takara, Shiga, Japan).

4.2.6. Isothermal titration calorimetry (ITC)

For ITC, Vivaspin 20 (10 kDa molecular weight cutoff, GE Healthcare) were used to exchange purified McpB LBD into ITC buffer (20 mM sodium phosphate, 100 mM NaCl, 10% (v/v) glycerol, pH 7.0). ITC experiments were performed on a MicroCal iTC 200 isothermal titration calorimeter (GE Healthcare) at 25°C. Test compounds were dissolved in ITC buffer. Protein solution (200 μM) was added to fill the sample cell and titrated with 1 mM compound solution. Data were analyzed using the One Set of Sites model of the MicroCal version of ORIGIN 7.0 software.

4.2.7. Circular dichroism (CD) analysis

For CD analyses, Vivaspin 20 columns (10 kDa molecular weight cutoff, GE Healthcare) were used to exchange purified McpB LBD into CD buffer (20 mM sodium phosphate,

100 mM NaCl, pH 7.0). CD experiments were performed on a J-820 CD spectrometer (JASCO, Tokyo, Japan) equipped with a 1-mm path length cuvette using 20 μM McpB LBD in the absence and presence of 100 μM boric acid. CD spectra (190–260 nm) were recorded at 25°C. For thermal denaturation experiments, CD at 222 nm was monitored from 20 to 70°C.

4.2.8. Gel filtration chromatography

Purified McpB LBD protein was subjected to gel filtration chromatography using ÄKTA explorer 10S (GE Healthcare) equipped with a Superdex 200 increase 10/300 GL column (GE Healthcare). The protein sample passed through a 0.22 μm cut-off filter was loaded column equilibrated with ITC buffer. A standard curve was made using a Gel Filtration Calibration Kit LMW (GE Healthcare) following the manufacturer's instruction.

4.2.9. Analytical ultracentrifugation

For analytical ultracentrifugation analyses, Vivaspin 20 (10 kDa molecular weight cutoff, GE Healthcare) were used to exchange purified McpB LBD into ITC buffer. Sedimentation velocity experiments were performed using an Optima XL-I analytical ultracentrifuge (Beckman Coulter, Brea, CA, USA) with a 4-chamber An60Ti rotor at 42,000 rpm at 25°C. Concentration gradients were measured by UV absorption at 280 nm without a time interval between successive scans. The data were analyzed using SEDFIT[75].

4.2.10. Construction of *mcpB* deletion mutant of MAFF106611

To construct the pNMMF11 plasmid for unmarked deletion of *mcpB* of MAFF106611, a

1.3-kb upstream and 1.1-kb downstream regions of the *mcpB* gene in *R. pseudosolanacearum* MAFF106611 were amplified by PCR using the NMMF11Uf/NMMF11Ur and NMMF11Df/NMMF11Dr, respectively, and the genomic DNA of MAFF106611. The amplified upstream and downstream fragments were digested with *Eco*RI and *Xba*I and *Xba*I and *Hin*dIII and ligated with the backbone of pK18*mobsacB* digested with *Eco*RI and *Hin*dIII. The *mcpB* deletion mutant of MAFF106611 was obtained by using the resulting plasmid as described in section 2.2.4.

4.2.11. Sand-soak inoculation virulence assay

The virulence assay was carried out as described in section 2.2.8 with some modifications. For analysis of boric acid taxis, boric-acid-free containers were used instead of borosilicate glass tubes. Plastic plant box (6 × 6× 10 mm) containing 140 g Mikawa quartz sand standard no.6 (grain size 0.1 to 0.3 mm) (Mikawa-keiseki Co., Ltd., Aichi, Japan) was autoclaved for 15 min at 121˚C. Sterile PNS medium (30 ml) was added to each autoclaved box. The wounded tomato seedling was planted at the center of plant box, 50 µl of cell suspension was inoculated near wall of the plant box (distance between the seedling and the inoculation spot was 30 mm). The plants were maintained in a climate-controlled growth chamber at 28 °C with a 16:8 h light:dark cycle for 10 days and observed daily. All virulence assays included 8 plants per treatment, and each experiment was repeated at least eight times.

Table 4.1. Bacterial strains and plasmids used in chapter 4.

Strain and plasmid	Relevant characteristic(s)[a]	Reference.
Bacterial strains		
Ralstonia pseudosolanacearum		
Ps29	Wild-type strain; race 1, biovar 3, phylotype, isolated from tobacco	[42]
DPS11	Ps29 derivative; Δ*mcpB* (LC005236)	This study (chapter 2)
MAFF106611	Wild-type strain; race 1, biovar 4, phylotype I, isolated from eggplant	[42]
DMF11	MAFF106611 derivative; Δ*mcpB*	This study
Pseudomonas aeruginosa		
PAO1	Wild-type strain	[76]
Pseudomonas fluorescens		
Pf0-1	Wild-type strain	[77]
Pseudomonas protegens		
CHA0	Wild-type strain	[78]
Pseudomonas putida		
F1	Wild-type strain	[79]
Escherichia coli		
JM109	*recA1*, *endA1*, *gyrA96*, *thi-1*, *hsdR17* (r_k^- m_k^+), *e14*$^-$ (*mcrA*$^-$), *supE44*, *relA1*, Δ(*lac-proAB*)/F' [*traD36*, *proAB*$^+$, *lacI*^{q}, *lacZ* ΔM15]	[34]
S17-1	MM294 derivative, RP4-2 Tc::Mu-Km::Tn7; chromosomally integrated	[43]
BL21(DE3)	F$^-$, *ompI*, *hsdS*$_B$ (r^-_B m^-_B)	[80]
Plasmids		
pK18*mobsacB*	Km^r pUC18 derivative, *lacZα*, mobs site, *sacB*	[36]
pNMMF11	pK18*mobsacB* with a 1.3-kb PCR fragment upstream of *mcpB* and a 1.1-kb PCR fragment downstream of *mcpB* from MAFF106611 genome; Km^r	This study
pRCII	*E. coli-Ralstonia* shuttle vector derived from pKZ27; IncQ, *lac* promoter; Km^r	This study (chapter 2)
pPS11	pRCII with a 1.9-kb PCR fragment including *mcpB* of Ps29	This study
pET28b(+)	Km^r, protein expression vector	Novagen
pET28_PsMcpB_LBD	pET28b(+) with a 471-bp PCR fragment encoding McpB LBD of Ps29	This study

[a] LC005236 in parenthesis indicates the accession no. of the *mcp* genes.

Table 4.2. Oligonucleotides used in chapter 4.

Oligonucleotide	Sequence (5' to 3')[a]
Unmarked gene modification	
NMRS11Uf	TACTGGAATTCGTTCACGCTGGCTGTGCTTC
NMRS11Ur	CGTTCTCTAGACTTTCTTGAGTGACGCGCTAAGG
NMRS11Df	GCTAATCTAGACCGCAGGCAACAAGAAGAGC
NMRS11Dr	TACATAAGCTTGCAATGGGCATGCCAATAATC
mcpB cloning for complementation analysis	
CLRS11f	ATGAATTCTAGCGCGTCACTCAAGAAAGG
CLRS11r	ATGGATCCAAGACATGGAAGCCAAGCTG
Cloning of LBD region of *mcpB*	
McpB_LBDf	AATTCATATGGGGCGCCAGGCCGCCGCGAC
McpB_LBDr	AATTGGATCCTTAGCGGGCCAATGCTGCCG

[a] Underlined sequences indicate restriction enzyme sites.

4.3 Results

4.3.1. Discovery of chemotaxis toward boric acid

I used a computer-assisted capillary assay method[35] to assess bacterial chemotaxis. In this method, a glass capillary containing a known concentration of a test compound plus 1% agarose in 10 mM HEPES buffer (pH 7.0) is inserted into a bacterial cell suspension. HEPES buffer is also used for cell suspensions. The bacteria sense the test compound diffusing from the orifice of the glass capillary, and if attracted by the test compound, swim toward the orifice of the capillary. HEPES buffer at the same concentration and pH was used as a negative control in the chemotaxis assay. *R. pseudosolanacearum* Ps29 showed a chemotactic response to HEPES buffer although it was weak (Fig. 4.1A), and sometimes, the bacteria exhibited very strong responses to HEPES buffer. Careful review of the experimental procedure revealed that *R. pseudosolanacearum* exhibited much stronger responses to HEPES buffer stored in a borosilicate glass bottle for an extended time (for example, overnight) than to generally used buffer stored in plastic bottles, and

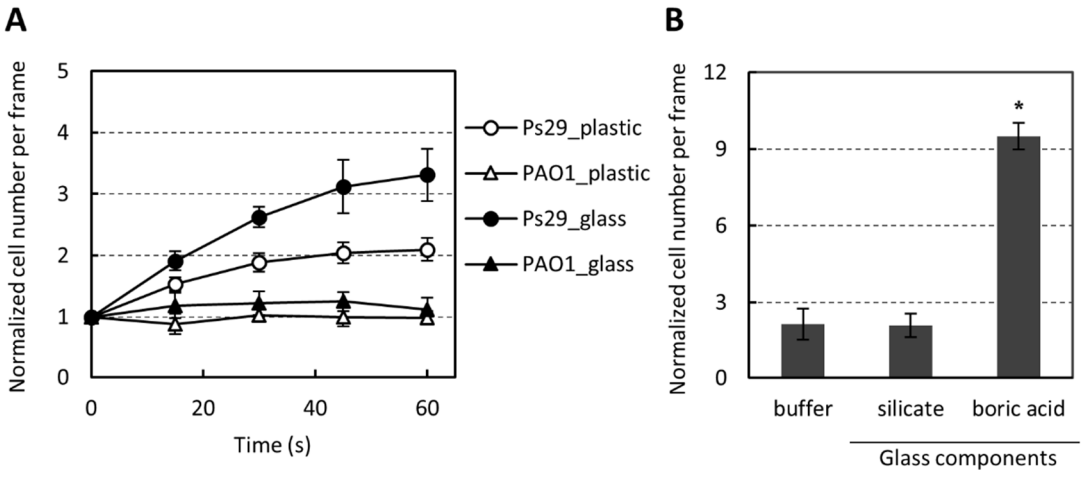

Fig. 4.1. Discovery of chemotaxis to boric acid. **A**, chemotaxis to negative control HEPES buffer by *R. pseudosolanacearum* Ps29 and *P. aeruginosa* PAO1. 'Plastic' and 'glass' indicate HEPES buffer stored in a plastic tube and glass bottle, respectively. **B**, chemotaxis to 5 mM silicate and 0.5 mM boric acid by *R. pseudosolanacearum* Ps29. HEPES buffer stored in a plastic tube was used as a control. Asterisk indicates a statistically significant difference compared with the response to buffer ($P < 0.05$ by Student's t test). Vertical bars represent the standard error of measurement for experiments performed at least in triplicate.

these responses were reproducible (Fig. 4.1A). By contrast, *Pseudomonas* strains including *P. aeruginosa* PAO1 (Fig. 4.1A), *P. fluorescen*s Pf0-1, *P. protegens* CHA0, and *P. putida* F1 (data not shown) exhibited no responses to HEPES buffer stored in either type of container. These results suggest that component(s) leaching from the borosilicate glass served as a chemoattractant(s) for *R. pseudosolanacearum* Ps29. Because boric acid and silicate should be the major compounds leaching from borosilicate glass, I assessed the chemotactic response of *R. solanacearum* Ps29 to these compounds. There was no significant difference between the responses to 5 mM silicate and the control (HEPES buffer stored in a plastic tube), but *R. pseudosolanacearum* Ps29 exhibited a significantly stronger response to 0.5 mM boric acid than to HEPES buffer ($P < 0.05$ by Student's *t* test) (Fig. 4.1B). This result clearly demonstrates that boric acid is a chemoattractant for *R. pseudosolanacearum* Ps29 and suggests that boric acid leaching from glassware was the cause of the chemotactic response of *R. pseudosolanacearum* Ps29 to the "negative" control. Therefore, all subsequent experiments were carried out without glassware (excepting glass capillaries and cover slips in the chemotaxis assay).

4.3.2. Characterization of chemotaxis to boric acid

As shown in Fig. 4.2A, *R. pseudosolanacearum* Ps29 showed a concentration-dependent chemotactic response to boric acid. The threshold concentration of boric acid for chemotaxis was 0.01 mM. I demonstrated that L-malate strongly attracts *R. pseudosolanacearum* Ps29 in chapter 2. I found that at high concentrations (>0.1 mM), boric acid elicited a chemotactic response comparable to or stronger than that elicited by L-malate, indicating that boric acid is also a strong chemoattractant for *R. pseudosolanacearum* Ps29.

The effect of pH on boric acid chemotaxis is shown in Fig. 4.2B. There was no significant difference between the strength of chemotaxis at pH 6.0 and 7.0. As a Lewis acid, boric acid abstracts OH from water[81]:

$$B(OH)_3 + H_2O \leftrightarrow B(OH)_4^- + H^+ \ (pK_a = 9.14) \qquad \text{eq. (1)}$$

The corresponding Henderson-Hasselbalch equation is:

$$pH = pK_a + \log ([B(OH)_4^-]/[B(OH)_3]) \qquad \text{eq. (2)}$$

Solving eq. 2 indicates that at pH 6.0, a concentration of borate $[B(OH)_4^-]$(0.058% boron) is 10-fold less than at pH 7.0 (0.57% boron). However, the strength of boric acid chemotaxis at pH 6.0 was comparable to that at pH 7.0, which suggests that the chemotaxis sensor detects boric acid ($B(OH)_3$) (alternatively, $B(OH)_3 + B(OH)_4^-$) but not $B(OH)_4^-$ alone.

4.3.3. Identification of chemoreceptor for boric acid

MCPs are transmembrane chemoreceptors that serve as sensor molecules in bacterial chemotaxis. To identify the gene encoding the MCP for boric acid, the library of *mcp*

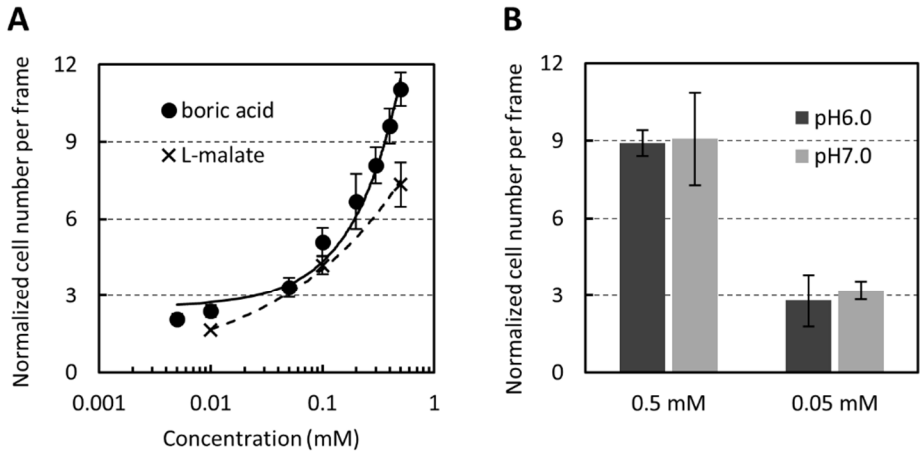

Fig. 4.2. Characterization of chemotaxis to boric acid by *R. pseudosolanacearum* Ps29. **A**, concentration-dependent chemotaxis toward boric acid and L-malate. **B**, chemotaxis to boric acid at pH6.0 and 7.0. Vertical bars represent the standard error of measurement for experiments performed at least in triplicate.

single-deletion mutants was screened for chemotactic responses to boric acid as described in chapter 2. Among 22 *mcp* single-deletion mutants, strain DPS11, in which the RS_RS17100 (old locus tag RSc3412) orthologue was deleted, failed to respond to boric acid (Fig. 4.3). Introduction of plasmid pPS11, which harbors the RS_RS17100 orthologue of *R. pseudosolanacearum* Ps29, restored the chemotactic response of strain DPS11 to boric acid, demonstrating that the RS_RS17100 homolog encodes an MCP for boric acid. The RS_RS17100 homologous protein of strain Ps29 was 99% identical (512 of 515 amino acids [aa]) to GMI1000 RS_RS17100 (Table 2.5). I accordingly renamed the RS_RS17100 homolog *mcpB* (MCP for boric acid).

4.3.4. Ligand specificity of McpB

To investigate ligand specificity of McpB, I measured chemotactic responses of *R. pseudosolanacearum* Ps29 to compounds having similar structures to boric acid (Fig. 4.4). They included methylboronic acid ($CH_3B(OH)_2$), methanediol ($CH_2(OH)_2$) (provided as formaldehyde), methanol (CH_2OH), aluminum hydroxide ($Al(OH)_3$), phosphate, sulfate, and arsenate (both methanetetrol ($C(OH)_4$) and methanetriol ($CH(OH)_3$) are hypothetical

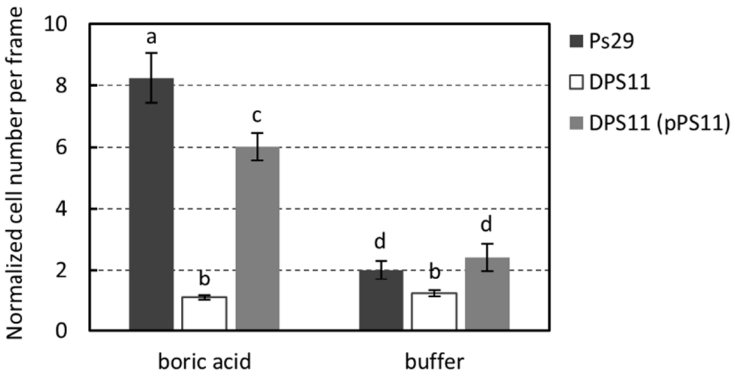

Fig. 4.3. Chemotaxis by *R. pseudosolanacearum* Ps29 strains to 0.1 mM boric acid. Ps29, wild type; DPS11, *mcpB* deletion mutant; DPS11 (pPS11), DPS11 harboring pPS11. Videotape frames were analyzed at the initiation of observation and 1.5 min after initiation. Vertical bars represent the standard error of measurement for experiments performed at least in triplicate. Different letters indicate significant differences ($P < 0.05$ by Student's *t* test).

compounds and thus unavailable). *R. pseudosolanacearum* Ps29 cells showed weak attractive responses to a negative control (HEPES buffer) because they responded to a small amount of boric acid diffused from a glass capillary. Although *R. pseudosolanacearum* Ps29 cells showed a strong responses to 0.5 mM boric acid, methanediol, methanol, aluminum hydroxide, and sulfate elicited only basal responses in Ps29 cells (i.e. the responses were not significantly different from that to the negative control). Responses to phosphate and arsenate were significantly higher than that to the negative control. To investigate whether McpB senses phosphate and arsenate, I compared responses of the wild-type strain and *mcpB* mutant of *R. pseudosolanacearum* Ps29 (Fig. 4.4B). The *mcpB* mutant showed decreased responses to phosphate and arsenate compared to those of the wild-type strain. However, the differences of the strength of chemotaxis to phosphate and arsenate between the wild-type strain and the mutant strain were similar to that to the negative control, suggesting that decreased responses of the *mcpB* mutant to phosphate and arsenate were due to the lack of boric

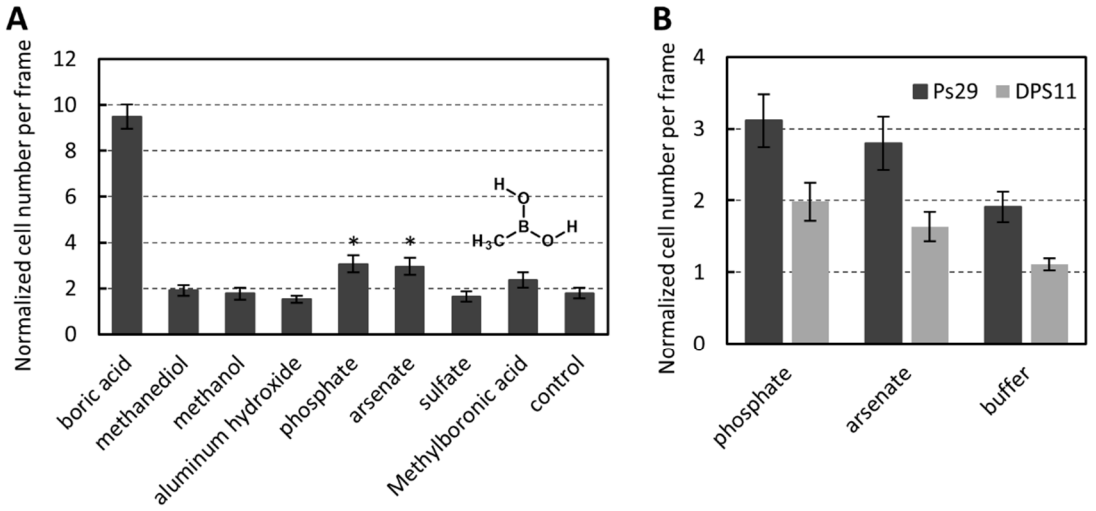

Fig. 4.4. Chemotaxis by *R. pseudosolanacearum* Ps29 strains to compounds with similar structure to boric acid. **A**, responses by wild-type strain. **B**, responses to phosphate and arsenate by wild-type and *mcpB* deletion mutant (DPS11). Boric acid and methylboronic acid, 0.5 mM; other compounds other than aluminum hydroxide, 5 mM; aluminum hydroxide, supernatant of suspension (because of low solubility). Vertical bars represent the standard error of measurement for experiments performed at least in triplicate. Asterisks indicate significant difference compared with the responses to buffer (P <0.05 by Student's t test).

acid chemotaxis. In addition, *R. pseudosolanacearum* Ps29 was not attracted to a boric acid derivative, methylboronic acid, in which the boron atom is bonded to only two hydroxyl groups (Fig. 4.4A). This result suggested that the three hydroxyl groups of boric acid are essential for recognition by *R. pseudosolanacearum* Ps29. When taken together, McpB does not sense these compounds with similar chemical structures.

4.3.5. Direct binding of boric acid to the McpB LBD

McpB shows structural characteristics typical of MCPs as described above. Chemotactic ligands are known to bind to the periplasmic domains (i.e., LBDs) of MCPs, thereby initiating chemotactic signaling. Dense alignment surface analysis[68] identified the LBD of McpB as a region spanning 157 amino acids (residues 33 to 187). To determine whether McpB recognizes boric acid directly, the LBD of McpB was overexpressed and purified from an *E. coli* lysate soluble fraction. Purified McpB LBD was then analyzed using isothermal titration calorimetry (ITC). Titration of buffer with 1 mM boric acid

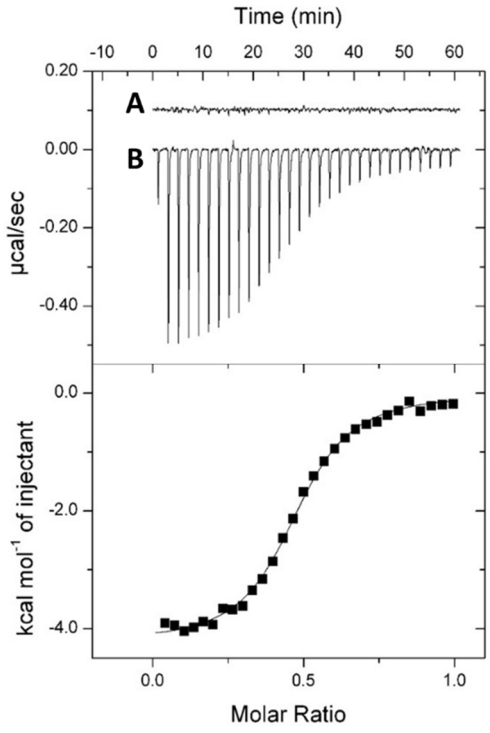

Fig. 4.5. Isothermal titration calorimetry (ITC). **A**, titration of ITC buffer with 1 mM boric acid; **B**, titration of 200 µM McpB LBD with 1 mM boric acid. Upper panel shows the raw titration data, and lower panel shows the integrated, dilution-corrected and concentration-normalized peak areas of the raw titration data. The data were fitted using the One Set of Sites model of the MicroCal version of Origin7.

generated almost no heat of dilution (Fig. 4.5A). By contrast, titration of 200 μM McpB LBD with 1 mM boric acid produced a large heat change that diminished as protein saturation approached (Fig. 4.5B). Analysis of the data revealed that binding of boric acid to the McpB LBD was driven by a favorable enthalpy change (ΔH = -4.52 kcal/mol), with a K_D of 5.44 μM. These results demonstrate that boric acid binds to McpB LBD directly.

4.3.6. Characterization of binding between the McpB LBD and boric acid

Several analytical techniques were used to characterize the McpB boric acid-sensing mechanism. The far-UV circular dichroism (CD) spectrum for the McpB LBD showed minima at 208 and 222 nm, which is typical of α-helical proteins (Fig. 4.6A). The α-helical content of the McpB LBD was calculated at 78%, which was similar to the α-helical content of 89% derived from the McpB LBD model (Fig. 4.7). The addition of boric acid produced no major changes in the CD spectrum of the McpB LBD, indicating that ligand binding does not significantly alter the McpB LBD secondary structure. Thermal unfolding of the McpB LBD was then assessed by monitoring the CD signal at

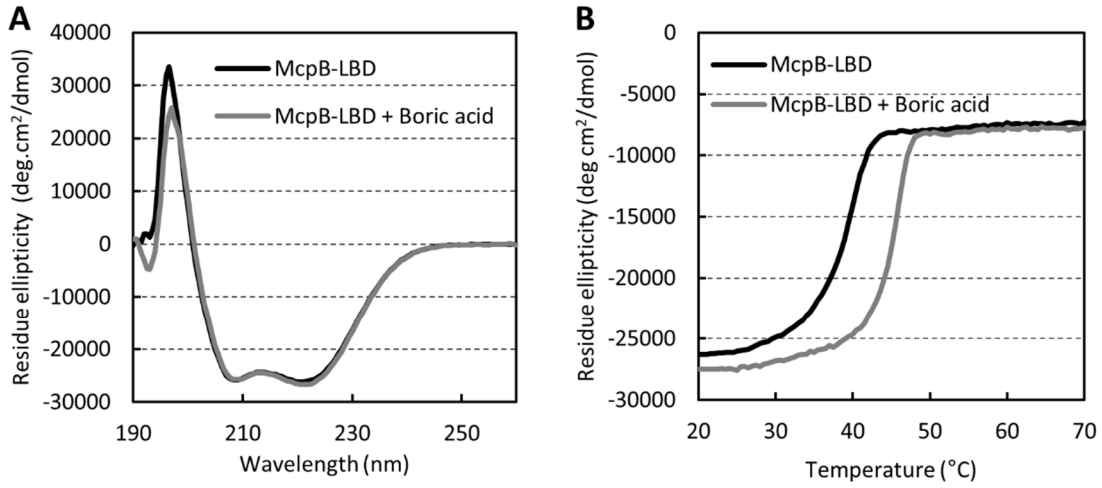

Fig. 4.6. Circular dichroism (CD) spectroscopic analysis of Mcp LBD. **A**, CD spectra of 20 μM McpB LBD in the absence and presence of 100 μM boric acid. **B**, thermal denaturation of 20 μM McpB LBD in the absence and presence of 100 μM boric acid as determined by CD ellipticity at 222 nm. Shown are average curves from triplicate experiments.

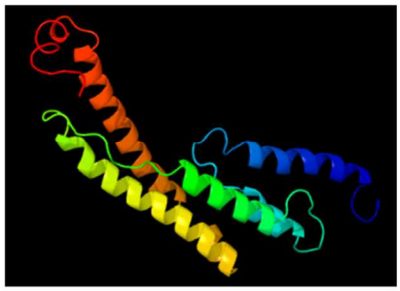

Fig. 4.7. The predicted three-dimensional (3D) structure of the *R. pseudosolanacearum* Ps29 McpB LBD. The 3D structure was predicted using the Phyre[2] algorithm (intensive mode). Blue, N-terminus; red, C-terminus.

222 nm (Fig. 4.6B). In the absence of boric acid, the midpoint of protein unfolding (T_m) was 39.3°C. However, a T_m of 45.2°C was observed in the presence of boric acid, corresponding to an increase of approximately 6°C.

As shown in Fig. 4.5, ITC analysis revealed that boric acid binds to the McpB LBD with an N value (binding ratio) of 0.4, suggesting that the McpB LBD dimer recognizes one boric acid molecule. Purified McpB LBD was subjected to gel filtration chromatography in the absence and presence of its ligand, and its molecular weights were estimated at 41.2 and 42.7 kDa, respectively, which were significantly higher than McpB LBD monomer size (19.3 kDa) (Fig. 4.8). This observation was confirmed in more detail by sedimentation velocity ultracentrifugation analysis. Fig. 4.9 shows the sedimentation coefficient distribution obtained for the McpB LBD in the absence and presence of boric acid. In the absence of ligand, a single peak with an *s* value (standardized to 20°C in water) of 2.53 S was observed, corresponding to an estimated molecular weight of 36.5 kDa, which is almost same size as an McpB LBD dimer. The sedimentation coefficient distribution of the McpB LBD in the presence of boric acid was essentially identical to that in the absence of boric acid. These results indicate that the McpB LBD is present exclusively as a dimer and recognizes one boric acid molecule.

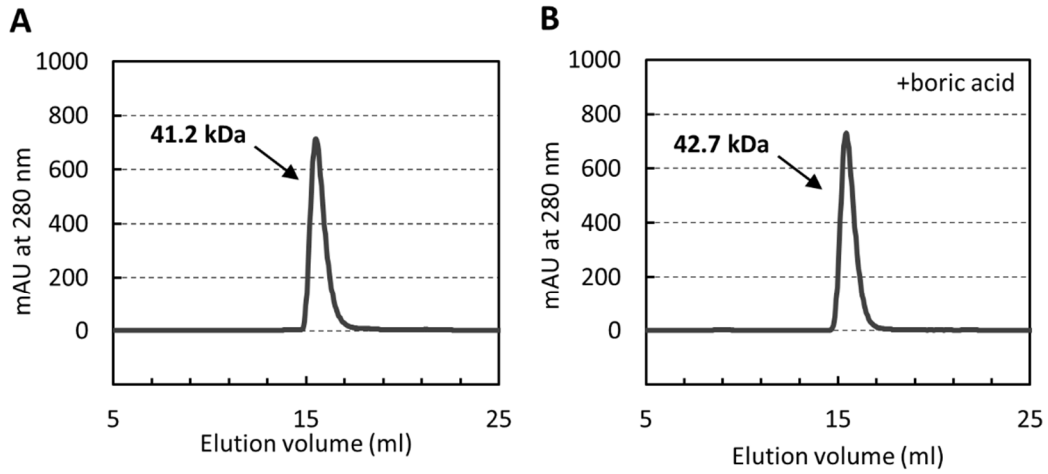

Fig. 4.8. Elution profiles of McpB LBD using gel filtration chromatography. **A**, McpB LBD in the absence of boric acid. **B**, McpB in the presence of 1 mM boric acid. Estimated molecular weights are shown in the panels.

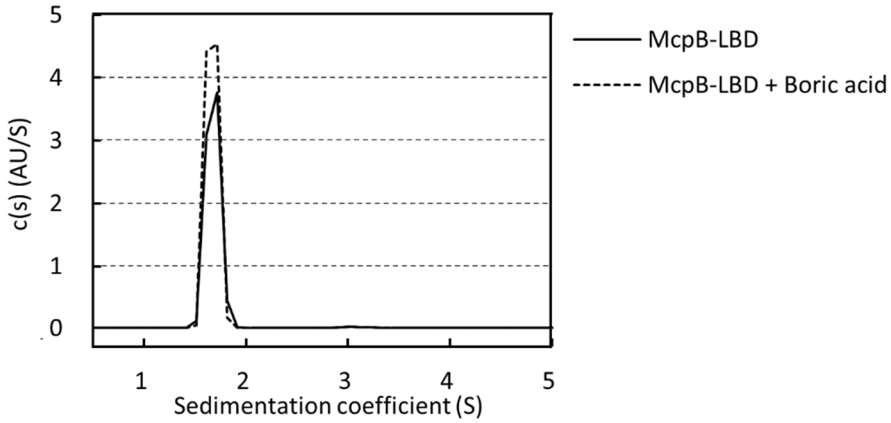

Fig. 4.9. Determination of the oligomeric state of McpB LBD using analytical ultracentrifugation. Shown are sedimentation coefficient distributions for 1.5 mg/ml McpB LBD in the absence and presence of 1 mM boric acid.

4.3.7. Biological meaning of boric acid taxis

The biological significance of chemotaxis in nature is generally that it enables bacteria to locate food sources. I therefore examined whether boric acid is essential for the growth of *R. pseudosolanacearum* Ps29. Strain Ps29 was cultured in plastic tubes with RSM medium containing different concentrations of boric acid (0-10 mM). There was no significant difference in growth at 0-1 mM boric acid, although growth at the highest

concentration (10 mM) of boric acid was significantly higher (1.7 fold) than in the absence of boric acid (Fig. 4.10).

Chemotaxis is also important for virulence in *R. pseudosolanacearum*[20]. I investigated the role of McpB-mediated chemotaxis in tomato plant infection using a highly virulent *R. pseudosolanacearum* MAFF106611 strains. Strain MAFF106611 also

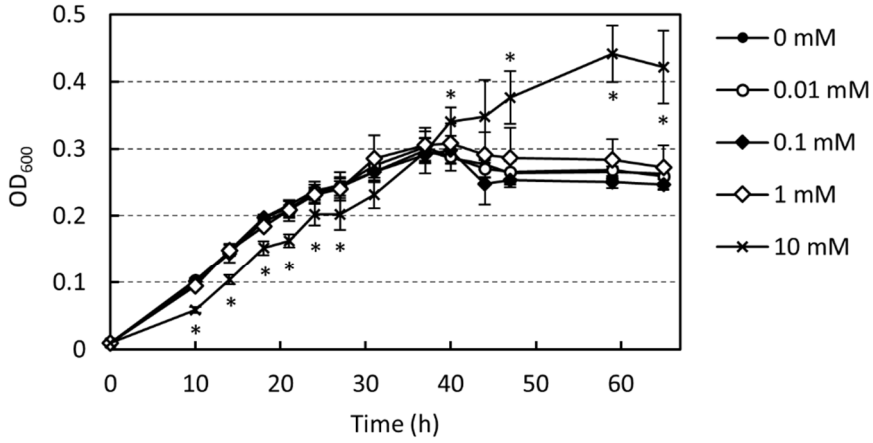

Fig. 4.10. Growth curves for wild type *R. pseudosolanacearum* Ps29 in RSM medium containing 5 g/l glucose and 0 to 10 mM boric acid. Vertical bars represent the standard error of measurement for triplicate experiments. Asterisks indicate significant differences in growth of the wild-type strain in the absence of boric acid and in the presence of 10 mM boric acid (P <0.05 by Student's t test).

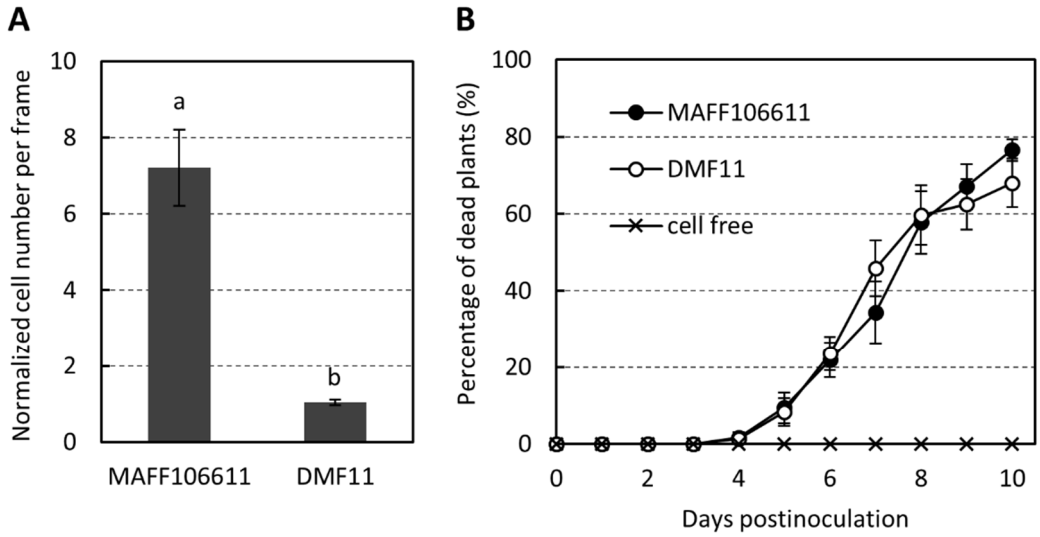

Fig. 4.11 Analyses using *R. pseudosolanacearum* MAFF106611 strains. **A**, chemotaxis to 5 mM boric acid. Videotape frames were analyzed at the initiation of observation and 2 min after initiation. Different letters indicate significant difference (P < 0.05 by Student's t test). **B**, Sand-soak inoculation virulence assay. MAFF106611, wild-type strain; DMF11, the *mcpB* deletion mutant.

has *mcpB* homologs, its product of which are 99% identical to the *R. pseudosolanacearum* Ps29 counterpart and showed chemotaxis to boric acid (Fig. 4.11A). The unmarked MAFF106611 *mcpB* deletion mutant (DMF11) failed to respond to boric acid (Fig. 4.11A). A sand-soak inoculation experiment, in which cells of test strains are inoculated into sand away from the target plant, was conducted to assess plant infection by the *R. pseudosolanacearum* strains. I found that the *mcpB* deletion mutant of MAFF106611 was as infectious as wild-type MAFF106611 in this assay (Fig. 4.11B).

4.4 Discussion

In this chapter, I conducted a detailed investigation of the positive chemotactic response of *R. pseudosolanacearum* Ps29 to "negative" control HEPES buffer and found that this response was directed toward boric acid leaching from borosilicate glass into the buffer. The most important finding in this chapter was the identification of boric acid as a novel chemoattractant. In addition, I identified the bacterial protein McpB as a chemoreceptor for boric acid by screening the library of *mcp* single-deletion mutants. The results of ITC assays examining the binding of boric acid to the LBD of McpB confirmed that this protein is a boric acid MCP.

The putative LBD of McpB belongs to the cluster-I group (120-210 amino acids), with a predicted LBD size of 157 amino acids and is annotated as 4-helix-bundle (4HB) in Pfam and InterPro. Protein structure predictions using the Phyre^2 fold recognition server[55] also suggested the presence of a 4HB domain in the *R. pseudosolanacearum* Ps29 McpB LBD (Fig. 4.7), similar to the structures predicted for McpM and McpT[59], as well as *E. coli* Tar and Tsr[51].

ITC analysis demonstrated that McpB LBD dimer binds one boric acid molecule.

Although *P. aeruginosa* does not respond to boric acid, it exhibits chemotactic responses to phosphate[10], which has a similar chemical structure to boric acid. Wu *et al*. identified two CtpH and CtpL as MCPs for phosphate in *P. aeruginosa*[37]. Rico-Jimènez *et al*. demonstrated that CtpL recognizes phosphate by biding of the periplasmic phosphate binding protein (PstS) in its phosphate loaded state, while CtpH binds directly phosphate[82]. They reported that CtpH LBD dimer bond one phosphate molecule. Since CtpH also has a 4HB in its LBD, binding of boric acid to McpB LBD has some parallels to binding of phosphate to CtpH LBD.

As performed in chapter 2 and 3, I performed a BLASTP using the McpB LBD as the query sequence. This similarity search indicated that several species of beta- and gamma-proteobacteria express proteins with highly similar sequence to the McpB LBD, most of which are putative MCPs. The *R. solanacearum* species complex, including strains GMI1000 (phylotype I), FQY_4 (phylotype I), SD54 (phylotype I), K60-1 (phylotype II), CFBP2957 (phylotype II), and PSI07 (phylotype IV), expresses McpB orthologues exhibiting a high degree of similarity to *R. pseudosolanacearum* Ps29 McpB LBD (>90% identity). Other beta-proteobacteria, such as *Parabukholderia* sp., *Massilia namucuonensis*, and *Burkholderia gladioli*, express MCPs with LBDs similar to that of McpB (approximately 50% identity). A number of gamma-proteobacteria express proteins with McpB LBD homologous sequences (up to 68% identity), including *Dickeya* sp., *Cedecea neteri*, *Pectobacterium carotovorum*, *Erwinia* sp., *Xanthomonas* sp., and *Pseudomonas syringae*. Interestingly, most of these bacteria are plant pathogens.

Boron serves as a micronutrient in prokaryotes and eukaryotes. Some bacteria produce biologically active compounds containing boron[83]. For example, *Streptomyces antibioticus*, *Streptomyces griseus*, and *Sorangium cellulosum* produce boromycin[84],

aplasmomycin[85], and tartrolons[86], respectively, all of which are antibiotics active against gram-positive bacteria. Many gram-positive and -negative bacteria produce furanosyl borate diester (known as autoinducer-2), which functions as a signaling compound in cell-to-cell communication[87]. Boron is also involved in the growth of nitrogen-fixing bacteria. Heterocystous cyanobacteria (*Nodularia* sp., *Chlorogloeopsis* sp., and *Nostoc* sp.) and actinomycetes *Frankia* strain BCU110501 require boron for growth under nitrogen-fixing conditions[88,89]. Boron plays a role in the stabilization of heterocysts in cyanobacteria and vehicle envelopes in *Frankia*, which are essential for the exclusion of nitrogenase-poisoning oxygen. Boron is reportedly required for the establishment of effective legume-*Rhizobium* symbiosis. In addition, boron is necessary for maintaining the cell wall structure of nodules[90] and the development of infection threads and nodule invasion[41]. In higher plants, boron is an essential micronutrient, as it is required for maintaining cell wall integrity[91]. The major components of plant cell walls are cellulose, hemicellulose, and pectin polysaccharides. Borate cross-links two chains of the pectin polysaccharide rhamnogalacturonan II by binding to their apiose residues; this cross-linking contributes to the maintenance of cell wall integrity[92].

What biological significance does boric acid chemotaxis have? Chemotaxis toward boric acid could be a “fortuitous” response mediated by McpB. In a previous study, co-worker identified McpT as an MCP for L-tartrate, which *R. pseudosolanacearum* Ps29 can utilize as a sole carbon source[59]. McpT recognizes D-malate, an unnatural enantiomer of malate, as a strong attractant, although strain Ps29 cannot utilize this compound. Our research group concluded that chemotaxis toward D-malate is a fortuitous response associated with McpT. To more clearly determine whether boric acid chemotaxis is a fortuitous response, I analyzed the chemotaxis of wild type strain Ps29 to

several compounds with similar structures to boric acid. Any of these compounds did not attract cells, suggesting that boric acid chemotaxis is not a fortuitous response.

Many attractants are growth substrates, for example amino acids, organic acids, sugars, and phosphate. Boric acid could be an important nutrient for the growth of *R. pseudosolanacearum* Ps29. I therefore confirmed whether there were differences in growth in a defined medium containing different concentration of boric acid. At 10 mM boric acid, cell growth was finally improved although it was inhibited at an early stage of growth. However, because 10 mM is not an environmentally relevant concentration with respect to boron (5 mg/kg in basalts; 100 mg/kg in shales[93]), the observed enhanced growth in 10 mM boric acid is probably not environmentally significant.

Chemotaxis also plays an important role in facilitating ecological interactions, including plant infection by *R. solanacearum*[20]. The distribution of McpB orthologues is limited to plant pathogenic bacteria belonging to the beta- and gamma-proteobacteria, and borate is a ubiquitous constituent of higher plants. These data suggest that boric acid functions as a chemotactic signaling compound that facilitates interactions between bacterial cells and plants. To confirm this possibility, I conducted infection assay using sand-soak inoculation method. The infectivity of strain DMF11 (MAFF106611 *mcpB* deletion mutant) did not differ significantly from that of wild-type MAFF106611. However, this result does not rule out the possibility that McpB-mediated chemotaxis is involved in plant infection, because borate is included in PNS medium used to support the growth of tomato plants. Therefore, a novel assay system should be developed to assess the role of boric acid chemotaxis in the infection of plants by *R. pseudosolanacearum*.

CHAPTER5
Conclusion

The *R. solanacearum* species complex requires chemotaxis to exert full virulence on host plants[20]. Since the soil-borne pathogen is attracted to plant root exudate, comportment(s) of root exudate might play a role as a signal molecule. However, chemotactic signal molecules involved in plant infection by the *R. solanacearum* species complex have not been identified. In this study, I attempted to elucidate the chemotaxis mechanism involved in plant infection of the bacterial wilt pathogen by identification of unknown MCPs function and using the *mcp* mutants.

In chapter 2, chemotaxis analysis using *R. pseudosolanacearum* strain Ps29 as a model of highly motile strain revealed that this strain showed attractive responses to 16 proteinogenic amino acids (excepting glycine, L-arginine, L-lysine and L-proline), organic acids (malate, citrate, tartrate, succinate and fumarate) and phosphate. To identify chemoreceptors for these attractants, I constructed a library of 22 *mcp* gene single-deletion mutants of *R. pseudosolanacearum* Ps29. Screening of the mutant library identified McpA and McpM as a chemoreceptor for L-amino acids and L-malate, respectively. Amino acids and L-malate are major components of plant root exudate[27]. Therefore, I next investigated whether chemotaxis to these compounds play an important role for plant infection of *R. pseudosolanacearum* using sand-soak inoculation virulence assay was used. In this assay, because bacterial cells were inoculated into sand at a spot about 30 mm away from a tomato plant, cells need to locate and invade plant from a distance to infect plant. The sand-soak inoculation virulence assay using *R. pseudosolanacearum* MAFF106611 as a model of highly virulent strain and its *mcp*

mutants revealed that the *mcpM* deletion mutant, which is deficient in L-malate taxis, showed significantly less infectious than wild-type strain. The infectivity of the *mcpA* deletion mutant, which is deficient in L-amino acids taxis, did not differ significantly from that of wild-type strain. On the other hand, the infectivity of the *mcpM* and *mcpA* mutants was similar to that of wild-type parent when these strains were directly inoculated into tomato roots. The results of the competitive tomato plant colonization assays were consistent with those of virulence assay. These results demonstrate that McpM-mediated chemotaxis to L-malate is required for the early stage of plant infection by *R. pseudosolanacearum* MAFF106611 while McpA-mediated chemotaxis to amino acids is not important for plant infection of the pathogen. However, the *cheA* deletion mutant, which is nonchemotactic but motile, had decreased infectivity compared to that of the *mcpM* deletion mutant, suggesting that chemotaxis to root exudate component(s) other than L-malate may be involved in plant infection by *R. pseudosolanacearum*.

Citrate, which is one of major component of plant root exudate[44] and strong chemoattractant for the *R. solanacearum* species complex, is a likely candidate for compound contributing to locate plant roots when plant infection. The failure to identify chemoreceptor(s) for citrate by the library of *mcp* single-deletion mutants in chapter 2 suggests that multiple receptors are involved in citrate taxis. In chapter 3, I therefore constructed multiple *mcp* deletion mutants of *R. pseudosolanacearum* Ps29 as a new library, and tried to identify citrate MCPs and to assess involvement of citrate taxis in plant infection. Analysis using the multiple-deletion mutant library successfully identified McpC and McpP as a chemoreceptor for citrate. Interestingly, McpC can also sense citrate/metal^{2+} complex, but McpP is not involved in this taxis. The sand-soak inoculation virulence assay and competitive plant colonization assay using tomato seedling and *R.*

pseudosolanacearum MAFF106611 strains revealed that the infectivity and colonization ability of *mcpC* and *mcpP* double-deletion mutant (DMF0516) did not differ from those of wild-type, suggesting that citrate taxis is not required for these ability. However, this result does not rule out the possibility that chemotaxis to citrate is involved in plant infection, because strain DMF0516 still has citrate MCP(s) other than McpC and McpP.

In chapter 4, I found boric acid as a novel chemoattractant by a detailed investigation of a unique phenomenon that *R. pseudosolanacearum* Ps29 responded to "negative" control. Screening of 22 *mcp* single-deletion mutants identified McpB as a boric acid chemoreceptor. Isothermal titration calorimetry and other several analyses using the purified McpB ligand-binding domain (LBD) revealed that McpB LBD dimer recognizes one boric acid molecule directly. This is the first report of a biological boric acid sensor. Interestingly, Protein BLAST analysis showed that MCPs with McpB LBD homologous sequences are differentially distributed in plant pathogens. This result suggests a possibility that boric acid taxis plays an important role in the infection by plant pathogens while in this study I could not experimentally demonstrate it.

In this study, I identified function of some chemoreceptors and partially elucidated hitherto unknown chemotactic mechanism involved in plant infection of the *R. pseudosolanacearum* by using the *mcp* mutants deficient in chemotaxis to particular compound. However, the specific functions and contributions to plant infection of more than half of 22 chemoreceptors are yet to be determined, and also the role of chemotaxis to boric acid in plant infection is unknown. Further studies are needed to more fully understand chemotaxis mechanism involved in the infection of the *R. solanacearum* species complex. The chemotaxis knowledge obtained in this and further studies could be useful for biocontrol of the bacterial wilt disease by this pathogen in the future.

References

1. Gillings MR and Fahy P. Genomic fingerprinting: towards a unified view of the *Pseudomonas solanacearum* species complex. In *Bacterial wilt: the disease and its causative agent,* Pseudomonas solanacearum. (ed. Hayward AC and Hartman GL), p 95-112. CAB International, Wallingford, United Kingdom (1994).
2. Safni I, Cleenwerck I, De Vos P, Fegan M, Sly L, and Kappler U. Polyphasic taxonomic revision of the *Ralstonia solanacearum* species complex: proposal to emend the descriptions of *Ralstonia solanacearum* and *Ralstonia syzygii* and reclassify current *R. syzygii* strains as *Ralstonia syzygii* subsp. syzygii subsp. nov., *R. solanacearum* phylotype IV strains as *Ralstonia syzygii* subsp. *indonesiensis* subsp. nov., banana blood disease bacterium strains as *Ralstonia syzygii* subsp. *celebesensis* subsp. nov. and *R. solanacearum* phylotype I and III strains as *Ralstonia pseudosolanacearum* sp. nov. *Int J Syst Evol Microbiol* **64**:3087-3103 (2014).
3. Hayward AC. Biology and epidemiology of bacterial wilt caused by *Pseudomonas solanacearum*. *Annu Rev Phytopathol* **29**:65-87 (1991).
4. Hayward AC. *Ralstonia solanacearum* In *Encyclopedia of microbiology, vol 4*. (ed. Lederberg J *et al*.) p32-42. Academic Press Inc, San Diego, CA. (2000).
5. Genin S. Molecular traits controlling host range and adaptation to plants in *Ralstonia solanacearum*. *New Phytologist* **187**:920-928 (2010).
6. Peeters N, Guidot A, Vailleau F, and Valls M. *Ralstonia solanacearum,* a wide spread bacterial plant pathogen in the post-genomic era. *Mol Plant Pathol* 14:651-662 (2013).
7. Adler J. Chemotaxis in bacteria. *Science* **153**:708-716 (1966).
8. Stock JB and Surette MG. Chemotaxis In Escherichia coli *and* Salmonella*: cellular and molecular biology, 2nd ed.* (ed. Neidhardt FC *et al*.) p1103-1129. ASM press, Washington DC, USA (1996).

9. Porter SL, Wadhams GH, and Armitage JP. Signal processing in complex chemotaxis pathways. *Nat Rev Microbiol* **9**:153-165 (2011).
10. Kato J, Ito A, Nikata T, and Ohtake H. Phosphate taxis in *Pseudomonas aeruginosa*. *J Bacteriol* **174**:5149-5151 (1992).
11. Oku S, Hayashida M, Tajima T, Nakashimada Y, and Kato J. Negative chemotaxis to trichloroethylene and its chemosensory protein in *Pseudomonas putida* F1. *J Biotechnol* **150**:S218-S218 (2010).
12. Oku S, Komatsu A, Tajima T, Nakashimada Y, and Kato J. Identification of chemotaxis sensory proteins for amino acids in *Pseudomonas fluorescens* Pf0-1 and their involvement in chemotaxis to tomato root exudate and root colonization. *Microbes Environ* **27**:462-469 (2012).
13. Moench TT and Konetzka WA. Chemotaxis in *Pseudomonas aeruginosa*. *J Bacteriol* **133**:427-429 (1978).
14. Moulton RC and Montie TC. Chemotaxis by *Pseudomonas aeruginosa*. *J Bacteriol* **137**:274-280 (1979).
15. Taguchi K, Fukutomi H, Kuroda A, Kato J, and Ohtake H. Genetic identification of chemotactic transducers for amino acids in *Pseudomonas aeruginosa*. *Microbiology* **143**:3223-3229 (1997).
16. Parales RE and Harwood CS. Bacterial chemotaxis to pollutants and plant-derived aromatic molecules. *Curr Opin Microbiol* **5**:266-273 (2002).
17. Miller LD, Yost CK, Hynes MF, and Alexandre G. The major chemotaxis gene cluster of *Rhizobium leguminosarum* bv viciae is essential for competitive nodulation. *Mol Microbiol* **63**:348-362 (2007).
18. de Weert S, Vermeiren H, Mulders IHM, Kuiper I, Hendrickx N, Bloemberg GV, Vanderleyden J, De Mot R, and Lugtenberg BJ. Flagella-driven chemotaxis towards exudate components is an important trait for tomato root colonization by *Pseudomonas fluorescens*.

Mol Plant Microbe Interact **15**:1173-1180 (2002).

19. Oku S, Komatsu A, Nakashimada Y, Tajima T, and Kato J. Identification of *Pseudomonas fluorescens* chemotaxis sensory proteins for malate, succinate, and fumarate, and their involvement in root colonization. *Microbes Environ* **29**:413-419 (2014).
20. Yao J and Allen C. Chemotaxis is required for virulence and competitive fitness of the bacterial wilt pathogen *Ralstonia solanacearum*. *J Bacteriol* **188**:3697-3708 (2006).
21. Tans-Kersten J, Huang H, and Allen C. *Ralstonia solanacearum* needs motility for invasive virulence on tomato. *J Bacteriol* **183**:3597-3605 (2001).
22. Yao J and Allen C. The plant pathogen *Ralstonia solanacearum* needs aerotaxis for normal biofilm formation and interactions with its tomato host. *J Bacteriol* **189**:6415-6424 (2007).
23. Lefeuvre P, Cellier G, Remenant B, Chiroleu F, and Prior P. Constraints on genome dynamics revealed from gene distribution among the *Ralstonia solanacearum* species. *PLoS One* **8**:e63155 (2013).
24. Gaworzewska ET and Carlile MJ. Positive chemotaxis of *Rhizobium leguminosarum* and other bacteria towards root exudates from legumes and other plants. *Microbiology* **128**:1179-1188 (1982).
25. Allard-Massicotte R, Tessier L, Lécuyer F, Lakshmanan V, Lucier J, Garneau D, Caudwell L, Vlamakis H, Bais HP, and Beauregard P. *Bacillus subtilis* early colonization of Arabidopsis thaliana roots involves multiple chemotaxis receptors. *mBio* **7**:e01664-16 (2016).
26. Antúnez-Lamas M, Cabrera-Ordóñez E, López-Solanilla E, Raposo R, Trelles-Salazar O, Rodríguez-Moreno A, and Rodríguez-Palenzuela P. Role of motility and chemotaxis in the pathogenesis of *Dickeya dadantii* 3937 (ex *Erwinia chrysanthemi* 3937). *Microbiology* **155**:434-442 (2009).
27. Dennis PG, Miller AJ, and Hirsch PR. Are root exudates more important than other sources of rhizodeposits in structuring rhizosphere bacterial communities? FEMS Microbiol Ecol **72**:313-327 (2010).

28. Vande Broek A and Vanderleyden J. The role of bacterial motility, chemotaxis, and attachment in bacteria-plant interactions. *Mol Plant Microbe Interact* **8**:800-810 (1995).
29. Brencic A and Winans SC. Detection of and response to signals involved in host-microbe interactions by plant-associated bacteria. *Microbiol Mol Biol Rev* **69**:155-194 (2005).
30. Neal AL, Ahmad S, Gordon-Weeks R, and Ton J. Benzoxazinoids in root exudates of maize attract *Pseudomonas putida* to the rhizosphere. *PLoS One* **7**:e35498 (2012).
31. Webb BA, Hildreth S, Helm RF, and Scharf BE.. *Sinorhizobium meliloti* chemoreceptor McpU mediates chemotaxis toward host plant exudates through direct proline sensing. *Appl Environ Microbiol* **80**:3404-3415 (2014).
32. Hendrick CA and Sequeira L. Lipopolysaccharide-defective mutants of the wilt pathogen *Pseudomonas solanacearum*. *Appl Environ Microbiol* **48**:94–101 (1984).
33. Clough SJ, Schell MA, and Denny TP. Evidence for involvement of a volatile extracellular factor in *Pseudomonas solanacearum* virulence gene expression. *Mol Plant Microbe Interact* **7**:621-630 (1994).
34. Sambrook J, Fritsch EF, and Maniatis T. *Molecular cloning: a laboratory manual, 2nd ed.* Cold Spring Harbor Laboratory Press, Cold Spring Harbor, NY (1989).
35. Nikata T, Sumida K, Kato J, and Ohtake H. Rapid method for analyzing bacterial behavioral responses to chemical stimuli. *Appl Environ Microbiol* **58**:2250-2254 (1992).
36. Schäfer A, Tauch A, Jäger W, Kalinowski J, Thierbach G, and Pühler A. Small mobilizable multi-purpose cloning vectors derived from the *Escherichia coli* plasmids pK18 and pK19: selection of defined deletions in the chromosome of *Corynebacterium glutamicum*. *Gene* **145**:69-73 (1994).
37. Wu H, Kato J, Kuroda A, Ikeda T, Takiguchi N, and Ohtake H. Identification and characterization of two chemotactic transducers for inorganic phosphate in *Pseudomonas aeruginosa*. *J Bacteriol* **182**:3400-3404 (2000).
38. Vieira J and Messing J. The pUC plasmids, an M13mp7-derived system for insertion

mutagenesis and sequencing with synthetic universal primers. *Gene* **19**:259-268 (1982).

39. Schweizer HP. *Escherichia-Pseudomonas* shuttle vectors derived from pUC18/19. *Gene* **97**:109–112 (1991).
40. Monteiro F, Sole M, van Dijk I, and Valls M. A chromosomal insertion toolbox for promoter probing, mutant complementation, and pathogenicity studies in *Ralstonia solanacearum*. *Mol Plant Microbe Interact* **25**:557-568 (2012).
41. Hoffland E, Findenegg GR, and Nelemans JA. Solubilization of rock phosphate by rape. *Plant Soil* **113**:161-165 (1989).
42. Yamada T, Kawasaki T, Nagata S, Fujiwara A, Usami S, and Fujie M. New bacteriophages that infect the phytopathogen *Ralstonia solanacearum*, *Microbiology*, **153**:2630-2639 (2007).
43. Simon R, Prifer U, and Pühler A. A broad host range mobilization system for in vivo genetic engineering: transposon mutagenesis in Gram negative bacteria. *Nat Biotechnol* **1**:784-791 (1983).
44. Kamilova F, Kravchenko LV, Shaposhnikov AI, Azarova T, Makarova N, and Lugtenberg B. Organic acids, sugars, and L-tryptophane in exudates of vegetables growing on stonewool and their effects on activities of rhizosphere bacteria. *Mol Plant Microbe Interact* **19**:250-256 (2006).
45. Falke JJ and Haselbauer GL. Transmembrane signaling in bacterial chemoreceptors. *Trends Biochem Sci* **26**:257-265 (2001).
46. Parales RE, Luu RA, Chen GY, Lui X, Wu V, Lin P, Hughes JG, Nesteryuk V, Parales JV, and Ditty JL. *Pseudomonas putida* F1 has multiple chemoreceptors with overlapping specificity for organic acids. *Microbiology* **159(Part 6)**:1086-1096 (2013).
47. Lacal J, Alfonso C, Liu X, Parales RE, Morel B, Conejero-Lara F, Rivas G, Duque E, Ramos J, and Krell T. Identification of a chemoreceptor for tricarboxylic acid cycle intermediates: differential chemotactic response towards receptor ligands. *J Biol Chem* **285**:23126-23136 (2010).

48. Alvarez-Ortega C and Harwood CS. 2007. Identification of a malate chemoreceptor in *Pseudomonas aeruginosa* by screening for chemotaxis defects in an energy taxis-deficient mutant. *Appl Environ Microbiol* **73**:7793-7795 (2007).

49. Kuroda A, Kumano T, Taguchi K, Nikata T, Kato J, and Ohtake H. Molecular cloning and characterization of a chemotactic transducer gene in *Pseudomonas aeruginosa*. *J Bacteriol* **177**:7019-7025 (1995).

50. Lacal J, García-Fontana C, Muñoz-Martínez F, Ramos JL, and Krell T. 2010. Sensing of environmental signals: classification of chemoreceptors according to the size of their ligand binding regions. *Environ Microbiol* **12**:2873-2884 (2010).

51. Ulrich LE and Zhulin IB. Four-helix bundle: a ubiquitous sensory module in prokaryotic signal transduction. *Bioinformatics* **21**(Suppl 3):iii45-iii48 (2005).

52. Stewart RC and Dahlquist FW. Molecular components of bacterial chemotaxis. *Chem Rev* **87**:997-1025 (1987).

53. Zhang Z and Hendrickson WA. Structural characterization of the predominant family of histidine kinase sensor domains. *J Mol Biol* **400**:335–353 (2010).

54. Reyes-Darias JA, Yang Y, Sourjik V, and Krell T. Correlation between signal input and output in PctA and PctB amino acid chemoreceptor of *Pseudomonas aeruginosa*. *Mol Microbiol* **96**:513-525 (2015).

55. Kelley LA, Mezulis S, Yates CM, Wass MN, and Sternberg MJ. The Phyre2 web portal for protein modeling, prediction and analysis. *Nat Protoc* **10**:845–858 (2015).

56. Anantharaman V and Aravind L. Cache - a signaling domain common to animal Ca^{2+}-channel subunits and a class of prokaryotic chemotaxis receptors. *Trends Biochem* **25**:535-537 (2000).

57. Ortega Á and Krell T. The HBM domain: introducing bimodularity to bacterial sensing. *Protein Sci* **23**:332-336 (2014).

58. Simons M, Permentier HP, de Weger LA, Wijffelman CA, and Lugtenberg BJJ. Amino acid synthesis is necessary for tomato root colonization by *Pseudomonas fluorescens* strain

WCS365. *Mol Plant Microbe Interact* **10**:102–106 (1997).

59. Tunchai M, Hida A, Oku S, Nakashimada Y, Tajima T, and Kato J. Identification of characterization of chemosensors for D-malate, unnatural enantiomer of malate, in *Ralstonia pseudosolanacearum*. *Microbiology* **163**:233–242 (2017).
60. Kuiper I, Kravchenko LV, Bloemberg GV, and Lugtenberg, BJ. *Pseudomonas putida* strain PCL1444, selected for efficient root colonization and naphthalene degradation, effectively utilizes root exudate components. *Mol Plant Microbe Interact* **15**: 734–741 (2002).
61. Yamamoto K and Imae Y. Cloning and characterization of the *Salmonella typhimurium*-specific chemoreceptor Tcp for taxis to citrate and from phenol. *Proc Natl Acad Sci USA* **90**: 217–221 (1993).
62. Ni B, Huang Z, Fan Z, Jiang C, and Liu S. *Comamonas testosteroni* uses a chemoreceptor for tricarboxylic acid cycle intermediates to trigger chemotactic responses towards aromatic compounds. *Mol Microbiol* **90**:813-823 (2013).
63. Ni B, Huang Z, Wu Y, Fan Z, Jiang C, and Liu S. A novel chemoreceptor MCP2983 from *Comamonas testosteroni* specifically binds to cis-aconitate and triggers chemotaxis towards diverse organic compounds. *Appl Microbiol Biotechnol* **99**:2773-2781 (2015).
64. Tunchai M, Hida A, Oku S, Nakashimada Y, Nikata T, Tajima T, Kato J. Negative chemotaxis of *Ralstonia pseudosolanacearum* to maleate and identification of the maleate chemosensory protein. *J Biosci Bioeng* **124**:647-652 (2017).
65. Lacal J, García-Fontana C, Callejo-García C, Ramos JL, and Krell T. Physiologically relevant divalent cations modulate citrate recognition by the McpS chemoreceptor. *J Mol Recognit* **24**:378-385 (2011).
66. Martín-Mora D, Reyes-Darias J, Ortega Á, Corral-Lugo A, Matilla MA, and Krell T. McpQ is a specific citrate chemoreceptor that responds preferentially to citrate/metal ion complexes. *Environ Microbiol* **18**:3284-3295 (2016).
67. Iwama T, Ito Y, Aoki H, Sakumoto H, Yamagata S, and Kawai K. Differential recognition of

citrate and a metal-citrate complex by the bacterial chemoreceptor Tcp. *J Biol Chem* **281**:17727-17735 (2006).

68. Cserzo M, Wallin E, Simon I, van Heiine G, and Flofsson A. Prediction of transmembrane alphahelices in prokaryotic membrane proteins: the dense alignment surface method. *Protein Eng* **10**:673-676 (1997).
69. Ingolia TD and Koshland DE Jr. Response to a metal ion-citrate complex in bacterial sensing. *J Bacteriol* **140**:798-804 (1979).
70. Doi R. and Ranamukhaarachchi SL. Soil dehydrogenase in a land degradation-rehabilitation gradient: observations from a savanna site with a wet/dry seasonal cycle. *Rev Biol Trop* **57**:223-234 (2009).
71. Pestana MN and Gomes AA. The effect of soil on cork quality. *Front Chem* **2**:80 (2014).
72. Lipton DS, Blanchar RW, and Blevins DG Citrate, malate, and succinate concentration in exudates from p-sufficient and p-stressed Medicago sativa L. seedlings. *Plant Physiol* **85**:315-317 (1987).
73. Qin R, Hirano Y, and Brunner I. Exudation of organic acid anions from poplar roots after exposure to Al, Cu and Zn. *Tree Physiol* **27**: 313-320 (2007).
74. López-Farfán D, Reyes-Darias JA, and Krell T. The expression of many chemoreceptor genes depends on the cognate chemoeffector as well as on the growth medium and phase. *Curr Genet* **63**:457-470 (2017).
75. Schuck P. Size-distribution analysis of macromolecules by sedimentation velocity ultracentrifugation and lamm equation modeling. *Biophys J* **78**:1606-1619 (2000).
76. Holloway BW, Krishnapillai V, and Morgan AF. Chromosomal genetics of *Pseudomonas*. *Microbiol Rev* **43**:73-102 (1979).
77. Compeau G, Alachi BJ, Platsouka E, and Levy SB. Survival of rifampin-resistant mutants of *Pseudomonas fluorescens* and *Pseudomonas putida* in soil systems. *Appl Environ Microbiol* **54**:2432-2438 (1988).

78. Stutz EW, Defago G, and Kern H. Naturally occurring fluorescent Pseudomonads involved in suppression of black root rot of tobacco. *Phytopathology* **76**:181-185 (1986).

79. Gibson DT, Koch JR, and Kallio RE. Oxidative degradation of aromatic hydrocarbons by microorganisms. I. Enzymatic formation of catechol from benzene. *Biochemistry* **7**:2653-2662 (1968).

80. Studier FW and Moffatt BA. Use of bacteriophage T7 RNA polymerase to direct selective high-level expression of cloned genes. *J Mol Biol* **189**:113-130 (1986).

81. Perelygin YP and Chistyakov DY. Boric acid. *Russ J Appl Chem* **79**:2041-2042 (2006).

82. Rico-Jiménez M, Reyes-Darias JA, Ortega Á, Peña AID, Morel B, and Krell T. Two different mechanisms mediate chemotaxis to inorganic phosphate in *Pseudomonas aeruginosa*. *Sci Rep* **6**:28967 (2016).

83. Řezanka T and Sigler K. Biologically active compounds of semi-metals. *Phytochemistry* **69**:585-606 (2008).

84. Hütter R, Keller-Schien W, Knüsel F, Prelog V, Rodgers GC, Suter P, Vogel G, Voser W, and Zähner H. Stoffwechselprodukte von Mikroorganismen. 57. Mitteilung. Boromycin. *Helv Chim Acta* **50**:1533–1539 (1967).

85. Okami Y, Okazaki T, Kitahara T, and Umezawa H. Studies on marine microorganisms. V. A new antibiotic, aplasmomycin, produced by a streptomycete isolated from shallow sea mud. *J Antibiot* **29**:1019-1025 (1976).

86. Irschik H, Schummer D, Gerth K, Höfle G, and Reichenbach H. The tartrolons, new boron-containing antibiotics from a myxobacterium, Sorangium cellulosum. *J Antibiot* **48**:26-30 (1995).

87. Chen X, Schauder S, Potier N, Van Dorsselaer A, Pelczer I, Bassler BL, and Hughson FM. Structural identification of a bacterial quorum-sensing signal containing boron. *Nature* **415**:545-549 (2002).

88. Bonilla I, Garcia-González M, and Mateo P. Boron requirement in cyanobacteria. Its possible

role in the early evolution of photosynthetic organisms. *Plant Physiol* **94**:1554-1560 (1990).

89. Bolaños L, Redondo-Nieto M,. Bonilla I, and Wall LG. Boron requirement in the *Discaria trinervis* (Rhamnaceae) and *Frankia* symbiotic relationship. Its essentiality for *Frankia* BCU110501 growth and nitrogen fixation. *Physiol Plant* **115**:563–570 (2002).
90. Bonilla I, Mergold-Villaseñor C, Campos ME, Sánchez N, Pérez H, López L, Castrejón L, Sánchez F, and Cassab GI. The aberrant cell walls of boron-deficient bean root nodules have no covalently bound hydroxyproline/proline-rich proteins. *Plant Physiol* **115**:1329-1340 (1997).
91. Bolaños L, Brewin NJ, and Bonilla I. Effects of boron on Rhizobium-legume cell-surface interactions and nodule development. *Plant Physiol* **110**:1249-1256 (1996).
92. O'Neill M. A, Ishii T, Albersheim P, and Darvill AG. Rhamnogalacturonan II: structure and function of a borate cross-linked cell wall pectic polysaccharide. *Annu Rev Plant Bio* **55**:109-139 (2004).
93. Shorrocks VM. The occurrence and correction of boron deficiency. *Plant soil* **193**:121-148 (1997).

Acknowledgements

This study has been carried out at Metabolic Engineering Lab. and Biomolecular Technology Lab., Graduate School of Advanced Sciences of Matter, Hiroshima University, and supported by JSPS KAKENHI Grant Number 15J05572.

I give a special thanks to Prof. Junichi Kato for their excellent guidance and kind supports. I am grateful to Prof. Nobukazu Tanaka and Prof. Akio Kuroda for carefully reviewing this thesis. I thank Assist. Prof. Takahisa Tajima, Prof. Yutaka Nakashimada, Assoc. Prof. Hidetoshi Kakizono, Dr. Shota Oku, Assoc. Prof. Makoto Fujie, and Assist. Prof. Takeru Kawasaki for their guidance and encouragement. I also would like to thank past and present members of these laboratories for their kindness.

I was also assisted by other persons in these laboratories. I am grateful to Prof. Hideaki Nojiri, Assist. Prof. Chiho Minakuchi, and Mr. Jun Matsuzawa for assistance with ITC analyses in Tokyo University, and Prof. Yoshihiro Sambongi, Mr. Yuki Kato, and Dr. Sotaro Fujii for assistance with CD analyses in Graduate School of Biosphere Science, Hiroshima University.

I really appreciate everyone’s assistance and kindness.

公表論文

(1) Identification of the *mcpA* and *mcpM* genes, encoding methyl-accepting proteins involved in amino acid and L-malate chemotaxis, and involvement of McpM-mediated chemotaxis in plant infection by *Ralstonia pseudosolanacearum* (formerly *Ralstonia solanacearum* phylotype I and III).
Hida A, Oku S, Kawasaki T, Nakashimada Y, Tajima T, Kato J.
Applied and Environmental Microbiology **81**:7420-7430 (2015).

(2) Identification of boric acid as a novel chemoattractant and elucidation of its chemoreceptor in *Ralstonia pseudosolanacearum* Ps29.
Hida A, Oku S, Nakashimada Y, Tajima T, Kato J.
Scientific Reports **7**:8609 (2017).

参考論文

(1) Identification and characterization of chemoresensors for D-malate, unnatural enantiomer of malate, in *Ralstonia pseudosolanacearum*
Tunchai M, **Hida A**, Oku S, Nakashimada Y, Tajima T, Kato J.
Microbiology **163**:233-242 (2017).

(2) Negative chemotaxis of Ralstonia pseudosolanacearum to maleate and identification of the maleate chemosensory protein.
Tunchai M, **Hida A**, Oku S, Nakashimada Y, Nikata T, Tajima T, Kato J.
Journal of Bioscience and Bioengineering **124**:647-652 (2017).

(3) Involvement of many chemotaxis sensors in negative chemotaxis to ethanol in *Ralstonia pseudosolanacearum* Ps29.
Oku S, **Hida A**, Tunchai M, Tajima T, Nakashimada Y, Kato J.
Microbiology **163**: 1880-1889 (2017).